DISCLAIMER

This contractor document was prepared for the U.S. Department of Energy (DOE), but has not undergone programmatic, policy, or publication review, and is provided for information only. The document provides preliminary information that may change based on new information to be used specifically for Total System Performance Assessment analyses. The document is a preliminary lower-level contractor document and is not intended for publication or wide distribution.

Although this document has undergone technical reviews at the contractor organization, it has not undergone a DOE policy review. Therefore, the views and options of authors expressed may not state or reflect those of the DOE. However, in the interest of the rapid transfer of information, we are providing this document for your information per your request.

WM-11
NM3567

OFFICE OF CIVILIAN RADIOACTIVE WASTE MANAGEMENT

ANALYSIS/MODEL COVER SHEET

Complete Only Applicable Items

1. QA: QA

2. ☒ Analysis — Check all that apply	3. ☐ Model — Check all that apply
Type of Analysis: ☐ Engineering ☐ Performance Assessment ☒ Scientific	Type of Model: ☐ Conceptual Model ☐ Abstraction ☐ Mathematical Model ☐ System Model ☐ Process Model
Intended Use of Analysis: ☒ Input to Calculation ☒ Input to another Analysis or Model ☒ Input to Technical Document ☐ Input to Other Technical Products	Intended Use of Model: ☐ Input to Calculation ☐ Input to another Model or Analysis ☐ Input to Technical Document ☐ Input to Other Technical Products
Describe use: Provides probabilistic basis for igneous consequence analyses	Describe use:

4. Title:

Characterize Framework for Igneous Activity at Yucca Mountain, Nevada (T0015)

5. Document Identifier (including Rev. No. and Change No., if applicable):

ANL-MGR-GS-000001, Rev 00

6. Total Attachments:	7. Attachment Numbers - No. of Pages in Each:
3	I-1; II-5; III-~~10~~ 16 R0 6-28-00

	Printed Name	Signature	Date
8. Originator	Frank Perry Bob Youngs	F.K. Perry, R. Youngs	6/27/2000
9. Checker	Steve Nelson Doug Walker	Steve Nelson for Doug Walker	6/27/00
10. Lead/Supervisor	Debra Bryan	Debra Bryan	6/27/2000
11. Responsible Manager	Debra Bryan	Debra Bryan	6/27/2000

12. Remarks:

INITIAL ISSUE

INFORMATION **COPY**

LAS VEGAS DOCUMENT **CONTROL**

ENCLOSURE 2

OFFICE OF CIVILIAN RADIOACTIVE WASTE MANAGEMENT
ANALYSIS/MODEL REVISION RECORD

Complete Only Applicable Items

1. Page: 2 of: 11

2. Analysis or Model Title:

Characterize Framework for Igneous Activity at Yucca Mountain, Nevada (T0015)

3. Document Identifier (including Rev. No. and Change No., if applicable):

ANL-MGR-GS-000001, Rev 00

4. Revision/Change No.	5. Description of Revision/Change
00	INITIAL ISSUE

CONTENTS

Page

1. PURPOSE 15

2. QUALITY ASSURANCE 17

3. COMPUTER SOFTWARE AND MODEL USAGE 19
   3.1 COMPUTER SOFTWARE 19
   3.2 MODELS 24

4. INPUTS 25
   4.1 DATA AND PARAMETERS 25
   4.2 CRITERIA 25
   4.3 CODES AND STANDARDS 25

5. ASSUMPTIONS 27
   5.1 USE OF QUATERNARY VOLCANOES 27
   5.2 ALL VOLCANIC EVENTS PRODUCE AT LEAST ONE ERUPTIVE CENTER .. 28
   5.3 LOCATION OF ERUPTIVE CENTERS ALONG THE LENGTH OF A DIKE OR DIKE SEGMENT 28
   5.4 POTENTIAL REPOSITORY DRIFT LOCATIONS FOR EDA II 29

6. ANALYSIS/MODEL 31
   6.1 INTRODUCTION 31
   6.2 VOLCANIC HISTORY OF THE YUCCA MOUNTAIN REGION 31
   6.3 THE PROBABILISTIC VOLCANIC HAZARD ANALYSIS (PVHA) 35
      6.3.1 The PVHA Process 35
         6.3.1.1 Selecting the Expert Panel Members 35
         6.3.1.2 Identifying Technical Issues 35
         6.3.1.3 Temporal and Spatial Aspects of Probability Models 36
         6.3.1.4 Eliciting the Experts' Judgments 37
         6.3.1.5 PVHA Results 37
         6.3.1.6 Significance of Buried Volcanic Centers on PVHA Results 38
         6.3.1.7 Alternative Estimates of the Intersection Probability 40
      6.3.2 Definitions and Parameters of a Volcanic Event and Implications for Alternative Probability Calculations 41
         6.3.2.1 Intrusive Versus Extrusive Events: Evidence from Analog Sites 44
         6.3.2.2 Alternative Event Lengths 46
      6.3.3 Conceptual Models of Volcanism and Formulation of Probability Models .. 47
   6.4 THE CRATER FLAT STRUCTURAL DOMAIN 50
      6.4.1 Internal Structure and Boundaries of the Crater Flat Basin 52
         6.4.1.1 Fault Orientations, Dip Directions, and Displacements 52

CONTENTS (Continued)

Page

6.4.1.2 Rotation of Faults 54
6.4.1.3 Quaternary Slip Rate 54
6.4.1.4 Basin Subsidence and Fault Displacement 55
6.4.1.5 Correlation with Volcanism 56
6.4.2 PVHA Volcanic Source Zones: Relationship to Crater Flat Structural Features and the Probability of Dike Intersection 56
6.5 RECALCULATION OF FREQUENCY OF INTERSECTION AND DEVELOPMENT OF DISTRIBUTIONS FOR LENGTH AND ORIENTATION OF DIKES AND FOR THE NUMBER OF ERUPTIVE CENTERS WITHIN THE POTENTIAL REPOSITORY FOOTPRINT 60
6.5.1 Formulation 62
6.5.1.1 Frequency of Intersection of the Potential Repository Footprint by a Dike 62
6.5.1.2 Conditional Distribution for Length and Azimuth of an Intersecting Dike 65
6.5.1.3 Conditional Distribution for the Number of Eruptive Centers 70
6.5.2 Implementation 76
6.5.2.1 Frequency of Intersection of the Potential Repository Footprint by a Dike 77
6.5.2.2 Distributions for Length, Azimuth, and Number of Eruptive Centers 78
6.5.3 Results 92
6.5.3.1 Frequency of Intersection of the Potential Repository Footprint by a Dike 92
6.5.3.2 Conditional Distributions for Intersection Length, Azimuth, and Number of Eruptive Centers within the Potential Repository Footprint 99

7. CONCLUSIONS 107
7.1 OUTPUTS OF THIS AMR 108

8. INPUTS AND REFERENCES 111
8.1 DOCUMENTS CITED 111
8.2 CODES, STANDARDS, REGULATIONS, AND PROCEDURES 116
8.3 SOFTWARE 116
8.4 SOURCE DATA, LISTED BY DATA TRACKING NUMBER 119
8.5 OUTPUT DATA, LISTED BY DATA TRACKING NUMBER 119

ATTACHMENTS
ATTACHMENT I: AMR FEEDS TO TSPA IGNEOUS ACTIVITY I-1
ATTACHMENT II: DEVELOPMENT OF FOOTPRINT POLYGONS FOR POTENTIAL REPOSITORY II-1

ATTACHMENT III: DEVELOPMENT OF DISTRIBUTIONS FOR NUMBER OF ERUPTIVE CENTERS PER VOLCANIC EVENT AND AVERAGE SPACING BETWEEN ERUPTIVE CENTERS III-1

INTENTIONALLY LEFT BLANK

FIGURES

Page

1. Flowchart for Computation of Frequency of Intersection of Potential Repository by a Dike 20

2. Flowchart for Computation of Conditional Distributions for Length and Azimuth of Intersecting Dike and Number of Eruptive Centers within the Potential Repository Given Intersection of the Potential Repository Footprint by a Dike 23

3. Location and Age of Post-Miocene (<5.3 m.y.) Volcanoes (or Clusters Where Multiple Volcanoes have Indistinguishable Ages) in the YMR 32

4. Composite Distribution for Dike Length Averaged Across All 10 PVHA Experts 43

5. Conceptual Diagram Comparing Event Definitions from the PVHA and Reamer (1999): Implications for Eruption and Intrusion Probabilities Based on Different Event Definitions 44

6. Composite Distribution for the Distance from the Point Volcanic Event to the End of the Dike Averaged Across All 10 PVHA Experts 48

7. Local Structural Domains and Domain Boundaries of the YMR and Internal Structures of the Crater Flat Basin and Selected Parts of Adjacent Domains 51

8. Schematic Cross Section of the Crater Flat Basin, from Seismic Reflection, Surficial Geology, and Borehole Information 53

9a. Local Structural Domains and Domain Boundaries of the YMR and Internal Structures of the Crater Flat Basin and Selected Parts of Adjacent Domains 58

9b. Local Structural Domains and Domain Boundaries of the YMR and Internal Structures of the Crater Flat Basin and Selected Parts of Adjacent Domains 59

10. Schematic Illustrating Procedure for Computing the Frequency of Intersection of the Potential Repository by a Volcanic Event 61

11a. Logic Tree Structure Used to Characterize Uncertainty in Volcanic Hazard 63

11b. Logic Tree Structure for Subtrees Addressing Uncertainty in Volcanic Hazard from Specific Sources 64

FIGURES (Continued)

Page

12. Definition of Parameters Used to Compute the Probability of Intersection of the Potential Repository Footprint by a Volcanic Event 66

13. Example Distributions for Dike Length, L, (part a); Normalized Location of the Point Volcanic Event Relative to the Total Length of the Dike, E^L, (part b); and the Resulting Distribution for Distance from the Point Volcanic Event to the End of the Dike, d (part c) 67

14. Example Simulations of the Distribution of Eruptive Centers along the Length of a Dike for: (a) the Independent, Uniformly Distributed (*IUD*) Spatial Distribution and (b) the Uniformly Spaced, Randomly Distributed (*USRD*) Spatial Distribution 72

15a. Probability for the Number of Eruptive Centers within the Potential Repository Footprint, r^{EC}, as a Function of Dike Length, L, for the Length of Intersection, $L^I = 1$ Kilometer, and the Number of Eruptive Centers Associated with the Volcanic Event, $n^{EC} = 2$ 74

15b. Probability for the Number of Eruptive Centers within the Potential Repository Footprint, r^{EC}, as a Function of Dike Length, L, for the Length of Intersection, $L^I = 1$ Kilometer, and the Number of Eruptive Centers Associated with the Volcanic Event, $n^{EC} = 3$ 75

16. Location of Primary Block and Primary + Contingency Blocks of Current Potential Repository Footprint (EDA II) Compared to Potential Repository Footprint Used in the PVHA 79

17. Spatial Distribution of Volcanic Hazard Defined by the PVHA Expert Panel: (a) Map of Expected Volcanic Event Frequency and (b) Map of Spatial Disaggregation of Expected Intersection Frequency 83

18. Distributions for Number of Eruptive Centers per Volcanic Event, n^{EC}, Derived from the PVHA Experts' Interpretations 85

19. Probability for the Number of Eruptive Centers within the Potential Repository Footprint, r^{EC}, Computed Using the *USRD-FD* Spatial Distribution of Eruptive Centers and for the Length of Intersection, $L^I = 1$ kilometer, and an Average Spacing of 2.5 kilometers between Eruptive Centers Compared to the Results for the *IUD* and *USRD* Models Shown on Figure 15a 87

20. Annual Frequency of Intersecting the Potential Repository Footprint for the Primary Block Case 97

FIGURES (Continued)

Page

21. Annual Frequency of Intersecting the Potential Repository Footprint for the Primary + Contingency Blocks Case 98

22. Marginal Conditional Distributions for Dike Intersection Length, L^I, for Mean and 95th Percentile Frequency of Intersection and for the Primary Block and Primary + Contingency Block Cases 100

23. Marginal Conditional Distributions for Dike Intersection Azimuth, ϕ, for Mean and 95th Percentile Frequency of Intersection and for the Primary Block and Primary + Contingency Block Cases 102

24. Marginal Conditional Distributions for the Number of Eruptive Centers within the Potential Repository Footprint, r^{EC}, for 5th Percentile, Mean, and 95th Percentile Frequency of Intersection and for the Primary Block and Primary + Contingency Block Cases 104

INTENTIONALLY LEFT BLANK

TABLES

Page

1. Software Routines Used to Compute Frequency of Intersection of the Potential Repository by a Dike 19

2. Software Routines Used to Compute Conditional Distributions for Dike Length, Azimuth, and Number of Eruptive Centers within the Potential Repository 21

3. Summary of Data Used as Inputs for Analyses in this AMR 25

4. Estimated Volume and $^{40}Ar/^{39}Ar$ Age of Quaternary Volcanoes in the YMR 34

5. PVHA Panel Members 35

6. Published Estimates of the Probability of Intersection of the Potential Repository at Yucca Mountain by a Volcanic Event 41

7. Average Eruptive Center Spacing 86

8. Frequency of Intersection for Primary Block (drifts 1-50) 93

9. Frequency of Intersection for Primary + Contingency Blocks (drifts 1-60) 95

10. Marginal Conditional Distributions for Dike Intersection Length, Conditional on the Occurrence of an Intersection 101

11. Marginal Conditional Distribution for Intersecting Dike Azimuth, Conditional on the Occurrence of an Intersection 103

12. Marginal Conditional Distribution for Number of Eruptive Centers within the Potential Repository, Conditional on the Occurrence of an Intersection 105

13. Summary Frequencies of Disruptive Volcanic Events 109

ACRONYMS

AMR	Analysis/Model Report
CDF	Cumulative probability density function
CM	Configuration Management
DOE	U.S. Department of Energy
DTN	Data tracking number
EDA	Enhanced design alternative
FEPs	Features, events, and processes
IUD-C	Independent, Uniformly Distributed eruptive centers with the number of centers Correlated with dike length
IUD-UC	Independent Uniformly Distributed eruptive centers with the number of centers UnCorrelated with dike length
LANL	Los Alamos National Laboratory
m.y.	Million years
NRC	Nuclear Regulatory Commission
OCRWM	Office of Civilian Radioactive Waste Management
QA	Quality assurance
QARD	Quality Assurance Requirements and Description
PA	Performance assessment
PMR	Process Model Report
PVHA	Probabilistic Volcanic Hazard Analysis
SAN	Software activity number
STN	Software tracking number
SR	Site recommendation
TBV	To be verified
TBD	To be determined
TSPA	Total System Performance Assessment
USRD-C	Uniformly Spaced, Randomly Distributed eruptive centers with the number of centers Correlated with dike length
USRD-FD	Uniformly Spaced, Randomly Distributed eruptive centers with the number of centers computed by a Fixed Density and dike length

USRD-UC	Uniformly Spaced, Randomly Distributed eruptive centers with the number of centers UnCorrelated with dike length
UTM	Universal Transverse Mercator
YMP	Yucca Mountain Site Characterization Project
YMR	Yucca Mountain region

INTENTIONALLY LEFT BLANK

1. PURPOSE

The purpose of this Analysis/Model report (AMR) is twofold. (1) The first is to present a conceptual framework of igneous activity in the Yucca Mountain region (YMR) consistent with the volcanic and tectonic history of this region and the assessment of this history by experts who participated in the Probabilistic Volcanic Hazard Analysis (PVHA) (CRWMS M&O 1996). Conceptual models presented in the PVHA are summarized and extended in areas in which new information has been presented. Alternative conceptual models are discussed as well as their impact on probability models. The relationship between volcanic source zones defined in the PVHA and structural features of the YMR are described based on discussions in the PVHA and studies presented since the PVHA. (2) The second purpose of the AMR is to present revised probability calculations based on PVHA outputs. Probability distributions are presented for the length and orientation of volcanic dikes within the repository footprint and for the number of eruptive centers located within the repository footprint (conditional on the dike intersecting the repository). The probability of intersection of a basaltic dike with the repository footprint is recalculated based on the current repository footprint and the probability of an eruptive center(s) forming within the current repository footprint is calculated. The probability of an eruptive center forming within the repository footprint is a calculation that was not included in the PVHA. Preparation of this AMR was conducted as defined by the AMR Development Plan (CRWMS M&O 1999a).

The U.S. Department of Energy (DOE) considers volcanism to be a potentially disruptive event in the Total System Performance Assessment (TSPA) analysis supporting Site Recommendation (SR) for the potential Yucca Mountain repository (DOE 1998). The two volcanic events (with individual probabilities and consequences) being modeled by TSPA-SR are: (1) the ascent of a basaltic dike or dike system (i.e., a set or swarm of multiple dikes comprising a single intrusive event) to repository level where it intersects drifts; and (2) the development of a volcano within the repository footprint with one or more conduits that intersect waste packages. As a consequence of the first event, which is non-eruptive, waste from breached packages may provide a source of radionuclides when groundwater moves through the damaged packages at some time in the future (igneous intrusion groundwater release). The potential consequence of the second event is that waste packages entrained within a conduit may be breached, releasing radionuclides in the erupting ash plume where they can be dispersed downwind to a critical group designated by DOE's Interim Guidance as being approximately 20 kilometers to the south of Yucca Mountain (Dyer 1999, Section 115(b)).

TSPA-SR requires consideration of both probability and consequence. The objective of the PVHA was to determine the probability of a basaltic dike intersecting the potential repository (CRWMS M&O 1996). The PVHA report was the outcome of an expert elicitation and forms the foundation of much of the igneous analysis for the SR. The PVHA included discussion of some aspects of the consequences of a volcanic event but not all the aspects required for the present analysis; therefore, additional analyses will be performed to complete supporting description of the volcanic risk. The risk from volcanism will be described by combining work from the PVHA (probability) and the present enhanced analysis of consequence.

The AMRs comprising the Disruptive Events Report, which support analysis of volcanic risk for TSPA-SR, are summarized in Attachment I. Broadly, information flows from left to right across this figure, culminating in support for the TSPA-SR. These AMRs directly or indirectly support the TSPA-SR analysis that calculates the overall performance of the system. This AMR, "Characterize Framework for Igneous Activity at Yucca Mountain, Nevada," describes the conceptual framework for volcanism near Yucca Mountain and how the conceptual framework provides the basis for probability calculations. This AMR also presents the probability results and associated uncertainties for intersection of the potential repository by a basaltic dike and the probability of an eruption through the repository, conditional on a dike intersection. These probability results provide the basis for all further igneous consequence analysis. This AMR provides direct input into the "Number of Waste Packages Hit" calculation (CRWMS M&O 2000c) and the "Igneous Consequence Modeling" AMR (CRWMS M&O 2000a).

2. QUALITY ASSURANCE

The activities documented in this AMR were evaluated in accordance with QAP-2-0, *Conduct of Activities* and were determined to be subject to the requirements of the U.S. Department of Energy (DOE) Office of Civilian Radioactive Waste Management (OCRWM) *Quality Assurance Requirements and Description* (QARD) (DOE 2000). This evaluation is documented in CRWMS M&O (1999b-d), and Wemheuer (1999) (Activity Evaluation for Work Package 1401213DM1). This AMR has been prepared in accordance with procedure AP-3.10Q, *Analyses and Models*.

The work activities documented in this AMR depend on electronic media to store, maintain, retrieve, modify, update, or transmit quality-affecting information. The applicable process controls identified through AP-SV.1Q, *Control of Electronic Management of Data*, are implemented for the activities documented in this AMR through procedure LANL-YMP-QP-S5.01, *Electronic Data Management*.

INTENTIONALLY LEFT BLANK

3. COMPUTER SOFTWARE AND MODEL USAGE

3.1 COMPUTER SOFTWARE

The calculations presented in this AMR were performed with the set of software routines described below. This software has been qualified following procedure AP-SI.1Q, Revision 2, ICN 4, *Software Management*. The software and routines used in support of this AMR were appropriate for this application and were used within their range of validation as described in the qualification documentation. The software is written in FORTRAN77 and operates on a PC equipped with a 486 or Pentium processor under DOS or in a Windows MSDOS window. The computations using these software routines were performed using the software routines acquired from Software Configuration Management. The software was designed to perform the calculations defined by the PVHA (CRWMS M&O 1996) and was used within the parameter limits defined by the PVHA.

The software routine titles are listed with the *.FOR* extension in the Software Configuration Management database, the Document Input Reference System (DIRS) database, and in Section 8.3 of this AMR. The routines are listed by their titles without the *.FOR* extension in Tables 1 and 2, Figures 1 and 2, and in the text of this AMR.

Table 1 lists the software routines used to compute the frequency of intersection of the repository footprint by a volcanic event through full enumeration of the PVHA experts' log trees. Figure 1 shows the data flow through the routines in Table 1. The software routines listed in Table 1 are qualified versions of the routines used in the PVHA calculation (CRWMS M&O 1996).

Table 1. Software Routines Used to Compute Frequency of Intersection of the Potential Repository by a Dike

Software Routine (STN Number)	Function
FITCD V1.0 (10262-1.0-00)	Computes discrete cumulative probability distributions for dike length from cumulative probabilities specified at selected values of length.
SFCD V1.0 (10275-1.0-00)	Computes discrete cumulative probability distributions for dike length using
DCPELD V1.0 (10258-1.0-00)	Computes discrete probability distribution for dike length from expert specified distributions (output of FITCD)
CPDI V1.0 (10257-1.0-00)	Computes conditional probability of intersection from volcanic events on an *x,y* grid using output of DCPELD and expert specified azimuth distributions.
UZVH V1.0 (10277-1.0-00)	Computes frequency of intersection from volcanic source zones using output of CPDI
FKVH V1.0 (10265-1.0-00)	Computes frequency of intersection using kernel density estimation with specified *h* and output of CPDI
UZVPVH V1.0 (10279-1.0-00)	Computes frequency of intersection from volcanic source zones using volume predictable volcanic event rate model and output of CPDI

Software Routine (STN Number)	Function
FKVPVH V1.0 (10267-1.0-00)	Computes frequency of intersection using kernel density estimation using volume predictable volcanic event rate model and output of CPDI
ZBCKVH V1.0 (10283-1.0-00)	Computes frequency of intersection using kernel density estimation with *h* constrained by a source zone boundary and output of CPDI
FITFIELD V1.0 (10263-1.0-00)	Computes parameters of a bivariate Gaussian distribution that approximates boundaries of a defined polygon
FIT2CNTR V1.0 (10261-1.0-00)	Computes parameters of a bivariate Gaussian distribution from locations of volcanic events
PFGVH V1.0 (10273-1.0-00)	Computes frequency of intersection using a bivariate Gaussian distribution with specified field parameters and output of CPDI. Bivariate Gaussian distribution parameters obtained from programs FIT2CNTR or FITFIELD
FPFGVH V1.0 (10269-1.0-00)	Computes frequency of intersection using a bivariate Gaussian distribution with parameters fit to volcanic event locations and output of CPDI
VHTREE V1.0 (10282-1.0-00)	Computes mean and fractiles of frequency of intersection over an individual expert's volcanic hazard logic tree and aggregate over all experts using outputs of UZVH, UZVHB, FKVH, UZVPVH, FKVPVH, ZBCLVH, PFGVH, and FPFGVH

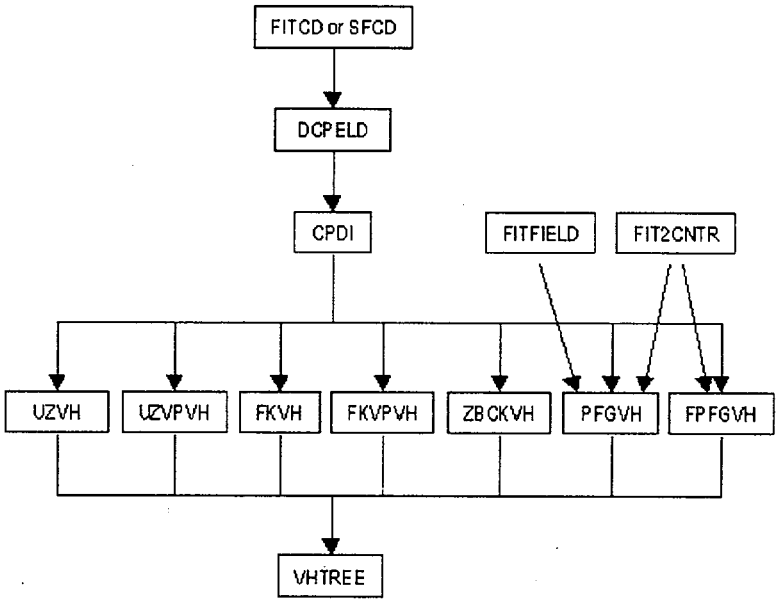

NOTE: Names in boxes denote software routines listed in Table 1.

Figure 1. Flowchart for Computation of Frequency of Intersection of Potential Repository by a Dike

Table 2 lists the software routines used to compute the conditional distributions for the length and azimuth of an intersecting dike within the potential repository footprint and the number of eruptive centers within this footprint. The data flow through the software routines for this calculation is shown in Figure 2.

Table 2. Software Routines Used to Compute Conditional Distributions for Dike Length, Azimuth, and Number of Eruptive Centers within the Potential Repository

Software Routine (STN Number)	Function
FITCD V1.0 (10262-1.0-00)	Computes discrete cumulative probability distributions for dike length from cumulative probabilities specified at selected values of length.
SFCD V1.0 (10275-1.0-00)	Computes discrete cumulative probability distributions for dike length using.
DCPELD V1.0 (10258-1.0-00)	Computes discrete probability distribution for dike length from expert specified distributions (output of FITCD)
CPDI V1.0 (10257-1.0-00)	Computes conditional probability of intersection from volcanic events on an *x,y* grid using output of DCPELD and expert specified azimuth distributions.
UZVHLH V1.0 (10278-1.0-00)	Computes simulations of contributions to frequency of intersection on an *x,y* grid from volcanic source zones using Latin Hypercube sampling and output from CPDI
FKVHLH V1.0 (10266-1.0-00)	Computes simulations of contributions to frequency of intersection on an *x,y* grid using kernel density estimation with specified *h* , Latin Hypercube sampling, and output from CPDI
UZVPVHLH V1.0 (10280-1.0-00)	Computes simulations of contributions to frequency of intersection on an *x,y* grid from volcanic source zones using volume predictable volcanic event rate model, Latin Hypercube sampling, and output from CPDI
FKVPVHLH V1.0 (10268-1.0-00)	Computes simulations of contributions to frequency of intersection on an *x,y* grid with kernel density estimation using volume predictable volcanic event rate model, Latin Hypercube sampling, and output from CPDI
ZBCKVHLH V1.0 (10284-1.0-00)	Computes simulations of contributions to frequency of intersection on an *x,y* grid using kernel density estimation with *h* constrained by a source zone boundary, Latin Hypercube sampling, and output from CPDI
FITFIELD V1.0 (10263-1.0-00)	Computes parameters of a bivariate Gaussian distribution that approximates boundaries of a defined polygon
FIT2CNTR V1.0 (10261-1.0-00)	Computes parameters of a bivariate Gaussian distribution from locations of volcanic events
PFGVHLH V1.0 (10274-1.0-00)	Computes simulations of contributions to frequency of intersection on an *x,y* grid using a 2D-Gaussian distribution with specified parameters, Latin Hypercube sampling, and output from CPDI. Gaussian distribution parameters obtained from programs FIT2CNTR or FITFIELD
FPFGVHLH V1.0 (10270-1.0-00)	Computes simulations of contributions to frequency of intersection on an *x,y* grid using a 2D-Gaussian distribution with parameters fit to volcanic event locations, Latin Hypercube sampling, and output from CPDI
VHTIELHS V1.0 (10281-1.0-00)	Computes mean and fractiles of simulations of contributions to frequency of intersection on an *x,y* grid over an individual expert's volcanic hazard logic tree using Latin Hypercube sampling and output from UZVHLH, FKVHLH, UZVPVHLH, FKVPVHLH, ZBCLVHLH, PFGVHLH, and FPFGVHLH
NECPDS V1.0 (10272-1.0-00)	Computes distributions for number of eruptive centers per volcanic event and compute average spacing between eruptive centers.

Software Routine (STN Number)	Function
FITIDSR V1.0 (10264-1.0-00)	Computes discrete incremental probability distributions for dike length using input to FITCD
SFIDSR V1.0 (10276-1.0-00)	Computes discrete incremental probability distributions for dike length using input to SFCD
DLECD V1.0 (10260-1.0-00)	Computes joint discrete probability distributions for dike length and number of eruptive centers per volcanic event using output from FITIDSR
DILECDLH V1.0 (10259-1.0-00)	Computes joint conditional distribution of dike intersection length, dike azimuth, and number of eruptive centers within the repository footprint from outputs of program VHTIELHS using Latin hypercube sampling of dike length and volcanic event location distributions from DIECDIST
CFRAC V1.0 (10254-1.0-00)	Locates individual expert's simulation results that represent specified percentiles of the composite distribution for frequency of intersection from outputs of VHTIELHS
COMBSM V1.0 (10256-1.0-00)	Computes composite joint distribution of dike intersection length, dike azimuth, and number of eruptive centers within the repository footprint across experts from outputs of DILECDLH and VHTIELHS for mean hazard
COMBSF V1.0 (10255-1.0-00)	Computes composite joint distribution of dike intersection length, dike azimuth, and number of eruptive centers within the repository footprint across experts from outputs of DILECDLH for selected percentiles of the hazard
MARGIN V1.0 (10271-1.0-00)	Computes marginal distributions for dike intersection length, dike azimuth, and number of eruptive centers within the repository footprint from output of COMBSM and COMBSF

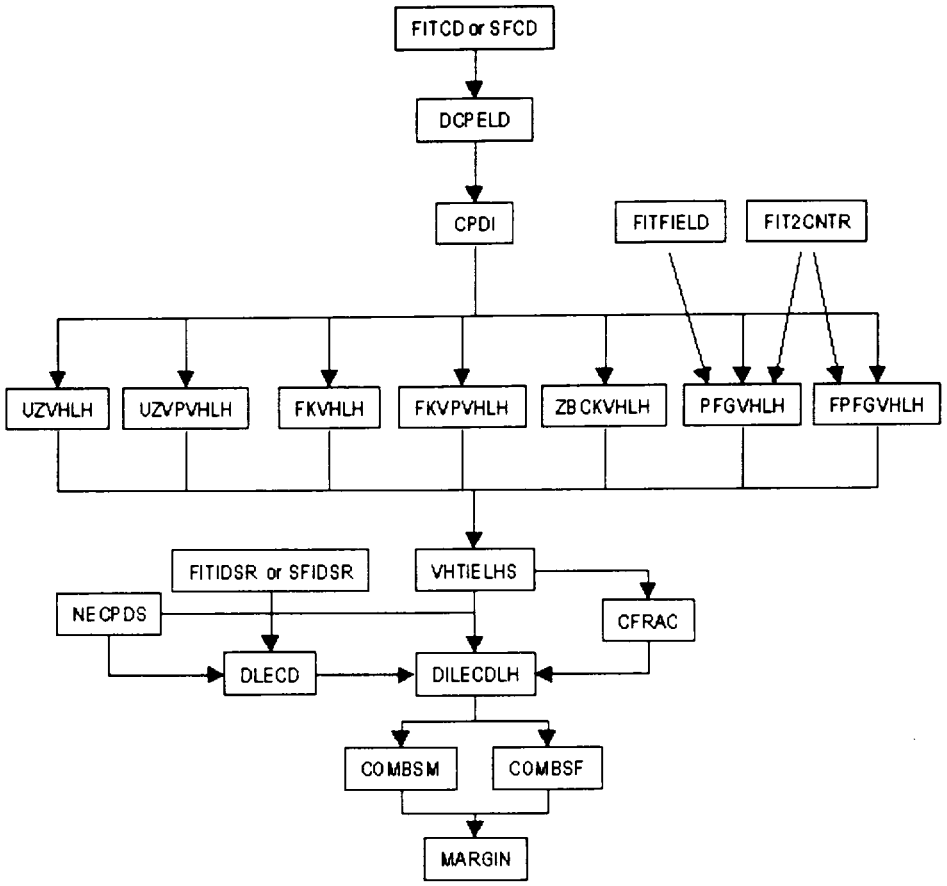

NOTE: Names in boxes denote software routines listed in Table 2.

Figure 2. Flowchart for Computation of Conditional Distributions for Length and Azimuth of Intersecting Dike and Number of Eruptive Centers within the Potential Repository Given Intersection of the Potential Repository Footprint by a Dike

In addition, software routine COMBDELD V1.0 (STN: 10288–1.0-00) was used to compute aggregate dike length and event length distributions across all 10 PVHA experts (Figures 4 and 6).

As part of development of a polygon representing the potential repository footprint, the drift coordinates obtained from CRWMS M&O (1999f) were converted from Nevada State Plane Coordinates to Universal Transverse Mercator (UTM) Coordinates. Yucca Mountain Site Characterization Project (YMP) Software EARTHVISION V4.0 (STN: 30035-1 V4.0) was used to transform the coordinates of 16 points that defined the northern and southern limits of the repository blocks. The calculation was performed on a Silicon Graphics Octane computer running the IRIX 6.4 operating system using software acquired from Software Configuration Management.

3.2 MODELS

The calculations performed in this AMR use as input the results of the PVHA (CRWMS M&O 1996). The PVHA is an expert elicitation study that assessed the scientific uncertainty in modeling the volcanic hazard at Yucca Mountain. The results of the PVHA consist of a set of alternative mathematical models, the probability that each model is the appropriate model, and probability distributions for the parameters of these models. The validation of these models is documented by the assessments of the experts presented in the PVHA (CRWMS M&O 1996, Appendix E).

4. INPUTS

4.1 DATA AND PARAMETERS

The location, a brief description, and the data tracking number (DTN) used as input for this AMR are listed in Table 3. The qualification status of data input is indicated in the electronic DIRS database.

The source of input data for this analysis is the PVHA expert interpretations presented in CRWMS M&O (1996). Because this AMR is an analysis of the PVHA (CRWMS M&O 1996), the use of the PVHA as input to this AMR is appropriate. The PVHA expert interpretations are used as inputs to the calculations described in Section 6.5 and Attachment III. The interpretations are also discussed in the conceptual framework described in Sections 6.1 through 6.4.

Table 3. Summary of Data Used as Inputs for Analyses in this AMR

Description	Data Source Listed by Data Tracking Number (DTN)	Location in AMR
PVHA (CRWMS M&O 1996): Expert Assessment of Volcanic Hazard in the YMR	MO0002PVHA0082.000	Entire Document

All other DTNs presented in this AMR are not used as direct input to this AMR and are used as reference only.

4.2 CRITERIA

This AMR addresses requirements presented in DOE Interim Guidance (Dyer 1999). Subparts of the Interim Guidance that apply to this analysis are those pertaining to the characterization of the Yucca Mountain site (Subpart B, Section 15), the compilation of information regarding geology of the site in support of the License Application (Subpart B, Section 21(c)(1)(ii)), and the definition of geologic parameters and conceptual models used in performance assessment (Subpart E, Section 114(a)).

4.3 CODES AND STANDARDS

No codes or standards are directly applicable to this analysis.

INTENTIONALLY LEFT BLANK

5. ASSUMPTIONS

This section describes the assumptions used for the analyses in Section 6.5, Attachment II, and Attachment III.

The calculation of the updated distribution for frequency of intersection of the potential repository footprint by a basaltic dike requires no assumptions because it uses the outputs defined by the PVHA (CRWMS M&O 1996) without modification. The update involves only a change in the potential repository footprint.

The calculation of conditional distributions for the length and azimuth of intersecting dikes within the potential repository requires no assumptions because it involves only a modification of the software to output an intermediate step of the "frequency of intersection of the potential repository footprint by a dike" calculation.

The calculation of conditional distributions for the number of eruptive centers within the potential repository footprint requires an assessment of the number of eruptive centers associated with a volcanic event and the spatial distribution for eruptive centers along the length of the dike. The PVHA experts were not asked to make this assessment part of their characterization of the volcanic hazard. However, the number of eruptive centers associated with a volcanic event can be derived from the PVHA experts' evaluation of the number of volcanic events that have occurred in the Quaternary using the following assumptions.

5.1 USE OF QUATERNARY VOLCANOES

Assumption: The mapped Quaternary volcanoes in the YMR are representative of the type being characterized for calculation of the consequences of an eruptive event through the potential repository. For the purposes of this AMR and for PA calculations, each eruptive center or vent equates to a one subsurface conduit.

Basis: The characteristics of Quaternary volcanoes in the YMR are used to define the distributions for the characteristics of future volcanic events (CRWMS M&O 2000b). The assumption that each volcano is associated with a conduit is consistent with the description of the eruptive process for YMR volcanoes described in CRWMS M&O (2000b). Volcanoes were also used by the PVHA experts as indicators of the occurrence of past volcanic events.

Confirmation Status: This assumption is consistent with DOE Interim Guidance (Dyer, 1999, section 114l) to "assume evolution of the geologic setting is consistent with present knowledge of natural processes." No work is needed to confirm it.

Use in the Analysis: This assumption is used in Attachment III to derive distributions for the number of eruptive centers per volcanic event and the average spacing between eruptive centers.

5.2 ALL VOLCANIC EVENTS PRODUCE AT LEAST ONE ERUPTIVE CENTER

Assumption: Each hypothetical volcanic event for which the associated dike intersects the repository has at least one eruptive center located somewhere along the length of the dike.

Basis: This assumption is justified on the basis of the PVHA expert panel's general belief that magma that ascends to within a few hundred meters of the surface will produce a surface manifestation of the volcanic event (CRWMS M&O 1996, Appendix E, e.g., pp. RC-10, BC-6, WD-6, WH-6, MK-12). The assumption is conservative in that the PVHA experts allowed for the possibility that not all past volcanic events reached the surface in assessing the rate of volcanic events. The rate of volcanic events used to compute the frequency of intersection of the potential repository footprint by a dike was obtained by multiplying the rate based on past volcanic events with observed surface manifestations by a "hidden events factor" greater than or equal to 1.0. Assuming all future volcanic events will produce an eruptive center produces the maximum rate of eruptive center occurrence.

Confirmation Status: The assumption is conservative in that it produces the maximum frequency of occurrence of eruptive centers and does not need to be confirmed.

Use in the Analysis: This assumption is used in Attachment III to develop distributions for the number of eruptive centers per volcanic event and in Section 6.5.2.2 in the computation of the conditional distribution for number of eruptive centers within the repository.

5.3 LOCATION OF ERUPTIVE CENTERS ALONG THE LENGTH OF A DIKE OR DIKE SEGMENT

Assumption: The location of an eruptive center along the length of a dike or dike segment is defined by a uniform probability distribution.

Basis: This assumption is justified on the basis that it is the minimum information assumption that maximizes the uncertainty in location of the eruptive center. Any other form of a probability distribution requires more information than the range of possible locations (in this case, the end points of a dike or dike segment). The assumption is conservative because it maximizes the probability for the occurrence of multiple eruptive centers within the potential repository.

Confirmation Status: The assumption does not need to be confirmed because it does not impose any additional information beyond the length of the dike, which is obtained from the PVHA experts' interpretations.

Use in the Analysis: This assumption is used in Section 6.5.2.2 in the computation of the conditional distribution for number of eruptive centers within the potential repository.

5.4 POTENTIAL REPOSITORY DRIFT LOCATIONS FOR EDA II

Assumption: The potential repository drift locations obtained from CRWMS M&O (1999e) and listed in Attachment II of this AMR (Table II-1) are appropriate portrayals of the design repository drift locations in place at the time this AMR was finalized.

Basis: Wilkins and Heath (1999) directed the use of the Enhanced Design Alternative II (EDA II), which is defined in CRWMS M&O (1999e), in analyses for SR design. CRWMS M&O (1999e) was received from the design organization as the current design of the potential repository drift locations.

Confirmation Status: Subsequent use of the results of these analyses will require confirmation that CRWMS M&O (1999) accurately reflects the current potential repository design layout.

Use in this Analysis: The potential repository drift locations for EDA II are used in Attachment II to develop potential repository footprints for input to the calculations described in Section 6.5.

INTENTIONALLY LEFT BLANK

6. ANALYSIS/MODEL

6.1 INTRODUCTION

This analysis discusses Potentially Disruptive Processes and Events and, therefore, directly supports the post-closure safety case as discussed in AP-3.15Q, *Managing Technical Product Inputs*. Consequently, this AMR is deemed to be of Level 1 importance in addressing the factors associated with the post-closure safety case.

In this AMR, a conceptual framework for volcanism at Yucca Mountain consistent with output and results of the PVHA is described. This report describes how this framework and alternative conceptual frameworks influence the results of models of the probability of dike intersection and volcanic eruption at the potential geologic repository at Yucca Mountain.

This AMR summarizes and extends the findings of the PVHA (CRWMS M&O 1996). For the PVHA, an expert panel was convened in 1995 to review all pertinent data relating to volcanism at Yucca Mountain and, based on these data, to quantify both the annual probability and associated uncertainty of a volcanic event intersecting a potential repository sited at Yucca Mountain. The data the experts reviewed was comprehensive, consisting of two decades of data collected by volcanologists who conducted studies to quantify the probability that a future volcanic eruption would disrupt the potential repository (e.g., CRWMS M&O 1998c and references therein). This AMR also describes the relationship between volcanic source zones defined in the PVHA and the current understanding of structural controls on volcanism in the YMR.

The results of the PVHA are a set of alternative models for assessing the volcanic hazard at Yucca Mountain, probabilities that each model is the appropriate model, and probability distributions for the parameters of the models. As such, the PVHA defines the scientific uncertainty in applying models to assess the volcanic hazard. The PVHA experts documented the basis for their assessments of the validity of the alternative models in Appendix E of CRWMS M&O (1996). Therefore, the results of the PVHA are considered valid for assessing the uncertainty in the volcanic hazard at Yucca Mountain.

Based on the PVHA outputs and assumptions in Section 5 of this AMR, probability distributions are developed for the length and orientation of dikes within the potential repository footprint and for the number of eruptive centers located within the repository footprint (conditional on a dike intersecting the repository). Lastly, the probability of dike intersection is recalculated based on the current potential repository footprint, and the probability of an eruptive center(s) forming within the current potential repository footprint is calculated (the latter is a calculation that was not included in the PVHA).

6.2 VOLCANIC HISTORY OF THE YUCCA MOUNTAIN REGION

Because several Quaternary basaltic volcanoes exist within 20 kilometers of the potential Yucca Mountain repository (Figure 3), volcanism must be assessed as a possible future disruptive event

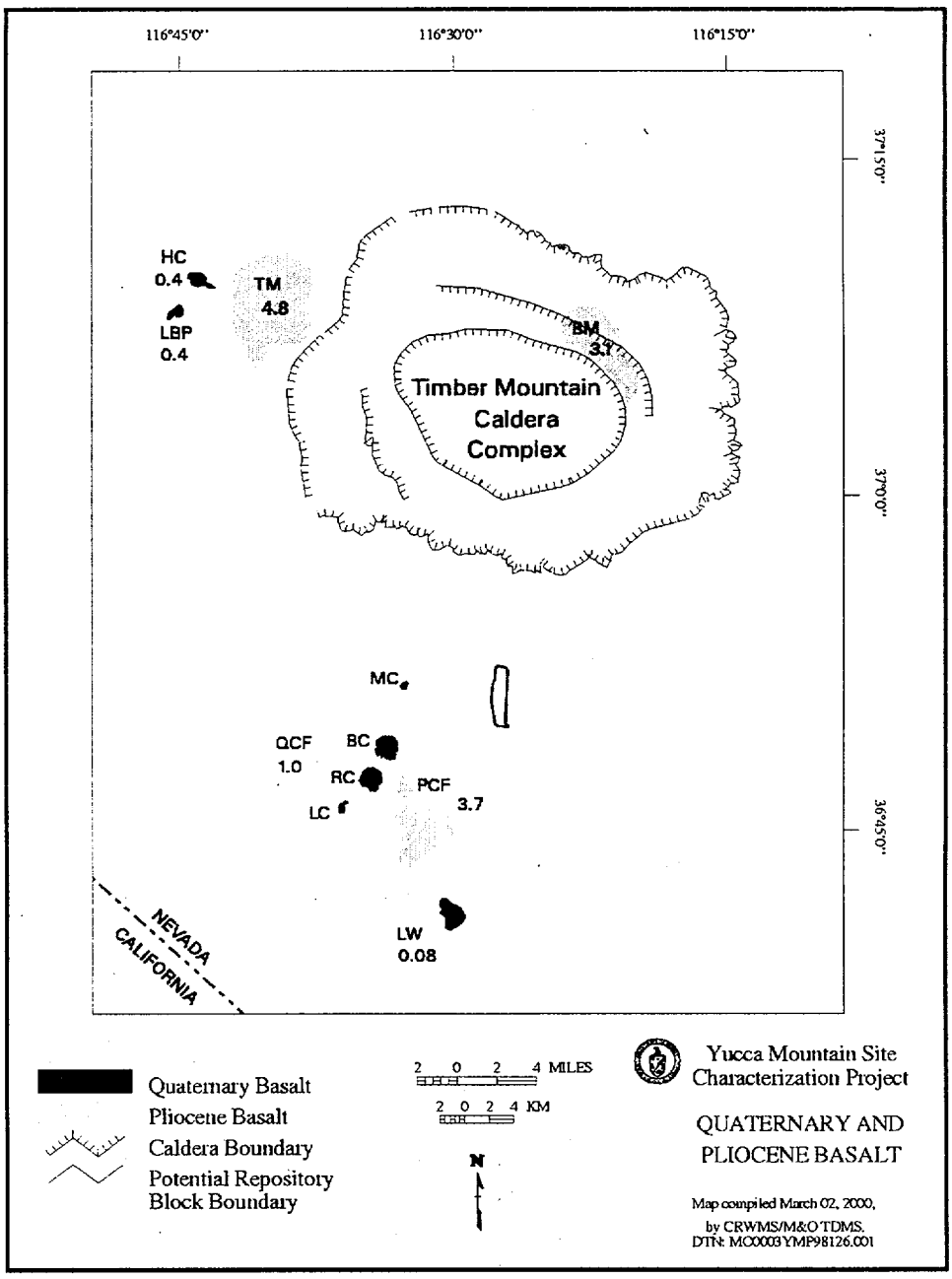

DTNs: LAFP831811AQ97.001; MO0003YMP98126.001 (both are used for reference only).

NOTES: Numbers by each volcano indicate approximate age in millions of years (CRWMS M&O 1998c, Chapter 2, Tables 2.B and 2.C, DTN: LAFP831811AQ97.001). TM: Thirsty Mesa, PCF: Pliocene Crater Flat, BM: Buckboard Mesa, QCF: Quaternary Crater Flat (MC: Makani Cone, BC: Black Cone, RC: Red Cone, LC: Little Cones), HC: Hidden Cone, LBP: Little Black Peak, LW: Lathrop Wells.

Figure 3. Location and Age of Post-Miocene (<5.3 m.y.) Volcanoes (or Clusters Where Multiple Volcanoes have Indistinguishable Ages) in the YMR

in TSPA. Two major types of volcanism have occurred in the YMR: an early phase of Miocene silicic volcanism, the recurrence of which is considered unlikely and not of regulatory concern, and a more recent phase of Miocene and post-Miocene basaltic volcanism that is of regulatory concern (Reamer 1999, p. 5).

The earliest volcanism in the YMR was dominated by a major episode of caldera-forming, silicic volcanism that occurred primarily between ~15 and 11 million years (m.y.), forming the southwestern Nevada volcanic field (Sawyer et al. 1994). Silicic volcanism was approximately coincident with a major period of extension, which occurred primarily between 13 and 9 m.y. (Sawyer et al. 1994, Figure 4). Yucca Mountain is an uplifted, erosional remnant of voluminous ash-flow tuff deposits formed during the early phase of silicic volcanism.

The commencement of basaltic volcanism occurred during the latter part of the caldera-forming phase, as extension rates waned, and small-volume basaltic volcanism has continued into the Quaternary. In terms of eruption volume, the 15-million-year history of volcanism in the YMR is viewed as a magmatic system that peaked between 13 and 11 m.y., with the eruption of over 5000 km^3 of ashflow tuffs, and has been in decline since, with relatively minor volumes of basalt erupted since 11 m.y. ago (CRWMS M&O 1998b, Figure 3.9-2). Approximately 99.9% of the volume of the southwestern Nevada volcanic field erupted by about 7.5 m.y. ago with the eruption of tuffs from the Stonewall Mountain volcanic center, which is the last active caldera system of the southwestern Nevada volcanic field. The last 0.1% of eruptive volume of the volcanic field consists entirely of basalt erupted since 7.5 m.y. ago (CRWMS M&O 1998b, Figure 3.9-5). Based on eruption volume, the southwestern Nevada volcanic field is considered to have virtually ceased eruptive activity since about 7.5 m.y. Considered in terms of total eruption volume, frequency of eruptions, and duration of volcanism, basaltic volcanic activity in the YMR defines one of the least active basaltic volcanic fields in the western United States (e.g., CRWMS M&O 1998c, Chapter 4, Figure 4-2, for post-Miocene basalts of Crater Flat).

Post-caldera basalts in the YMR can be divided into two episodes: Miocene (eruptions between ~9 and 7.3 m.y.) and post-Miocene (eruptions between ~4.8 and 0.08 m.y.). The time interval of about 2.5 m.y. between these episodes is the longest eruptive hiatus of basalt in the YMR during the last 9 million years (CRWMS M&O 1998c, Chapter 3, Table 3.1). This eruptive hiatus also marks a distinct shift in the locus of post-caldera basaltic volcanism in the YMR to the southwest (CRWMS M&O 1998b, Figure 3.9-6). The Miocene basalts and post-Miocene basalts are, thus, both temporally and spatially distinct. This observation emphasizes the importance of considering the age and location of the post-Miocene basalts (~ the past 5 million years of the volcanic history of the YMR) when calculating the volcanic hazard to the potential Yucca Mountain repository. The PVHA experts almost exclusively considered the time period of interest to be post-5 m.y. (with significant weight given to the post-1 m.y. period) as the time period of interest in assessing volcanic hazard at Yucca Mountain (CRWMS M&O 1996, Figure 3-62).

The post-Miocene basalts formed during at least six episodes of volcanism (based on age groupings) that occurred within 50 kilometers of the potential Yucca Mountain repository (Figure 3). These six episodes, in order of decreasing age, consist of the (1) basalt of Thirsty Mesa, (2) Pliocene Crater Flat and Amargosa Valley, (3) Buckboard Mesa, (4) Quaternary Crater

Flat, (5) Hidden Cone and Little Black Peak (the Sleeping Butte centers), and (6) Lathrop Wells. Three basalt episodes are in or near the Crater Flat topographic basin, within 20 kilometers of Yucca Mountain. Several aeromagnetic anomalies in the Amargosa Valley have characteristics that indicate buried basaltic volcanic centers (Langenheim et al 1993, p. 1840). One of these anomalies (anomaly B of Langenheim et al. 1993) was drilled and basalt cuttings dated at 3.85 m.y. using the $^{40}Ar/^{39}Ar$ method (CRWMS M&O 1998c, Chapter 2, Table 2.B). Because of the similarity in age to the 3.75 m.y. Pliocene Crater Flat episode, the buried basalts of Amargosa Valley are considered here as part of the same episode.

The total eruption volume of the post-Miocene basalts is about 6 km^3. The volume of individual episodes has decreased progressively through time, with the three Pliocene episodes having volumes of approximately 1 to 3 km^3 each and the three Quaternary episodes having a total volume of only ~0.5 km^3 (CRWMS M&O 1998b, Figure 3.9-2; Table 3). All of the Quaternary volcanoes are similar in that they are of small volume (~0.1 km^3 or less, Table 4) and typically consist of a single main scoria cone surrounded by a small field of *aa* basalt flows, which commonly extend ~ 1 kilometer from the scoria cone.

The seven or eight (if Little Cones is counted as two volcanoes) Quaternary volcanoes in the YMR occur to the south, west, and northwest of Yucca Mountain in a roughly linear zone defined as the Crater Flat Volcanic Zone (Crowe and Perry 1990, p. 328). Five of seven Quaternary volcanoes are in or near Crater Flat and lie within 20 kilometers of the Yucca Mountain Site (Figure 3). Models that attempt to relate volcanism and structural features in the YMR have emphasized the Crater Flat basin because of the frequency of volcanic activity associated with Crater Flat and its proximity to the potential Yucca Mountain repository (e.g., Smith et al. 1990, p. 84; Connor and Hill 1995, p. 10122).

Table 4. Estimated Volume and $^{40}Ar/^{39}Ar$ Age[a] of Quaternary Volcanoes in the YMR

Volcano	Volume (km^3)[b]	Volume (km^3)[c]	Age (m.y.)[e]
Makani Cone	0.006		1.16-1.17
Black Cone	0.105	0.07	0.94-1.10
Red Cone	0.105		0.92-1.08
Little Cones	0.002	>0.01[d]	0.77-1.02
Hidden Cone	0.03		0.32-0.56
Little Black Peak	0.03		0.36-0.39
Lathrop Wells Cone	0.14		0.074-0.084

DTNs: LA0004FP831811.002; LAFP831811AQ97.001 (both are used for reference only)

NOTES:
[a] $^{40}Ar/^{39}Ar$ dates provide the most complete and self-consistent chronology data set for Quaternary volcanoes of the YMR. A full discussion of other chronology methods used to date basaltic rocks in the YMR can be found in CRWMS M&O (1998c, Chapter 2). Other chronology methods may not provide consistent or accurate estimates of the time of eruption.
[b] CRWMS M&O (1998c, Chapter 3, Table 3.1), (DTN: LA0004FP831811.002)
[c] Stamatakos et al. (1997) p. 327
[d] Accounts for volume of buried flows detected by ground magnetic surveys
[e] Range of ages from CRWMS M&O (1998c, Chapter 2, Table 2.B). Lathrop Wells ages (Heizler et al. 1999, Table 3) represent the range of plateau ages measured, except for sample LW157, a statistical outlier (DTN: LAFP831811AQ97.001).

6.3 THE PROBABILISTIC VOLCANIC HAZARD ANALYSIS (PVHA)

In 1995-96, the DOE sponsored the PVHA project to assess the probability of a future volcanic event intersecting the potential repository at Yucca Mountain. To ensure that a wide range of approaches was considered for the PVHA, the DOE identified 10 experts in the field to participate in the project and evaluate the data. Their evaluations (elicitations) were then combined to produce an integrated assessment of the volcanic hazard that reflects a range of alternative scientific interpretations. This assessment, which focused on the volcanic hazard at the site expressed as the probability of intersection of the potential repository by a basaltic dike, provided input to an assessment of volcanic risk, which expresses the probability of radionuclide release due to volcanic eruption.

6.3.1 The PVHA Process

The major procedural steps in the PVHA were selecting the expert panel members, identifying the technical issues, eliciting the experts' judgments, applying temporal and spatial aspects of probability models, and compiling and presenting the results.

6.3.1.1 Selecting the Expert Panel Members

From more than 70 nominees, 10 individuals were selected to participate in the PVHA project. Efforts were made to balance the panel with respect to technical expertise (geology, geochemistry, and geophysics) and institutional/organizational affiliation. The 10 experts and their affiliations are listed in Table 5 (CRWMS M&O 1996, Table 1-2).

Table 5. PVHA Panel Members

Expert	Abbreviation	Affiliation
Dr. Richard W. Carlson	RC	Carnegie Institute of Washington
Dr. Bruce M. Crowe	BC	Los Alamos National Laboratory
Dr. Wendell A. Duffield	WD	United States Geological Survey, Flagstaff
Dr. Richard V. Fisher	RF	University of California, Santa Barbara (Emeritus)
Dr. William R. Hackett	WH	WRH Associates, Salt Lake City
Dr. Mel A. Kuntz	MK	United States Geological Survey, Denver
Dr. Alexander R. McBirney	AM	University of Oregon (Emeritus)
Dr. Michael F. Sheridan	MS	State University of New York, Buffalo
Dr. George A. Thompson	GT	Stanford University
Dr. George P. L. Walker	GW	University of Hawaii, Honolulu

DTN: MO0002PVHA0082.000.

6.3.1.2 Identifying Technical Issues

The PVHA panel of experts convened between February and December 1995. A technical facilitator/integrator led carefully structured, intensive interactions among the panel members.

The experts participated in workshops, field trips, and other interactions, which were used to identify sources of agreement and disagreement among them. Each expert played the role of an informed technical evaluator of data, rather than a proponent of a particular interpretation. On occasion, however, some experts were asked to present particular interpretations to facilitate discussion and consideration of alternative interpretations. In all of the interactions, it was made clear that the purpose of the PVHA was to identify and understand uncertainty, not to eliminate it. It was also emphasized that the purpose was not necessarily to achieve consensus. Instead, disagreement was expected and accepted.

At the core of the PVHA project were four workshops. The primary objective of the workshops was to ensure the experts' understanding of the issues, alternative volcanic hazard models, and the data available on which they would base their technical assessments. The first three workshops focused on the data, volcanic hazard models, and interpretations relevant to the PVHA. The workshops included presentations of data and interpretations by technical specialists from Los Alamos National Laboratory (LANL), the United States Geological Survey (USGS), the University of Nevada, Las Vegas, the Center for Nuclear Waste Regulatory Analysis, as well as from some PVHA experts. During the fourth workshop, the experts reviewed the preliminary assessments developed by the panel members, after which the individual elicitations were revised, based on feedback received. Two field trips held during the course of the PVHA provided the opportunity for the panel members to observe geologic relationships pertaining to eruptive style, the definition of volcanic events, and the distribution and timing of volcanic activity in the YMR.

6.3.1.3 Temporal and Spatial Aspects of Probability Models

Before the third PVHA workshop, an interactive meeting was held for the benefit of the expert panel, in order to focus on the methods available to calculate volcanic hazard. The methods were used to calculate the two main aspects of volcanic hazard probability models: the temporal and spatial aspects.

Temporal models describe the frequency of occurrence of volcanic activity and include homogeneous and nonhomogeneous models. Many of the experts used homogeneous Poisson models to define the temporal occurrence of volcanic events, which assumes a uniform rate of volcanism based on the number of volcanic events that occurred during various periods in the past. Nonhomogeneous models were used by some experts to consider the possibility that volcanic events are clustered in time or to describe the possible waning or waxing of volcanic activity in the region during the period of time the experts believed was relevant to hazard analysis.

Spatial models describe the spatial distribution (location) of future volcanic activity. The most common PVHA models considered the future occurrence of volcanoes to be homogeneous within particular defined regions or "source zones" (CRWMS M&O 1996, Figure 3-62). Source zones were defined based on several criteria: the spatial distribution of observed basaltic volcanoes (especially post-5 m.y. volcanoes), structurally-controlled regions, regions defined based on geochemical affinities, tectonic provinces, and other criteria. Nonhomogeneous parametric spatial distributions of future volcano occurrences were also modeled, for example, that the location of future volcanoes will follow a bivariate Gaussian distribution based on the

location of volcanoes in Crater Flat. Finally, nonhomogeneous, nonparametric spatial density models were used by some experts to assess the spatial distribution of future volcanoes. These models make use of a kernel density function and smoothing parameter based on locations of existing centers to obtain the spatial distribution for location of future volcanoes.

6.3.1.4 Eliciting the Experts' Judgments

Formal elicitation followed the third workshop. The process consisted of a two-day individual interview with each expert. To provide consistency, the same interview team was used for all elicitations. Following the elicitation interview, each expert was provided with a written summary of his elicitation, which was prepared by the interview team. The expert reviewed and clarified the summary and had the opportunity to revise any assessments. To promote a full understanding of each individual's judgment, the preliminary assessments made by each member of the expert panel were presented and discussed at the fourth workshop. Following this workshop, each expert had a final opportunity to revise his assessments before the results of the PVHA were finalized (CRWMS M&O 1996, Appendix E). A summary of input parameters for the PVHA probability models is found in CRWMS M&O (1998a, Table 10-5).

6.3.1.5 PVHA Results

The product of the PVHA was a quantitative assessment of the probability of a volcanic event intersecting the potential repository and the uncertainty associated with the assessment (CRWMS M&O 1996, Figure 4-32). Specifically, a probability distribution of the annual frequency of intersection of a basaltic dike with the potential repository footprint was defined.

Each of the 10 experts independently arrived at a probability distribution for the annual frequency of intersection of the potential repository footprint by a dike that typically spanned ~2 orders of magnitude (CRWMS M&O 1996, Figure 4-31). From these individual probability distributions, an aggregate probability distribution for the annual frequency of intersection of the potential repository footprint by a dike was computed that reflected the uncertainty across the entire expert panel (CRWMS M&O 1996, Figure 4-32). The individual expert's distributions were combined using equal weights to obtain the aggregate probability distribution. The mean value of the aggregate probability distribution was $1.5 \cdot 10^{-8}$ dike intersections per year, with a 90% confidence interval of $5.4 \cdot 10^{-10}$ to $4.9 \cdot 10^{-8}$ (CRWMS M&O 1996, p. 4-10). (Note that these values are updated in this AMR for the EDA II potential repository footprint in Section 6.5.3.) The composite distribution spanned about three orders of magnitude for intersection frequency. The range in the mean frequencies of intersection for the individual experts' interpretations spanned about one order of magnitude (CRWMS M&O 1996, Figure 4-32). The variance for frequency of intersection defined by the composite distribution was disaggregated to identify the contributions from each of the sources of uncertainty, including variability between the experts' interpretations (CRWMS M&O 1996, Figure 4-33). Most of the uncertainty in characterizing the hazard arose from uncertainty in an individual expert's interpretations of the hazard rather than differences in scientific interpretation between the experts (CRWMS M&O 1996, p. 4-10, Figure 4-33). The probability distribution arrived at by the PVHA accounted for undetected events (buried volcanic events, or intrusive events that never reached the surface). The

undetected event frequency ranged from 1 to 5 times that of observed events, with most estimates in the range of 1.1 to 1.5 (CRWMS M&O 1996, Figure 3-62).

The PVHA results indicated that the statistical uncertainty in estimating the event rate was the largest component of intra-expert uncertainty (CRWMS M&O 1996, Figure 4-33). The next largest uncertainty was uncertainty in the appropriate spatial model. Other important spatial uncertainties included the spatial smoothing distance, Gaussian field parameters, zonation models, and event lengths. The temporal issues of importance included the time period of interest, event counts at a particular center, and the frequency of hidden events (CRWMS M&O 1996, Figure 4-33).

6.3.1.6 Significance of Buried Volcanic Centers on PVHA Results

The uncertainty in the event rate accounted for about 40% of the total intra-expert uncertainty (CRWMS M&O 1996, Figure 4-33). The event rate depends on the number of events estimated for a particular time period and for a particular source zone, and can be expressed as events/year/square kilometer (CRWMS M&O 1996, p. 3-2; Figure 17a of this report). A key parameter for estimating event rates is, therefore, an estimate of the number of volcanic events that have occurred in the YMR, particularly since the Miocene. Since all post-Miocene volcanic centers observable at the surface in the YMR have been identified (Figure 3), the only factor that could significantly change PVHA estimates of event counts and the event rate would be evidence not considered by the PVHA of a significant number of previously unidentified buried volcanic centers or intrusions.

Langenheim et al. (1993) presented data for aeromagnetic anomalies in Amargosa Valley, and interpreted them as shallowly buried basaltic volcanic centers. These data were available to the PVHA experts (CRWMS M&O 1996, p. B-4) and data and interpretations concerning the Amargosa Valley anomalies were also presented by Langenheim during Workshop 1 of the PVHA project (CRWMS M&O 1996, p. C-3). In the PVHA, 9 of 10 experts included volcanic events of the Amargosa Valley in their YMR event counts (CRWMS M&O 1996, Appendix E, pp. RC-8, BC-17, WD-5, WH-7, MK-10, AM-8, MS-8, GT-6, GW-6). The only expert who did not include events of the Amargosa Valley in their YMR event counts considered only the past 2 million years to be the relevant time period (CRWMS M&O 1996, Appendix E, RF-6), thus excluding the period of time during which the anomalies were probably formed. The most common expert assessment of the number of volcanic events represented by the aeromagnetic anomalies in Amargosa Valley was 5, with slightly less weight assigned to 3, 4, and 6 events (CRWMS M&O 1996, Figure 3-63). In addition, the PVHA experts assessed a hidden event factor, allowing for additional undetected events not counted in the total YMR event counts that already included the Amargosa Valley event counts (CRWMS M&O 1996, Figure 3-62, 3-63). These factors typically resulted in an increase of 10 to 50 percent in the rate of volcanic events over that computed from the observed volcanic events.

New data that could potentially change the assessment of the number of volcanic events by the PHVA experts include an analysis of existing aeromagnetic data for the YMR (Earthfield Technology 1995) and new ground magnetic surveys of aeromagnetic anomalies (Connor et al. 1997; Magsino et al. 1998). A map presented by Earthfield Technology (1995, Appendix II) indicates the presence of as many as 40-60 aeromagnetic anomalies within ~35-40 kilometers of

Yucca Mountain that are interpreted as intrusive bodies; six of these lie within ~5 kilometers of the potential repository site. The Earthfield Technology (1995) results were based on the merging of three aeromagnetic data sets, the Timber Mountain, Lathrop Wells, and Yucca Mountain surveys. Subsequent to release of the Earthfield Technology (1995) report, it was discovered that the report "was flawed by an incomplete and mislocated Timber Mt. Survey" (Feighner and Majer 1996, p. 1). Inspection of the flight survey map in Earthfield Technology (1995, Figure 2) and a corresponding map enclosed in Appendix I of Feighner and Majer (1996) indicates that the Timber Mountain Survey, which encompasses about 50% of the coverage area and the majority of the aeromagnetic anomalies, was mislocated approximately 20 km to the south-southwest of its correct location. For this reason, further analysis of the anomalies as presented by Earthfield Technology (1995, Appendix II), and that lie within the Timber Mountain survey, is not warranted. The six anomalies located within 5 kilometers of the potential repository site (the Yucca Mountain survey) are associated with mapped faults and are probably due to faulting of magnetic Topopah Springs Tuff, due to the variation of magnetic properties within juxtaposed rock masses (Feighner and Majer 1996, p. 2; Reamer 1999, p. 32).

The most reliable and detailed data available for magnetic anomalies in the YMR is presented in Connor et al. (1997) and Magsino et al. (1998). These data were obtained using ground magnetic surveys of 14 selected aeromagnetic anomalies located to the north, east, west, and south of the potential repository site (Magsino et al. 1998, Figure 1-1). Collectively, these surveys represent a comprehensive assessment of aeromagnetic anomalies nearest the proposed repository site and provide confidence that the geologic record of basaltic volcanism near Yucca Mountain is adequately understood. Of the 14 surveys, 7 provide no evidence of buried basalt and 3 were conducted over areas with known surface exposures of basalt, partly to enhance understanding of the relationship between volcanism and geologic structure (Magsino et al. 1998, Section 4). Four of the 14 surveys provide evidence of buried volcanic centers. Two of these (Anomalies A and F/G of the PVHA) were known to the PVHA experts as possible buried basaltic volcanic centers (from the data of Langenheim et al. 1993; Crowe et al. 1995, Figure 2.5), but the data presented in Connor et al. (1997) and Magsino et al. (1998) provide increased detail and confidence of their volcanic origin. Of the two remaining surveys, anomalies in the Steve's Pass area on the southwest margin of Crater Flat are interpreted as buried basalt. Interpretation of a buried, reversely magnetized body of rock southwest of Northern (or Makani) Cone is less certain, and may be either a basalt body or Miocene tuff (Magsino et al. 1998, Sections 4.4 and 4.11). Each of the four anomalies representing probable buried volcanic centers occur within volcanic source zones previously specified by the PVHA experts (CRWMS M&O 1996, Appendix E), except for the anomalies in the Steve's Pass area, which lie slightly to the southwest of most experts' volcanic source zones, in a direction away from Yucca Mountain.

On the basis of evidence for buried volcanic centers presented in Connor et al. (1997), Brocoum (1997) conducted sensitivity analyses to assess the potential impact on the PVHA results of increased event counts in Amargosa Valley and Crater Flat. Considering the experts' method for assessment of event counts, particularly for northeast alignments of vents (as in the case of Amargosa anomaly F/G), the mean value for the number of buried volcanic centers was increased from the original PVHA value of 4.7 events to 6.1 events (Brocoum 1997, Enclosure 1, p. 5). The mean annual frequency of intersection of a dike with the potential repository footprint was recalculated using the revised event count distributions, resulting in an increase in the mean

annual frequency of intersection of 4% (Brocoum 1997, Enclosure 1, p. 5). Given the uncertainty factored into the PVHA by assessment of alternative event counts and hidden event factors, small changes in the PVHA event counts have an insignificant impact on the annual frequency of intersection distribution derived from the PVHA. A later sensitivity analysis presented by CRWMS M&O (1998c, Chapter 6, pp. 6-83 and 6-84) conservatively assumed that all known aeromagnetic anomalies in Crater Flat and Amargosa Valley were Quaternary age, instead of Pliocene. Using this assumption, the most likely number of Quaternary volcanic events near Yucca Mountain based on PVHA event counts was increased from 3.8 to 8 events. This increase in the Quaternary event count resulted in a disruption probability of $\sim 2.5 \cdot 10^{-8}$ per year (CRWMS M&O 1998c, Chapter 6, p. 6-84), a result not significantly different from the mean PVHA result of $1.5 \cdot 10^{-8}$ per year (CRWMS M&O 1996, pp. 4-10, 4-14).

In summary, the data presented by Connor et al. (1997) and Magsino et al. (1998) provide stronger evidence that Anomalies A and F/G (as defined in the PHVA) represent buried volcanic centers, and that at least one anomaly not considered by the PVHA experts represents a probable buried volcanic center. Sensitivity studies (Brocoum 1997; CRWMS M&O 1998c, Chapter 6) show that the addition of several volcanic events located within already defined volcanic source zones does not significantly impact the results of the PVHA. Significantly, the four anomalies east of Yucca Mountain (Magsino et al. 1998, Figure 1-1) show no evidence of buried volcanic centers and provide confirmatory evidence that the volcanic source zones specified by the experts to the south and west of Yucca Mountain are a valid representation of the spatial distribution of post-Miocene volcanism in the YMR.

6.3.1.7 Alternative Estimates of the Intersection Probability

Several alternative estimates of the intersection probability (the annual probability of a volcanic event intersecting of the potential repository footprint) were presented between 1982 and 1998 (Table 6). As discussed in the following section (6.3.2), volcanic events in hazard calculations have been represented as both points and lines (Table 6). For point events, volcanic source zone areas or the potential repository area have generally been increased to account for the fact that volcanic events have dimension due to the length of associated dikes. The shorter the event length, the more comparable intersection probability results are for calculations representing volcanic events as either points or lines. Intersections probabilities near 10^{-7} intersections/year (Ho and Smith 1998, pp. 507-508; Reamer 1999, p. 61) reflect unusually small volcanic source zone areas or unusually long event lengths (Table 6).

Most of the published intersection probabilities, including the mean intersection probability estimated in the PVHA, cluster at values slightly greater than 10^{-8} per year (Table 6), indicating that this probability estimate is fairly robust given the range of alternative temporal and spatial models, and event geometries considered in probability calculations.

Table 6. Published Estimates of the Probability of Intersection of the Potential Repository at Yucca Mountain by a Volcanic Event

Reference	Intersection Probability (per year)	Comment	Event Representation
Crowe et al. (1982), pp. 184-185	$3.3 \cdot 10^{-10} - 4.7 \cdot 10^{-8}$	Range of alternative probability calculations	point
Crowe et al. (1993), p. 188	$2.6 \cdot 10^{-8}$	Median value of probability distribution	point
Connor and Hill (1995), pp. 10,121	$1–5 \cdot 10^{-8}$	Range of 3 alternative models	point
Crowe et al. (1995), Table 7.22	$1.8 \cdot 10^{-8}$	Median value of 22 alternative probability models	point
Ho and Smith (1998), pp. 507-508	(1) $1.5 \cdot 10^{-8}$, (2) $1.09 \cdot 10^{-8}$, $2.83 \cdot 10^{-8}$, (3) $3.14 \cdot 10^{-7}$	3 alternative models; 3rd model assumes a spatial intersection ratio (using a Bayesian prior) of 8/75 or 0.11, approximately one order of magnitude higher than other published estimates, because volcanic events are forced to occur within a small zone enclosing Yucca Mountain	point
CRWMS M&O (1998c), Chapter 6, p. 6-84	$2.5 \cdot 10^{-8}$	Sensitivity analysis that conservatively assumes all aeromagnetic anomalies in Amargosa Valley are Quaternary age	point
Reamer (1999) pp. 61, 131, Figs. 29, 30	$10^{-8}–10^{-7}$	Value of 10^{-7} assumes maximum event length of 20 km and that crustal density variations contribute to event location.	line

N/A - Reference only

6.3.2 Definitions and Parameters of a Volcanic Event and Implications for Alternative Probability Calculations

An important issue in the PVHA and in alternative volcanic hazard assessments of the potential Yucca Mountain repository is the definition of a "volcanic event." The definition of a volcanic event can affect the outcome of probability calculations and must be clearly understood to meaningfully compare the results of alternative probability calculations. A volcanic event was defined slightly differently by each PVHA expert, but the experts generally agreed that a volcanic event is the formation of a volcano (with one or more vents) resulting from the ascent of basaltic magma through the crust as a dike or system of dikes (CRWMS M&O 1996, Appendix E). For the purposes of probability models discussed in this report (Section 6.5), a volcanic event is defined as a point (x,y) in space representing a volcano, and an associated dike having length, azimuth and location relative to the point event (Figure 10 and 12, this AMR). The possibility that a dike system (e.g., multiple dikes) has width is not part of the calculations in this AMR but is included in the "Number of Waste Packages Hit" calculation (CRWMS M&O 2000c). The duration of a volcanic event was generally estimated by each PVHA expert to be no more than a few years or tens of years (CRWMS M&O 1996, Appendix E, e.g., pp. BC-4, WD-2, RF-2, MK-4, AM-2, GW-2). Although the PVHA assumed volcanic events to have both an extrusive and intrusive component (volcano and dike), the output of the PVHA was the annual frequency of intersection of the potential repository footprint by an intrusive basaltic dike

(CRWMS M&O 1996, Section 3.1.6, Figure 4-32). The PVHA did not calculate the conditional probability that a dike intersecting the potential repository footprint would result in an extrusive volcanic eruption through the repository.

Typical dike dimensions assigned by the experts were a dike width of one meter and a dike length of 1 to 5 kilometers (CRWMS M&O 1996, Appendix E; Figure 4). The most likely values for maximum dike lengths were estimated at 17 to 22 kilometers (CRWMS M&O 1996, Figure 3-62). The values of maximum dike length represent tails of distributions that have a small impact on the probability of dike intersection. The individual PVHA expert dike length distributions can be aggregated to derive a PHVA aggregate dike length distribution. The aggregate dike-length distribution derived from the PVHA has 5th-percentile, mean, and 95th-percentile values of 0.6, 4.0, and 10.1 kilometers, respectively (Figure 4). The most commonly assigned dike orientation centers around N30°E (CRWMS M&O 1996, Figure 3-62).

Prior to the PVHA, most assessments of volcanic hazard to the potential repository represented volcanic events as points having no physical dimension (CRWMS M&O 1996, p. 3-16). The physical dimension of events was generally taken into account by appropriately expanding the area of the potential repository or of volcanic source zones (e.g., Crowe et al. 1995, p. 7-64). The PVHA and probability calculations presented by the Nuclear Regulatory Commission (NRC) since the PVHA have represented volcanic events as having both length and orientation (Reamer 1999). It is important to compare the different representations of volcanic events in order to compare probability results meaningfully. The Reamer (1999, Sections 4.1.6.3.2 and 4.1.6.3.3, Figures 29 and 30) calculated disruption probabilities using vent and vent alignment (e.g., the alignment of Quaternary vents from Makani Cone to Little Cones [Figure 3]) as the volcanic event. Conceptually, use of either the PVHA or NRC volcanic event should result in the same intersection probability, if the same temporal/spatial models and assumptions are used, as well as the same probability distributions for event length and orientation (Figure 5). However, these probabilities represent different physical occurrences, and PVHA and NRC model parameters are not equivalent. The PVHA intersection probability represents the probability of a dike intersection. Thus, the probability of an eruption (conditional on dike intersection) through the potential repository must be lower. The NRC intersection probability values are based on the interpretation that every intersection of a vent alignment with the potential repository footprint results in an eruption through the potential repository (Reamer 1999, p. 57), and that the probability of intersection by shallow intrusive events that do not erupt is necessarily higher, possibly by a factor of 2-5 (Reamer 1999, p. 60, Figure 5).

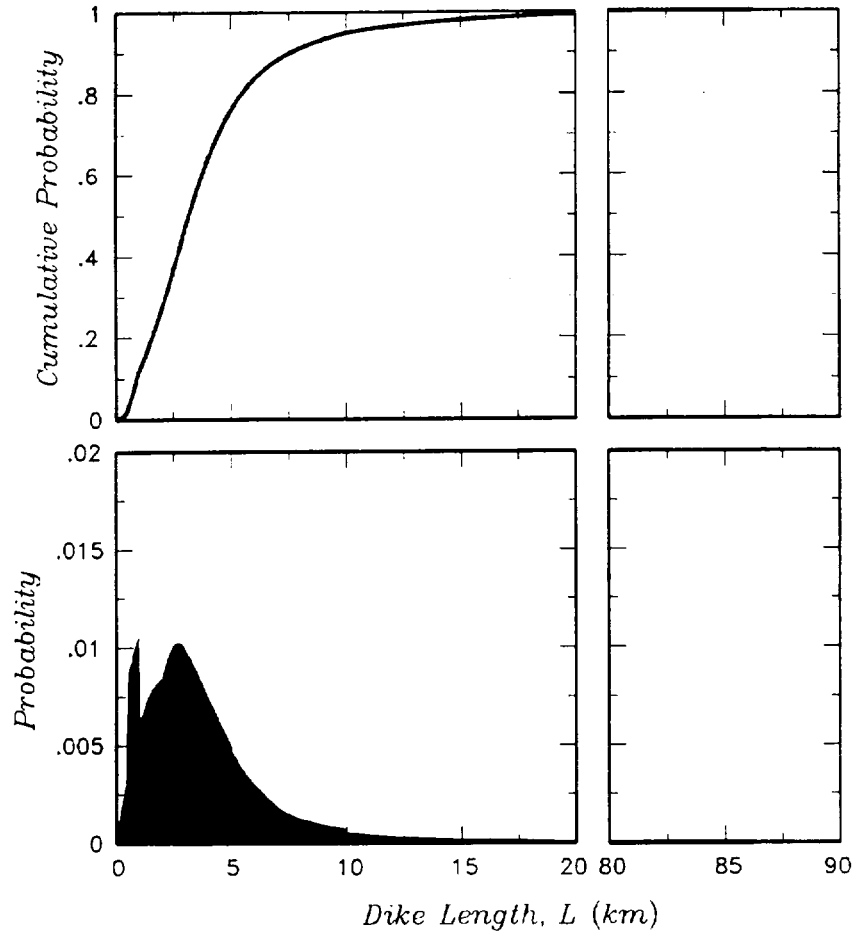

Output data. DTN: LA0005FP831811.001

NOTES: The 5th-percentile, mean, and 95th-percentile values are 0.6, 4.0, and 10.1, km, respectively. The distribution contains a very long upper tail extending to 86 km. The irregular shape of the probability mass function in the lower plot reflects the variation in the distributions defined by the individual experts.

Figure 4. Composite Distribution for Dike Length Averaged Across All 10 PVHA Experts

The NRC assumes that every vent alignment intersection will result in an eruption through the potential repository because they conclude that vent spacings along alignments are small compared to the potential repository footprint (Reamer 1999, Sections 4.1.4.3.3 and 4.1.6.3.2). The technical basis for this conclusion is unclear. In Section 6.5.1.3, five alternative approaches for the number and spatial distribution of vents along the dike associated with a volcanic event are formulated, based on PVHA expert output and observed vent spacing in the YMR, to test for sensitivity of model choice. According to these approaches, the eruption probability is always less than the dike intersection probability, by a factor of ~2 (Figure 5, Table 13).

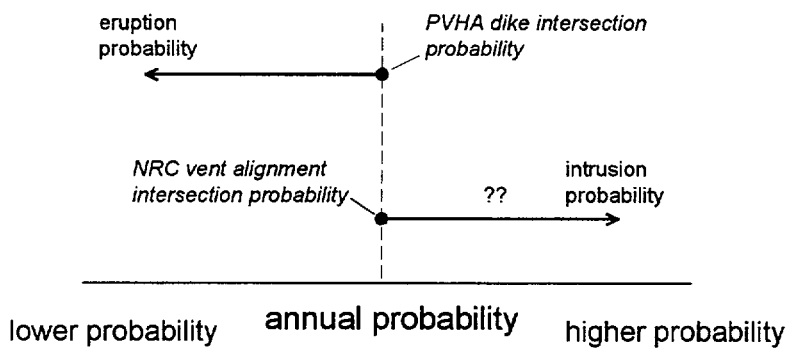

N/A - For illustration purposes only

Figure 5. Conceptual Diagram Comparing Event Definitions from the PVHA and Reamer (1999): Implications for Eruption and Intrusion Probabilities Based on Different Event Definitions

6.3.2.1 Intrusive Versus Extrusive Events: Evidence from Analog Sites

Another issue requiring discussion is whether dikes or dike systems can reach the near surface without any portion of the system erupting. The NRC (Reamer 1999) assumption that all vent alignment intersections result in eruption through the potential repository implies that intrusive events that intersect the potential repository and do not erupt represent entirely separate temporal events. Using the San Rafael volcanic field as an analog, the NRC assumes for PA purposes that the probability of separate intrusive events that do not erupt is 2 to 5 times higher than the probability of eruptive events (Reamer 1999, Section 4.1.6.4). Thus, for example, if 5 volcanic events resulting in volcanic eruptions have occurred in the YMR in the past 1 million years, the NRC's assumption requires that 10 to 25 additional intrusive events have also occurred, independent in time and location from the events that produced the volcanic eruptions. In the PVHA definition of a volcanic event, intrusive and extrusive events in the YMR are generally considered to be linked on a one-to-one basis–a volcanic event is defined as an extrusive volcano and its associated intrusive dike or dike system. Dikes that reach depths of < 0.5 to 1 kilometers are thought to erupt at some point along the length of the dike, mainly because of volatile exsolution (CRWMS M&O 1996, Appendix E, pp. RC-10, BC-6, WH-6, MK-12). The most common multiplier assigned for undetected intrusive events was 1.1 to 1.2 times that of known volcanic events (CRWMS M&O 1996, Figure 3.62), a number lower than the NRC multiplier of 2 to 5.

An appropriate analog in the YMR for understanding the relationship between intrusive and extrusive components of a volcanic event is the Paiute Ridge intrusive/extrusive center (Byers and Barnes 1967) on the northeastern margin of the Nevada Test Site. Paiute Ridge is a small-volume Miocene volcanic center comparable in volume and composition to Quaternary volcanoes near Yucca Mountain (CRWMS M&O 1998c, Chapter 5, p. 5-29). Paleomagnetic, geochronologic, and geochemical data indicate that the entire intrusive/extrusive complex formed during a brief magmatic pulse and, thus, represents a single volcanic event (Ratcliff et al. 1994; CRWMS M&O 1998c, Chapter 5, p. 5-29). The vents and associated dike system formed within an NNW-trending extensional graben and provide excellent exposures of a variety of depths of the system including remnants of surface lava flows, volcanic conduits, and dikes and sills intruded into tuff country rock at depths of up to 300 meters (CRWMS M&O 1998c, Chapter 5, pp. 5-27 through 5-41). There is evidence of shallow structural control of dike emplacement at Paiute Ridge, including dike emplacement along fault planes (Byers and Barnes 1967; CRWMS M&O 1998c, Chapter 5, pp.5-27 through 5-28). Dike lengths at Paiute Ridge range from < 1 to 5 kilometers (CRWMS M&O 1998c, Chapter 5, p. 5-31), comparable to the range estimated for post-Miocene volcanism near Yucca Mountain (Figure 4).

Field observations at Paiute Ridge clearly show that, while some portions of individual dikes stagnated within about 100 meters of the surface without erupting, other portions of the same volcanic event did erupt, as evidenced by associated lava flows and volcanic conduits (Byers and Barnes 1967; CRWMS M&O 1998c, Chapter 5, pp. 5-29 to 5-33). During the time period considered most significant by the PVHA experts for evaluating volcanic hazard (the past 5 m.y., CRWMS M&O 1996, Figure 3-62), there is no known episode of dike intrusion to within a few hundreds meters of the surface in the YMR that has not been accompanied by an extrusive component. Thus, there is no evidence in the YMR geologic record to suggest that dike intrusions without accompanying eruptions occur 2 to 5 times more frequently than eruptions. (Reamer 1999, Figure 5, Sections 4.1.6.3.4 and 4.1.6.4).

The NRC assumption of higher intrusion probabilities in the YMR is based on analogy to the San Rafael volcanic field on the western Colorado Plateau, where an extensive system of shallowly intruded dikes is well exposed (Delaney and Gartner 1997). Delaney and Gartner (1997, p. 1180) estimate that 174 dikes are represented in the San Rafael dike swarm. Breccias are present along portions of 45 of these dikes, which are interpreted to represent the subsurface beneath eruptive centers (Delaney and Gartner 1997, pp. 1178, 1191). No attempt is made in Delaney and Gartner (1997) to estimate the frequency of temporally discrete intrusive versus eruptive events. They suggest only that at least 45 dikes show evidence of eruption along some segment of a dike; other parts of the same dike, or other parts of the same dike system, may have erupted, as is observed at Paiute Ridge. Given the Paiute Ridge analogy and the Delaney and Gartner (1997) interpretation that the San Rafael swarm likely represents the subsurface beneath a large volcanic field active for about a million years (Delaney and Gartner 1997, pp. 1177, 1178-1179), it is likely that many individual intrusive/extrusive events are represented at San Rafael, with some portion of a dike system erupting during each event, and other portions of the same dike system not erupting. Thus, while the data and discussion presented in Delaney and Gartner (1997), have been used to argue that intrusive events without an eruptive component occur 2 to 5 times more frequently than intrusive events with an eruptive component, an alternative interpretation is that the intrusion/extrusion ratio is closer to 1. This alternative interpretation is

more consistent with the geologic record of the YMR, as demonstrated at the Paiute Ridge analog site.

6.3.2.2 Alternative Event Lengths

The length of dikes or vent alignments (Reamer 1999, Figure 30) can significantly affect intersection probabilities, depending partly on how far areas of high-event frequency are from the potential repository. When volcanic events primarily occur far from the potential repository, they must have sufficient length to intersect the repository, and longer event lengths will result in higher intersection probabilities. When volcanic events occur more frequently nearer the potential repository, volcanic events with shorter lengths are able to intersect the repository with higher frequency.

As evaluated by experts in the PVHA, the mean dike length associated with a volcanic event in the YMR is 4 kilometers and 95% of dikes are shorter than 10.1 kilometers (Figure 4). These values are consistent with observed volcanic features in the YMR. For instance, the maximum vent spacing in the YMR is 5.4 kilometers between Black and Makani Cones, and volcanic vent alignments lengths are typically in the range of 2 to 5 kilometers (e.g., Hidden Cone-Little Black Peak, Amargosa Aeromagnetic Anomaly A, Red Cone-Black Cone). The longest proposed vent alignment in the YMR, assuming it represents one volcanic event, is the Quaternary Crater Flat alignment with a length of about 11 kilometers (Figure 3). Observed dikes, such as at Paiute Ridge, range in length from < 1 to 5 kilometers. Dike and vent alignments of the 3.7 m.y. basalts in southeast Crater Flat (Figure 3) are no more than 4 kilometers in length.

Event lengths used in probability models by researchers from the University of Nevada, Las Vegas (e.g., Smith et al. 1990) and the NRC (Reamer 1999, Figures 29 and 30) are significantly longer than those assessed by the experts in the PVHA. For example, Smith et al. (1990, p. 81) based the dimensions of "high-risk" volcanic source zones, used as a spatial control on event distribution in probability models, on the length of volcanic vent alignments at analog sites. The analog site chosen to define the dimensions of the "high-risk" zone is the relatively large-volume Fortification Hill volcanic field near Lake Mead, 200 kilometers southeast of Yucca Mountain. In terms of volume, Smith et al. (1990, p. 85) acknowledge that this volcanic field is not analogous to Quaternary volcanism near Yucca Mountain. The vent alignment length defined at Fortification Hill is 25 kilometers (Smith et al. 1990, p. 85). Smith et al. (1990, p. 87) consider this length to be an upper bound, and it corresponds to the > 99th-percentile value of the PVHA event length distribution (Figure 4).

Vent alignment lengths are used directly in NRC probability calculations (Reamer 1999, Sections 4.1.6.3.2 and 4.1.6.3.3, Figures 29 and 30) and have a maximum half-length range of 5.2 to 10.2 kilometers, corresponding to a total-length range of 10.4 to 20.4 kilometers. These values are based on the half-length of the Quaternary Crater Flat vent alignment (5.6 kilometers, the longest half-length observed in the YMR), and the observation that vent alignment half-lengths of 10 kilometers or more occur in other volcanic fields (Reamer 1999, p. 40). It is notable that ~97% of the 174 dike lengths measured in the San Rafael volcanic field (discussed above), which the NRC uses as a YMR analog, have total lengths of < 5 kilometers (Delaney and Gartner 1997, Figure 4). The median of the length distribution at San Rafael is ~1.1 kilometers,

and the maximum dike length is 8 to 9 kilometers (Delaney and Gartner 1997, Figure 4), a distribution not dissimilar to that used in the PVHA (Figure 4).

A measure comparable to dike half-length, the distance from the end of the dike nearest the potential repository to the point of origin of the volcanic event, can be derived from information elicited in the PVHA (Figure 6). This distribution has a 5th-percentile, mean, and 95th-percentile values of 0.2, 2, and 5.6 kilometers, which, given the previous discussions of observed dike lengths, vent spacings, and maximum observed half-length vent alignment of 5.6 kilometers, is in excellent agreement with observed volcanic event features in the YMR. Note that the range of maximum event length values (10 to 20 kilometers) used in NRC probability models (Reamer 1999, Figures 29 and 30), are comparable to the maximum dike lengths assessed by the PVHA experts. However, the NRC's use of a uniform distribution for dike half-length results in a much greater weighting in NRC probability models for dike lengths that represent the > 95th-percentile values assessed by the 10 PVHA experts (Figure 4). The NRC intersection probability value of 10^{-7} per year, assumed for purposes of NRC performance assessment (Reamer 1999, p. 61), depends on a maximum vent alignment length of 20 kilometers (Reamer 1999, Figure 30).

6.3.3 Conceptual Models of Volcanism and Formulation of Probability Models

In the PVHA and alternative assessments of volcanic hazard to the potential Yucca Mountain repository, the conceptual model of volcanism–how and where magmas form, and what processes control the timing and location of magma ascent through the crust to form volcanoes–has a fundamental impact on how probability models are formulated and the consequent results of probability models (e.g, Smith et al. 1990; CRWMS M&O 1996; Reamer 1999).

In general, the PVHA experts viewed the YMR as part of the same extensional tectonic and volcanic regime as the rest of the southern Great Basin portion of the Basin and Range province, but several members of the panel noted the possible additional influence on volcanism of the Walker-Lane structural zone (CRWMS M&O 1996, Appendix E, e.g., pp. WD-1, WH-1). The smaller volumes of basalt erupted in the YMR since the Miocene reflects waning of both tectonism and magmatism in this part of the Basin and Range Province (CRWMS M&O 1996, Appendix E, e.g. pp. RC-1, BC-3, WD-2, RF-3, WH-1, MK-1, AM-3).

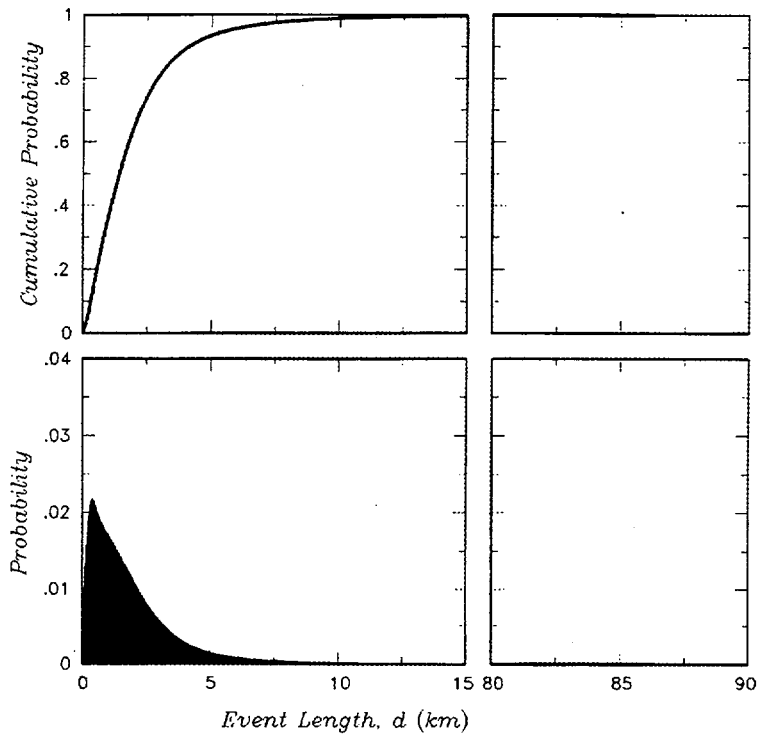

Output data. DTN: LA0005FP831811.001

NOTES: This distribution is obtained by convolving the distributions for dike length with those for the location of the point event relative to the dike. The 5th-percentile, mean, and 95th-percentile values are 0.2, 2.0, and 5.6, km, respectively. The distribution contains a very long upper tail extending to 86 km.

Figure 6. Composite Distribution for the Distance from the Point Volcanic Event to the End of the Dike Averaged Across All 10 PVHA Experts

Some PVHA experts distinguished between deep (mantle source) and shallow (upper crustal structure and stress field) processes when considering different scales (regional and local) of spatial control on volcanism (CRWMS M&O 1996, Appendix E, e.g., pp. MK-2, AM-1). The PVHA experts generally view volcanism in the YMR as a regional-scale phenomenon because of melting processes in the upper lithospheric mantle that produce small volumes of alkali basalt, which is a basalt type generated by relatively small percentages of mantle melting compared to other basalt types (CRWMS M&O 1998c, Chapter 4, p. 4-4). The exact mechanism of mantle melting in the YMR is poorly understood but may be controlled by a complex combination of processes including the effect of residual heat in the lithospheric mantle from previous episodes of volcanism and the presence of a plate subduction system, local variations in volatile (water) content, variations in mantle mineralogy and chemistry, and the effect of regional lithospheric extension (CRWMS M&O 1996, Appendix E). Researchers who have analyzed magmatic processes in the YMR generally agree that the magnitude of mantle melting has drastically decreased since the middle Miocene and that all melts in the past few million years have been generated within relatively cool (compared to asthenospheric mantle) ancient lithospheric mantle, a factor that may contribute to the relatively small and decreasing volume of basaltic

melt erupted in the YMR since the Miocene (Farmer et al. 1989; Yogodzinski and Smith 1995; CRWMS M&O 1996, Appendix E; Reamer 1999, pp. 17, 47).

On a more local and shallow scale, most researchers conclude that (1) volcanism is correlated with zones of past or present crustal extension, and (2) once dikes feeding volcanoes enter the shallow upper crust, their location and orientation is influenced by the orientation of the local stress field and the presence of faults that may locally control vent location and alignment. The evidence cited for these two conclusions includes several northeast-oriented vent alignments in the YMR and the association of eruptive centers with known or inferred faults (Smith et al. 1990, p. 83; CRWMS M&O 1996, Appendix E, e.g., AM-4; Connor et al. 1997, p. 78; Reamer 1999, Section 4.1.3.3.3; Fridrich et al. 1999, p. 211).

A mechanistic model relating mantle melting and lithospheric extension has recently been proposed for the YMR by the NRC (Reamer 1999, Section 4.1.5.3.2) and, additionally, is used as the geologic basis for weighting spatial density models based on crustal density variations across the YMR (Reamer 1999, Section 4.1.6.3.3). The conceptual basis of the model is that crustal density variations across the YMR control variations in lithostatic pressure at the base of the crust. These pressure variations in turn control the location of decompression melting within the mantle, which in turn controls the location of future igneous activity within the YMR (Reamer 1999, Section 4.1.5.3.2, pp. 47-48).

As formulated, a finite-element model that calculates lateral pressure changes in the YMR based on upper crustal density variations (Reamer 1999, Section 4.1.5.3.2) is a poor predictor of volcano distribution in the YMR. The model predicts that maximum melting (and, hence, more frequent occurrence of volcanism) will occur farthest from the region of high crustal density (Reamer 1999, Figure 20[b]), but note that this model predicts the opposite of what is observed for the occurrence of post-Miocene volcanism in the YMR (e.g., Reamer 1999, Figure 22) because volcanism is concentrated near high-density crust of the Bare Mountain domain rather than farther to the east (Figure 7).

Inspection of a map of apparent crustal density variation (Reamer 1999, Figure 22) shows that low average crustal density extends fairly uniformly for a distance of at least 50 kilometers east of the Bare Mountain Fault. Within the context of the NRC conceptual model, (i.e, crustal density exerts a primary control on location of volcanism), post-Miocene volcanism should occur somewhat randomly across this broad region. Instead, all post-Miocene volcanism near Yucca Mountain is located within 5 to 10 kilometers of the Bare Mountain fault, or near the southern ends of the Windy Wash and Stagecoach Road faults (Fridrich et al. 1999, p. 211), indicating that local zones of extension and upper crustal faulting may exert more direct control on the location of volcanism than the effect of shallow crustal processes on deep mantle processes (CRWMS M&O 1996, Appendix E, e.g., pp. AM-5, MS-2; Fridrich et al. 1999, p. 211; Reamer 1999, Section 4.1.5.3.3). This is not to say that areas of low crustal density and volcanism do not often coincide, but instead that both are independently influenced or caused by upper crustal faulting and extension.

The NRC uses crustal density as a primary "tectonic" or "geologic" control on volcano distribution (Reamer 1999, Section 4.1.6.3.3), even though volcano distribution is not randomly

distributed over broad areas of low crustal density as predicted by this model. An alternative method of weighting spatial density models would be to weight by estimated percent of extension within the Crater Flat basin (e.g., Fridrich et al. 1999, Figure 5), thereby tying probability models more directly to a geologic process (faulting and extension) that many researchers agree exerts an important geologic control on volcano location (Smith et al. 1990, p. 83; CRWMS M&O 1996, Appendix E, e.g., pp. AM-5, MS-2 ; Connor et al. 1997, p. 78; Reamer 1999, Section 4.1.3.3.3, p. 47). The strong southward and westward increase in extension rate across the Crater Flat basin corresponds well to sites of most recent volcanism in the basin (Fridrich et al. 1999, Figures 1 and 5), as opposed to crustal density variations that are hypothesized to control volcano location but do not correspond well with volcano location (Reamer 1999, Figure 22). In terms of alternative conceptual models, models based on observable geologic features in the YMR provide a more defensible framework and technical basis for probability calculations than models relying on unobservable processes that remain largely speculative (i.e., Reamer 1999, Section 4.1.5.3.2; see also Probability Acceptance Criteria 3, Reamer 1999, p. 24).

In summary, the NRC probability model that relies on spatial density functions weighted by crustal density (Reamer 1999, Section 4.1.6.3.3) is not well supported based on observations of volcano distribution within the YMR. Significantly, this probability model is the basis for calculating the highest annual probability value for a volcanic eruption within the potential repository boundary ($9 \cdot 10^{-8}$ per year, Reamer 1999, Figure 30), which is the value (rounded up to "10^{-7}" per year) that the NRC will use for the purposes of performance assessment (Reamer 1999, p. 61). It should also be noted that this probability model results in an approximately two-fold increase in the intersection probability compared to unweighted spatial density models (Reamer 1999, Figure 29). As discussed previously in section 6.3.2.2, the results of this probability model also depend to a large extent on dike lengths that are inconsistent with the geologic record of the YMR.

6.4 THE CRATER FLAT STRUCTURAL DOMAIN

Clearly, post-Miocene volcanoes in the YMR are spatially clustered (Crowe et al. 1995, Chapter 3; Connor and Hill 1995, Figure 2). For probability models that incorporate clustering of volcanoes (Connor and Hill 1995) or specify volcanic source zones based primarily on the location or clustering of volcano centers (CRWMS M&O 1996), estimation of the hazard to Yucca Mountain is often dominated by the presence of the Crater Flat cluster. This is due to the relatively high occurrence and Quaternary age of volcanoes in the Crater Flat basin (including Lathrop Wells, which lies within the Crater Flat structural domain and is the youngest volcano in the YMR), and because of the close proximity of Crater Flat volcanoes to Yucca Mountain, compared to other volcanic clusters in the YMR (Figure 3).

The Crater Flat structural domain as defined by Fridrich (1999, pp. 170-178) is a structural basin or graben. It is bounded on the west by the Bare Mountain fault and on the east by structures buried beneath Jackass Flats (Figure 7). It includes the Crater Flat topographic basin on the west and Yucca Mountain near the center of the structural basin (Figure 7). Because the potential Yucca Mountain repository lies within the Crater Flat structural basin, the structural and geophysical features of the basin, and to what degree they influence the location of volcanism

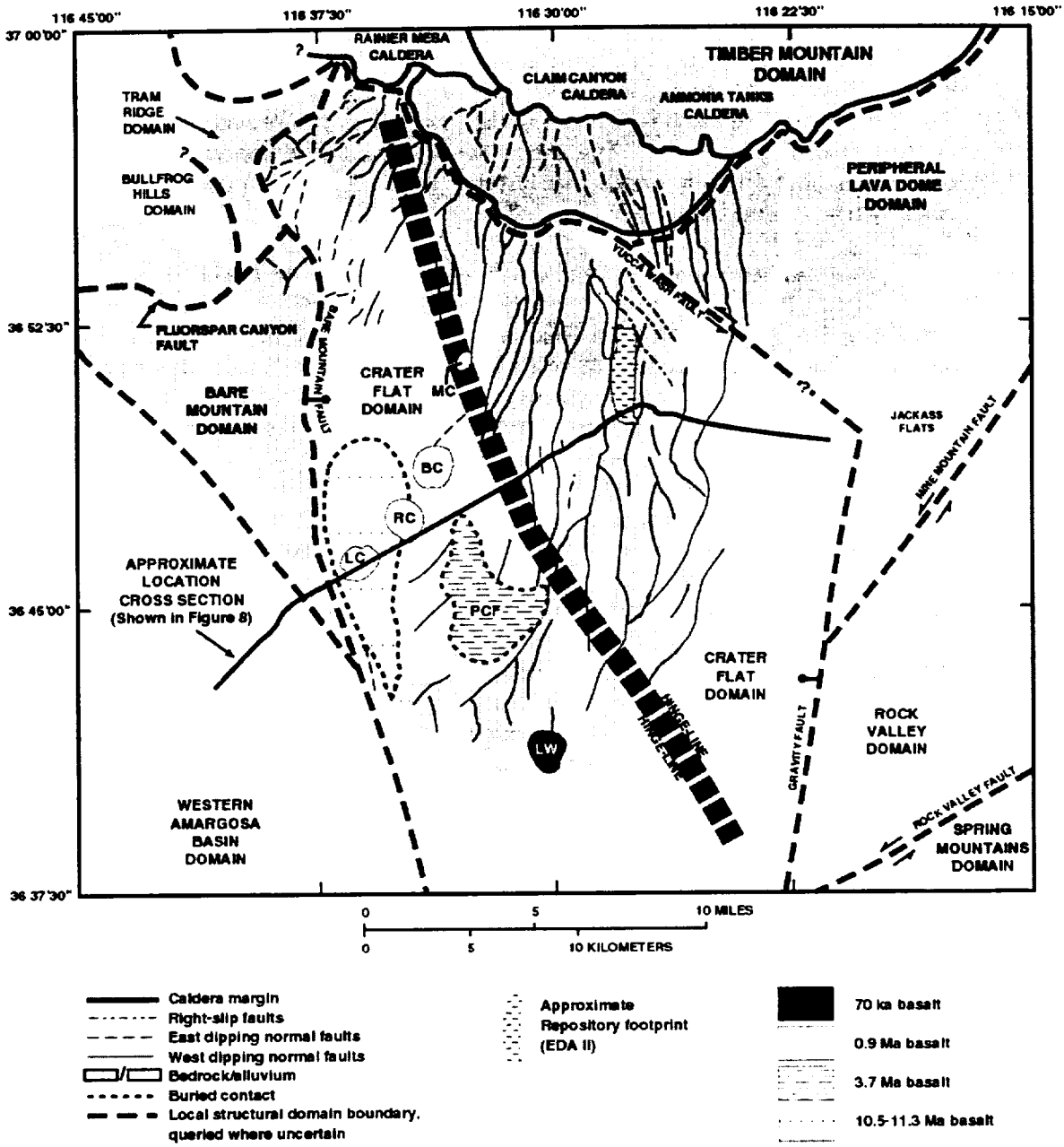

NOTES: Basalts of different ages are shown in relation to basin structure (modified from Fridrich et al. 1999, Figure 1). The 70-ka age of the Lathrop Wells volcano indicated in the legend was estimated based on preliminary data subsequently published in Heizler et al. (1999), which indicates an age closer to 80 k.y.. MC: Makani Cone, BC: Black Cone, RC: Red Cone, LC: Little Cones, LW: Lathrop Wells.

Figure 7. Local Structural Domains and Domain Boundaries of the YMR and Internal Structures of the Crater Flat Basin and Selected Parts of Adjacent Domains (from Fridrich et al. 1999, Figure 1)

within the basin, have been a key factor in conceptual models of volcanism that provide the geologic framework for assessing hazards to the potential repository.

The following sections describe the internal structure of the Crater Flat basin, as well as how the PVHA experts and subsequent investigators have interpreted the influence of structural characteristics of the basin in estimating the locations of future volcanic events. Based largely on work published since the PVHA, the evidence that the northeastern and southwestern portions of the basin have different extensional histories that may have influenced the location of basaltic volcanism within the basin is summarized below.

6.4.1 Internal Structure and Boundaries of the Crater Flat Basin

The Crater Flat structural domain (also referred to herein as the "Crater Flat basin") comprises the Crater Flat topographic basin (west of Yucca Mountain), Yucca Mountain, and the western part of Jackass Flats. Based on geologic mapping and interpretation of subsurface structures from geophysical surveys (discussed below), the Crater Flat structural domain appears to comprise a single, westward-sloping, faulted basin (Figure 8). The western boundary of the Crater Flat basin coincides with the Bare Mountain fault and the northward extension of the fault into the Tram Ridge and Tate's Wash faults (Fridrich 1999, p. 174). The Bare Mountain fault dips steeply (64±5° near the southern end) and can be imaged by seismic reflection to depths of at least 3.5 kilometers and possibly to depths of 6 kilometers (Brocher et al. 1998, pp. 956, 966). Logically, this major fault probably extends to the brittle-ductile transition in the middle crust. The northern boundary consists of a gradational termination of intrabasin structure at the perimeter of the Timber Mountain caldera complex (Fridrich 1999, p. 174). As defined by Fridrich (1999, pp. 174, 176), the northeastern boundary coincides with Yucca Wash, which is an alluvium-filled valley inferred to be underlain by a small northwest-striking right-lateral strike slip fault or zone of faults (Fridrich 1999, pp. 174, 176). The fault is nowhere exposed but is inferred from the fact that Yucca Wash is a linear valley separating Yucca Mountain from a domain to the northeast in which the 12.7-12.8-m.y. Paintbrush Group and older rocks are more extended than on northern Yucca Mountain (Fridrich 1999, p. 176). Day et al. (1998, p. 11) summarize evidence indicating that a major fault is not present beneath Yucca Wash.

The eastern and southern margins of the domain are not physiographically distinct but rather merge with adjacent portions of the Basin and Range. The eastern margin of the Crater Flat basin is probably a buried, down-to-the-west fault known as the Gravity Fault (Fridrich 1999, p. 176, Figure 7). The southern margin is inferred from gravity and magnetic data, and from discontinuous outcrops, to be a fault structure buried beneath young alluvium. It is typically drawn in a northwestern direction along the Amargosa Valley (Fridrich 1999, p. 176). Fundamental changes in the style, timing, and magnitude of extension and other deformation occur across all of the boundaries of the Crater Flat basin.

6.4.1.1 Fault Orientations, Dip Directions, and Displacements

In the center of the Crater Flat basin, a sequence of 12.7 to 12.8 m.y. ash-flow tuffs (primarily the Tiva Canyon and Topopah Spring Tuffs of the Paintbrush Group) crop out. These exposed tuff units comprise Yucca Mountain and adjacent mesas. Much of the information about

orientation, offset, and timing of faulting is based on examination of faults that cut through the exposed tuffs. Because both Crater Flat and Jackass Flats are basins that have undergone alluviation in the late Quaternary, much of the structure of these basins is not accessible to direct observation. Information on structures beneath Crater Flat and Jackass Flats is derived mainly from seismic, gravity, and aeromagnetic and ground magnetic data.

The Crater Flat basin is characterized by an array of closely spaced, small-to-moderate sized extensional faults that generally dip towards the center of the basin (Figure 8). Normal faults within the Crater Flat basin strike northerly in the northeastern part of the basin but change to increasingly northeasterly to the south and west across the basin (Figure 7). These orientations can be measured directly where faults are exposed on Yucca Mountain and can be inferred from the strike of aeromagnetic and gravity anomalies where buried beneath young basin fill. In general, the fault pattern within Crater Flat basin is roughly radial to the caldera complex to the north and curved from north to south across the basin. Based on the strike directions of faults within the Crater Flat basin, a northwest-trending "hinge line" can be defined (Fridrich et al. 1999, p. 208) that separates an area of predominantly north-striking faults on the northeast from an area of predominantly northeast-striking faults on the southwest (Figure 7). The hinge line marks the approximate location of (1) the 20° contour of clockwise rotation of the Tiva Canyon Tuff, (2) a subtle yet abrupt decline in elevation to the southwest, and (3) an increase in Quaternary displacement for faults southwest of the hinge line (Fridrich et al. 1999, p. 208; Stamatakos et al. 1997, p. 327). These observations are consistent with a division of the Crater Flat basin into two portions, separated at the approximate position of the hinge line (Figure 7): (1) a northeastern, less extended portion, and (2) a southwestern, more extended portion (Fridrich et al. 1999, p. 208; Stamatakos et al. 1997, pp. 327-328).

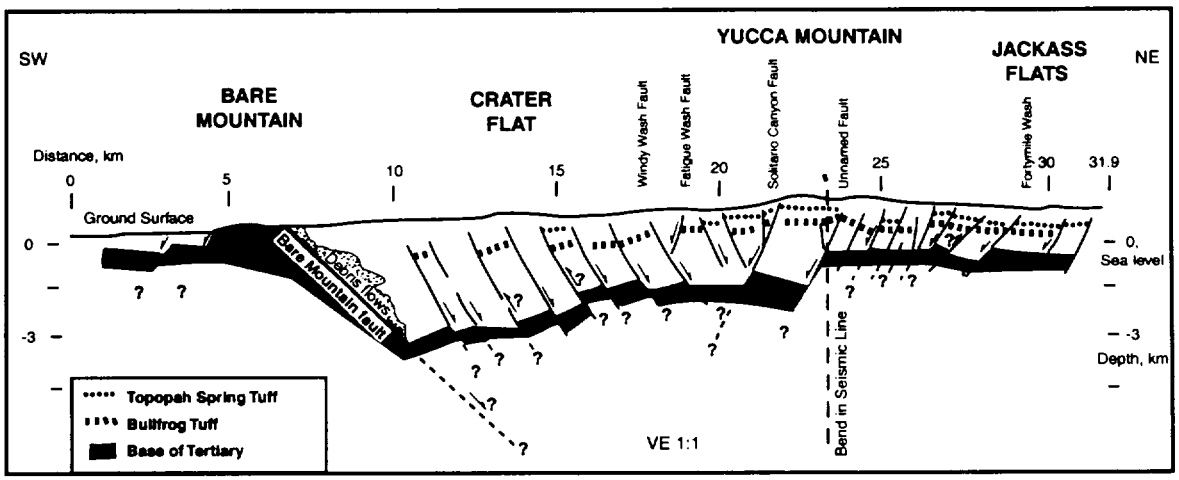

NOTE: Location of cross section is indicated in Figure 7.

Figure 8. Schematic Cross Section of the Crater Flat Basin, from Seismic Reflection, Surficial Geology, and Borehole Information (modified from Brocher et al. 1998)

Seismic reflection surveys show that the Crater Flat basin is deepest to the west (Brocher et al. 1998, Figure 6; see also Ferrill et al. 1996, Figure 1b), implying that extension is also greatest to the west. Stratigraphic thickening of Miocene volcanic rocks to the west support this interpretation (Fridrich et al. 1999, p. 198). Thus, Crater Flat basin is a single, westward-dipping graben, with less fault displacement in the eastern half, within which no major faults dominate (Figure 8).

Nearly all faults of the Crater Flat basin have at least a small component of oblique offset (Fridrich 1999, p. 177). Stratal tilts increase strongly to the west and south from an area of minimum tilts in the northeastern part of the basin on north Yucca Mountain. Faults in the southern part of the basin have a shallower dip and generally greater hanging wall tilt. In the northeastern part of the basin, cumulative extension is 7 to 15%. In contrast, cumulative extension in the southwestern part of the basin is at least 50 to 100%. This greater extension results from decreased spacing between the intrabasin faults and to increased average throw of the major faults (Fridrich et al. 1999, pp. 197-198).

6.4.1.2 Rotation of Faults

The curved pattern of faults and the difference in orientation of faults from northeast to southwest in the Crater Flat basin is attributed to southward increasing clockwise vertical-axis rotation, whereby fault blocks together with their bounding faults were rotated from their original positions. On the scale of the basin as a whole, the spatial variation of declination (i.e., interpreted as vertical-axis rotation) is very smooth (Rosenbaum et al. 1991, pp. 1976-1977; Hudson et al. 1996; Fridrich et al. 1999, Figure 8). The hinge line that is defined from the strike directions of faults corresponds approximately to the contour of 20° clockwise rotation of the Tiva Canyon Tuff. In general, more than 20° of clockwise rotation is present southwest of this line, and less than 20° of rotation is present northeast of the hinge line. In the northeastern part of the basin, cumulative clockwise rotation is generally <5°; in contrast, cumulative rotation in the southwestern part of the basin is > 45° (Fridrich et al. 1999, p. 197). Paleomagnetic data from the Crater Flat basin are interpreted to show that older stratigraphic units are rotated more than younger units and that the major pulse of vertical-axis rotation followed the major episode of extension by about 1 m. y. The major pulse of rotation occurred between 11.6 and 11.45 m.y. (Hudson et al. 1996; Fridrich et al. 1999, p. 210). The close association in the areal pattern of vertical axis rotation with the magnitude of extension in the Crater Flat basin suggests that the rotation and extension are related as a consequence of fan-like opening of the basin (Fridrich et al. 1999, p. 210).

6.4.1.3 Quaternary Slip Rate

Based on the areal variation in the pattern of late Quaternary extension in the Crater Flat basin, a strong southward increase in deformation rate exists. Slip rates determined on individual faults generally increases to the south (Fridrich et al. 1999, pp. 197, 208; Fridrich 1999, p. 177). In addition, cumulative late Quaternary (900 to 100 k.y.) extension measured along three profiles yields 0.025, 0.1, and 0.2% per m.y. from north to south across the basin (Fridrich et al. 1999, p. 207). Thus, the original fan-like pattern of basin opening established in the Miocene still persists. The continuing pattern of oblique basin opening indicates that vertical-axis rotation

must still be occurring at a rate that is significant relative to the rate of extension (Fridrich et al. 1999, pp. 207-208).

Wernicke et al. (1998, p. 2098) presented data from global positioning system surveys that they interpreted as indicating a strain rate near Yucca Mountain 3-4 times the Basin and Range average. Based on this conclusion, they suggested that the volcanic hazard at Yucca Mountain may have been underestimated by an order of magnitude (Wernicke et al. 1998, p. 2099). A more recent study (Savage et al. 1999) using data covering a longer time period than Wernicke et al. (1998) interpreted the data to suggest that within the error of the measurements, the strain rate near Yucca Mountain measured between 1983-1998 was not significantly different from zero (Savage et al. 1999, p. 17631).

The suggestion that postulated anomalous strain rates near Yucca Mountain would lead to an order-of-magnitude increase in the volcano recurrence rate is not consistent with the post-Miocene volcanic record of the YMR. The total volume of basalt erupted during the past million years near Yucca Mountain is less than 0.5 km^3, and is part of a systematic decline in the volume of basalt erupted over the past 5 m.y. (CRWMS M&O 1998c, Chapter 4, p. 4-12). This million-year record of low-volume volcanism is inconsistent with the hypothesis that approximate 100,000 year time intervals within this period have involved particularly high strain rates that would lead to an order-of-magnitude increase in magmatic activity, as stated by Wernicke et al. (1998, p. 2099). Furthermore, the youngest episode of volcanism near Yucca Mountain occurred as a temporally isolated event ~80 k.y. ago at Lathrop Wells, with no volcanism occurring since (CRWMS M&O 1998c, Chapter 2, Sections III and IV). This observation is inconsistent with the Wernicke et al. (1998, p. 2099) hypothesis that Lathrop Wells may represent the onset of a cluster of volcanic events that may continue for several tens of thousands of years. Connor et al. (1998, p. 1007b) calculated that an order-of-magnitude increase in the volcano recurrence rate would result in a 90% probability of a new volcano forming since 80 ka. No such event has occurred. Connor et al. (1998, Figure 1) also presented fault displacement data showing that deformation rates in the YMR have decreased since about 60 k.y. ago, suggesting that the region is not currently within a period of anomalous strain rate that would couple to increased volcano recurrence rate.

6.4.1.4 Basin Subsidence and Fault Displacement

A greater subsidence in the southwestern part of the Crater Flat basin can be inferred from a lower elevation and, therefore, a greater sedimentation rate compared to the northeastern part of the basin. A subtle topographic decline (lower on the southwest side) corresponds with the hinge line, defined from the strike directions of faults (discussed above), along most of its length. The lower elevation is a function of greater total amount of extension to the southwest of the hinge line. Most faults that cross the hinge line show a pronounced southward increase in both Quaternary displacement and total bedrock displacement across it (Fridrich et al. 1999, p. 197, 208; Fridrich 1999, p. 177), especially near the western margin (Bare Mountain fault) and central part (southern Yucca Mountain) of the basin. Miocene and Pliocene sediments are only slightly offset at the northern end of the Bare Mountain fault, whereas Holocene sediments are significantly offset near the southern end of the fault (Stamatakos et al. 1997, p. 327). Also, growth of alluvial fans is greater along the southern part of the fault. Differences in fan growth

are indicative of increased fault slip in the southwestern part of the basin and are compatible with measured slip rates along the Bare Mountain fault from 0.02 mm/yr in the north to 0.21 mm/yr along the southern part of the fault (Ferrill et al. 1996, p. 562). Along the eastern side of Crater Flat, cumulative offset on the Solitario Canyon fault is approximately 1000 meters greater to the south compared to the north (Stamatakos et al. 1997, p. 327). Greater differential subsidence in the southwestern part of the Crater Flat basin is correlated with a greater thickness of Quaternary alluvium in this part of the basin compared to adjacent parts. For example, lava flows associated with Little Cones are buried beneath approximately 15 meters of alluvium, whereas Red and Black Cones, of approximately the same age, are more completely exposed.

To summarize, a variety of structural data, including fault orientations, direction of dip, total and late Quaternary extension, vertical-axis rotation, and basin subsidence, are interpreted to show that the northeastern part of the Crater Flat basin is significantly different from the southwestern part of the basin. That is, each part of the basin has a distinctive style of deformation; the two regions of the basin can be distinguished from each other across a well-defined though gradational boundary, the hinge line extending obliquely across the Crater Flat basin (Figure 7). Thus, the northeastern and southwestern parts of the Crater Flat basin comprise structurally distinct portions of the basin with the southwestern portion characterized by a history of greater extension.

6.4.1.5 Correlation with Volcanism

The post-Miocene basaltic centers of the Crater Flat basin lie within the southwestern part of the basin (Figure 7). This portion of the basin is coincident with the zone of greatest transtensional deformation, between the hinge line of the basin and the Bare Mountain fault, suggesting that this extensional zone controlled the ascent of basalt through the upper crust (Fridrich et al. 1999, p. 210). The youngest volcano in the Crater Flat basin, the 80-ka Lathrop Wells volcano, lies between the southern ends of the Windy Wash and Stagecoach Road faults, the most active site of late Quaternary faulting in the Crater Flat basin (Fridrich et al. 1999, p. 211). Thus, there is a close spatial and temporal relationship between sites of extension and volcanism throughout the Crater Flat Basin (Fridrich et al. 1999, p. 211). The restriction of three episodes of post-Miocene volcanism to the transtensional zone in the Crater Flat basin suggests that volcanism is less likely to occur at Yucca Mountain, which lies outside of the transtensional zone, in an area where no post-Miocene volcanism has occurred (Fridrich et al. 1999, p. 210, Figure 17a). As discussed in the next section, the PVHA experts recognized the close association between volcanism and areas of maximum extension in the YMR (CRWMS M&O 1996, pp. RC-5, BC-12, AM-5, MS-2, GT-2). Subsequent geologic and geophysical studies provide corroborative evidence that areas of maximum extension in the Crater Flat basin correspond closely to volcanic source zones defined in the PVHA (Stamatakos et al. 1997; Brocher et al. 1998; Fridrich et al. 1999).

6.4.2 PVHA Volcanic Source Zones: Relationship to Crater Flat Structural Features and the Probability of Dike Intersection

The correlation between the structurally active portion of the Crater Flat basin and sites of volcanism within the basin indicate that Yucca Mountain is near, but not within, a local volcanic zone that may produce small volumes of future volcanism (CRWMS M&O 1996, Appendix E,

expert zone maps). Although local source zones were chosen by PVHA experts based largely on the location of past volcanic events, they correspond to the areas of highest cumulative extension and most active faulting in the Crater Flat basin (Fridrich et al. 1999, Figures 5 and 6), an association recognized by several of the PHVA experts (CRWMS M&O 1996, pp. RC-5, BC-12, AM-3–5, GT-2). In all cases in which local zones were defined, they were restricted to the southwestern portion of the Crater Flat basin or defined elongated, northwest-trending belts that included the southwestern portion and stretched to the Timber Mountain area (Figures 9a and 9b). All of the local zones excluded the northeastern portion of the Crater Flat basin, in which the potential Yucca Mountain repository is located (Figures 9a and 9b). Based on structural arguments, therefore, and the past patterns of the close association of volcanism and extension, the eastern boundaries of local volcanic source zones defined in the PVHA separate more tectonically active and less tectonically active portions of the Crater Flat basin and may be reasonable predictors of the eastern extent of volcanism expected in the future.

In terms of probability calculations, the volcanic source zones defined in the PVHA represent local regions of higher event frequency (southwestern Crater Flat), whereas northeastern Crater Flat (which includes Yucca Mountain) falls within a regional background source zone of lower event frequency (Figure 17a). According to the intersection probability models used in the PVHA, two mechanisms can generate a disruptive event at Yucca Mountain: either a volcanic event is generated within a local source zone (higher probability event) to the west of Yucca Mountain and has the appropriate location and dike characteristics (length and azimuth) to intersect the potential repository, or a volcanic event is generated within a regional background zone (lower probability event) and intersects the repository. Because the probability of intersection of a volcanic event with the potential repository includes components of both mechanisms, the intersection probability estimated for the repository should reflect spatial event frequencies that lie between local source zone values and regional background values, consistent with the results of the PVHA, and appropriate for a site that lies outside of a local volcanic source zone but near enough to possibly be affected by dikes generated within the source zone.

In summary, many models of the experts related the areas of greatest likelihood for future volcanic activity to the region where previous volcanism has occurred and in which extensional deformation has been and continues to be greatest, i.e., to the southwestern portion of the Crater Flat basin (CRWMS M&O 1996, pp. RC-5, BC-12, AM-5, MS-2, GT-2, and expert zone maps; Figures 9a and b). Analysis by the NRC also indicates that the highest likelihood of future volcanic activity is in southwestern Crater Flat (Reamer 1999, Sections 4.1.5.4 and 4.1.6.3.3; Figure 28). Given that the southern and southwestern portion of the Crater Flat Basin is the most extended (Ferrill et al. 1996; Stamatakos et al. 1997, Fridrich et al. 1999; Reamer 1999, p. 47) and that the locus of post-Miocene volcanism in the Crater Flat basin lies in the south and southwestern portion of the basin (Fridrich et al. 1999; Reamer 1999, p. 47), volcanic source zones defined in the PVHA and centered in southwestern Crater Flat are consistent with the tectonic history and structural features of the Crater Flat structural domain (Figures 9a and b, 17a).

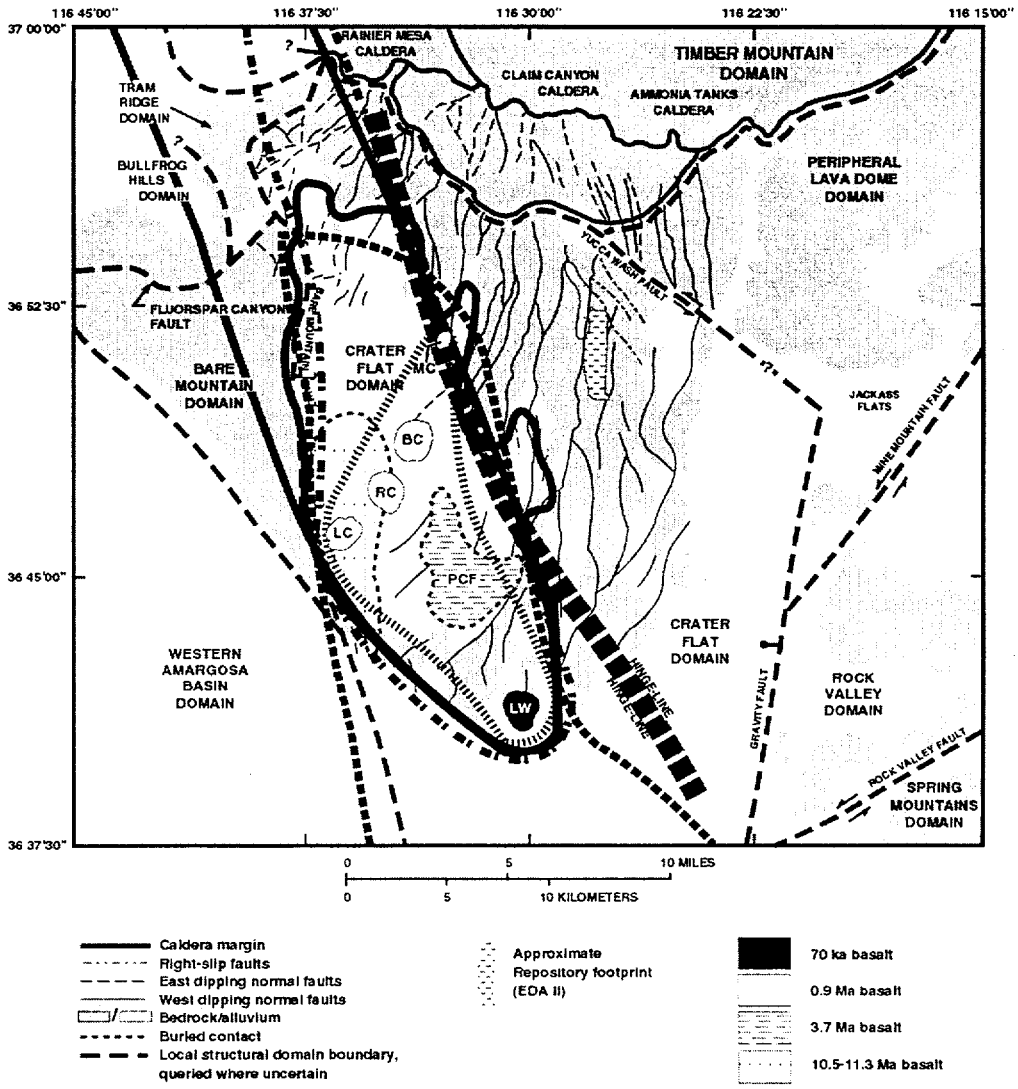

PVHA VOLCANIC SOURCE ZONE BOUNDARIES NEAR YUCCA MOUNTAIN

Crowe — Kuntz

Duffield — Hackett

DTN: MO0002PVHA0082.000 (for zone boundaries only)

NOTES: Superimposed on the Fridrich et al. (1999) map are boundaries of selected volcanic source zones (locally homogeneous spatial and temporal model, CRWMS M&O 1996, Section 3.13) defined by the PVHA experts that lie within the Crater Flat basin (CRWMS M&O 1996, Appendix E). MC: Makani Cone, BC: Black Cone, RC: Red Cone, LC: Little Cones, LW: Lathrop Wells.

Figure 9a. Local Structural Domains and Domain Boundaries of the YMR and Internal Structures of the Crater Flat Basin and Selected Parts of Adjacent Domains (from Fridrich et al. 1999, Figure 1)

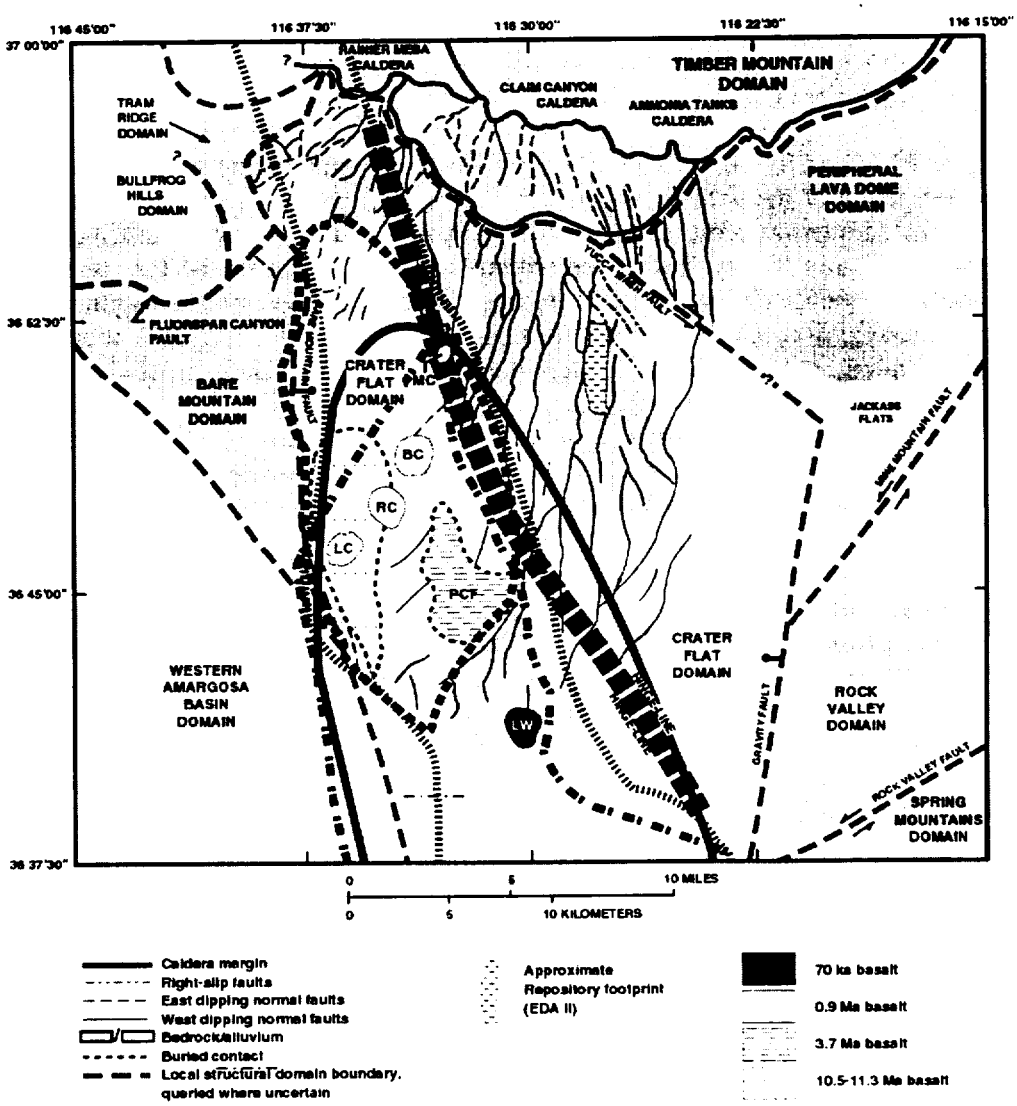

PVHA VOLCANIC SOURCE ZONE BOUNDARIES NEAR YUCCA MOUNTAIN

Fisher — McBirney
Walker — Thompson

DTN: MO0002PVHA0082.000 (for zone boundaries only)

NOTES: Superimposed on the Fridrich et al. (1999) map are boundaries of selected volcanic source zones (locally homogeneous spatial and temporal model, CRWMS M&O 1996, Section 3.13) defined by the PVHA experts that lie within the Crater Flat basin (CRWMS M&O 1996, Appendix E). MC: Makani Cone, BC: Black Cone, RC: Red Cone, LC: Little Cones, LW: Lathrop Wells.

Figure 9b. Local Structural Domains and Domain Boundaries of the YMR and Internal Structures of the Crater Flat Basin and Selected Parts of Adjacent Domains (from Fridrich et al. 1999, Figure 1)

6.5 RECALCULATION OF FREQUENCY OF INTERSECTION AND DEVELOPMENT OF DISTRIBUTIONS FOR LENGTH AND ORIENTATION OF DIKES AND FOR THE NUMBER OF ERUPTIVE CENTERS WITHIN THE POTENTIAL REPOSITORY FOOTPRINT

The PVHA (CRWMS M&O 1996) presented a methodology for calculating the frequency of intersection of the potential repository footprint by a dike associated with a volcanic event and presented interpretations of 10 experts that were used to compute a distribution for the frequency of intersection that quantified the scientific uncertainty in the PVHA assessment. To evaluate the consequences of an intersection, information is needed on the length and orientation of the intersecting dike and the probability that an eruptive center (the vent above the conduit feeding an erupting volcano) forms within the footprint. This section of the AMR develops these assessments. In addition, the current configuration of the potential repository, EDA II, has a different footprint from that used to compute the frequency of intersection by a dike in the PVHA (CRWMS M&O 1996). Consequently, the distribution for frequency of intersection by a dike was recalculated as part of this AMR, using the potential repository footprints based on EDA II.

The approach used to compute the frequency of intersection of the potential repository by a dike is illustrated in Figure 10. The PVHA experts specified spatial and temporal models that define the frequency of occurrence of volcanic events in the region around Yucca Mountain. A grid is constructed over this region with a spacing of 1 kilometer in the x (east-west) and y (north-south) directions. At each location in the grid, x and y, the annual frequency of occurrence of volcanic events, $\lambda(x,y,t)$, is computed from the experts' spatial and temporal models. The variable t indicates that this rate is defined to be the present day rate. The volcanic events occurring at point (x,y) will have an associated dike. The experts defined distributions for the length and orientation of the possible dikes that may be associated with volcanic events. Shown schematically on Figure 10 are four possible dikes associated with the volcanic event. Of these four, two are at the proper orientation and of sufficient length to intersect the potential repository. Using the distributions for dike length and orientation, the fraction of all dikes associated with volcanic events at point (x,y) that intersect the potential repository is computed. This is defined as the conditional probability of intersection for volcanic events at point (x,y), $P^I(\,|\,x,y)$. The frequency of intersecting volcanic events at point (x,y) is then the frequency of volcanic events, $\lambda(x,y,t)$, multiplied by the conditional probability of intersection. The process is repeated for all locations in the grid, producing the frequency of intersection at each point. The sum of these values over all locations in the grid is the annual frequency of intersection of the potential repository by volcanic events, the computed result of the PVHA.

The PVHA analysis did not make any assessment of the consequences of an intersection of the potential repository footprint by a dike. Consequently, a potential dike that extended all the way through the potential repository, such as dike 2 on Figure 10, has the same contribution to the frequency of intersection as a shorter dike that only extends part way into the potential repository, such as dike 4 on Figure 10. However, an assessment of consequences requires information on the length and orientation of the intersecting dikes within the potential repository. Consequently, the PVHA calculation process was modified to provide this information. This is accomplished by a straightforward disaggregation of the intersection frequency into relative

frequencies for discrete increments of length and azimuth. A series of bins with length increments of 0.05 kilometer and azimuth increments of 5° were set up. This discretization is sufficiently fine to provide an accurate picture of the distribution of lengths and azimuths of intersecting dikes. Then, when a volcanic event produces an intersection in the hazard calculation, the resulting length and azimuth within the potential repository footprint are computed, and the event is assigned to the appropriate bin. At the end of the calculation, the value in each bin represents the frequency of intersections that produce the specific values of length and azimuth represented by the bin. The sum of the numbers in all of the length-azimuth bins equals the frequency of intersection. The values in each bin divided by the frequency of intersection provide a conditional distribution for length and azimuth given an intersection. This calculation is completely defined by the interpretations developed by the PVHA expert panel (CRWMS M&O 1996, Appendix E) and requires no additional assumptions.

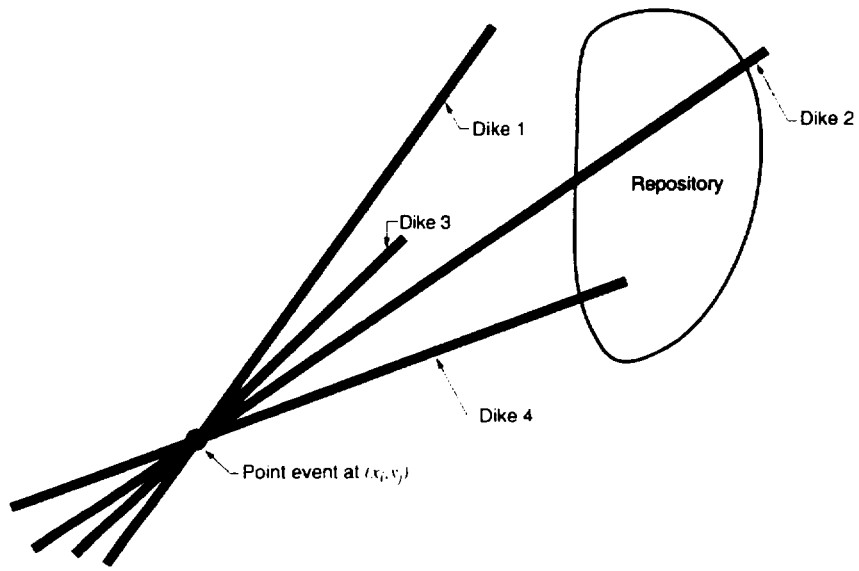

N/A - For illustration purposes only

Figure 10. Schematic Illustrating Procedure for Computing the Frequency of Intersection of the Potential Repository by a Volcanic Event

The additional evaluation needed for consequence analyses is a conditional distribution for the number of eruptive centers that occur within the potential repository footprint given that there is an intersection by a dike associated with a volcanic event. Evaluation of this distribution requires an assessment of the number of eruptive centers associated with a volcanic event and the

spatial distribution for eruptive centers along the length of the dike. The PVHA experts were not asked to make these assessments as part of their characterization of the volcanic hazard. The PVHA experts did assess the number of volcanic events represented by the observed eruptive centers in the YMR. These assessments, together with the characteristics of Quaternary volcanoes in the YMR and a limited number of assumptions, are used to derive empirical distributions for the number of eruptive centers per volcanic event (presented in Attachment III). Application of these assessments in the calculation of the number of eruptive centers within the potential repository requires assessment of the possible correlation between number of eruptive centers and dike length and on the spatial distribution of eruptive centers along the length of the dike. Calculations are performed in this AMR using a range of possible assessments to incorporate these uncertainties into the analysis.

The assessments of the distributions for length and orientation of intersecting dikes developed in this AMR use the geometric representation of a dike employed in the PVHA (CRWMS M&O 1996). As such, dikes are linear features having only length and orientation. The evaluation of the consequences of a dike intersection of the potential repository footprint requires additional information on the width of the intersecting feature. Assessments of the width of intersecting dikes in presented in CRWMS M&O (2000b).

6.5.1 Formulation

This section describes the mathematical formulation required to compute the conditional distributions for the length and azimuth of intersecting dikes within the potential repository footprint and the number of eruptive centers within this footprint. The formulation is an extension of the mathematical formulation used to compute the frequency of intersection of the potential repository footprint by a dike in the PVHA (CRWMS M&O 1996, Section 3).

6.5.1.1 Frequency of Intersection of the Potential Repository Footprint by a Dike

This section restates the PVHA formulation (CRWMS M&O 1996, Section 3) to introduce terms and notation.

The PVHA study provided a distribution for the annual frequency of intersection of the potential repository, $\nu^I(t)$, computed using the relationship (CRWMS M&O 1996, p. 3-2):

$$\nu^I(t) = \iint_R \lambda(x,y,t) \cdot P^I(|x,y)\mathrm{d}x\mathrm{d}y \qquad \text{(Eq. 1)}$$

where $\lambda(x,y,t)$ is the rate of volcanic events at location (x,y) for the current time t; $P^I(\,|\,x,y)$ is the conditional probability that a dike associated with the volcanic event at point (x,y) intersects the potential repository boundary; and R is the region surrounding the potential repository. [Note that the notation for intersection has been changed from a subscript I in CRWMS M&O (1996) to a superscript I in this AMR for clarity.]

The actual calculation was performed on a 0.5-km × 0.5-km grid spacing using the numerical summation:

$$\nu^{I}(t) = \sum_{i}\sum_{j} \lambda(x_i, y_j, t) \cdot P^{I}(x_i, y_j)\Delta x \Delta y \qquad \text{(Eq. 2)}$$

The PVHA experts quantified the uncertainty in $\nu^{I}(t)$ by developing a set of alternative probability models and model parameters for all aspects of the hazard calculation. These were organized in the logic tree format shown in Figures 11a and b.

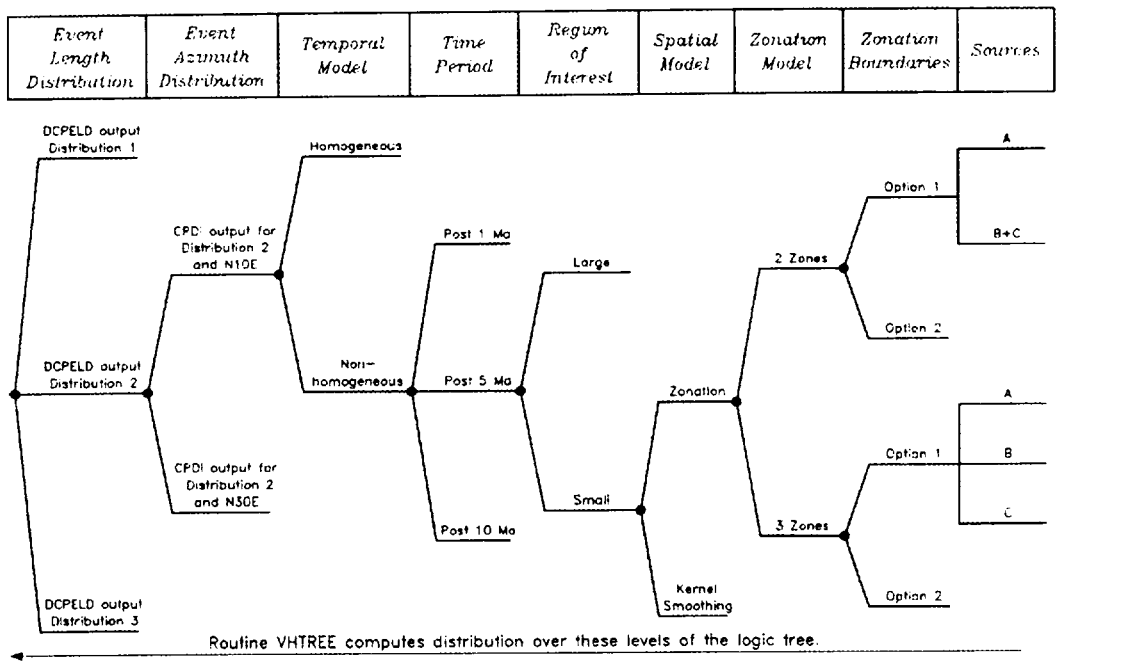

N/A - For illustration purposes only

Figure 11a. Logic Tree Structure Used to Characterize Uncertainty in Volcanic Hazard (modified from CRWMS M&O 1996)

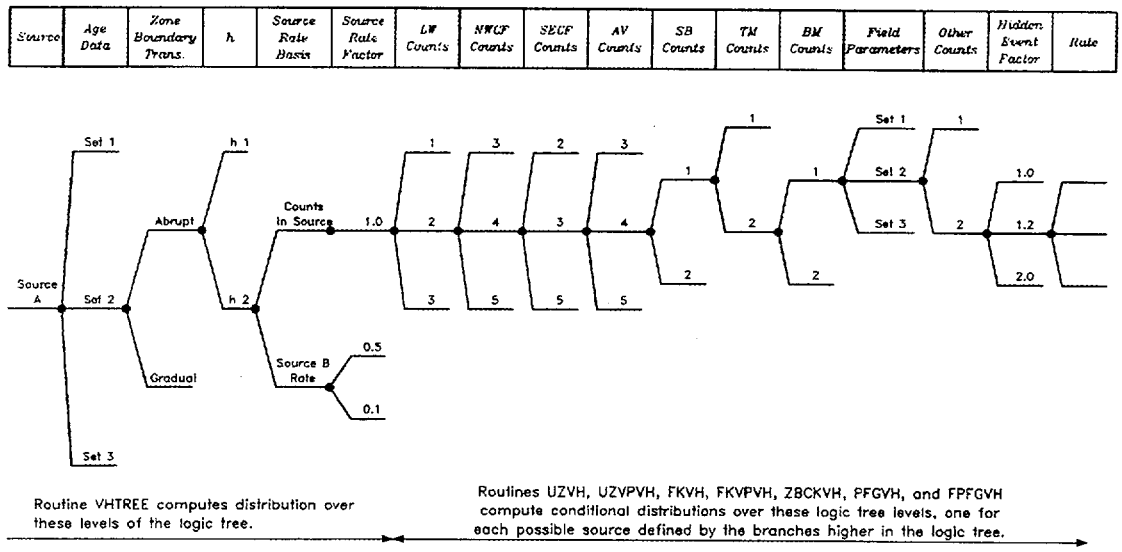

NA - For illustration purposes only

NOTE: These subtrees are attached to the overall logic tree shown on Figure 11a (modified from CRWMS M&O 1996).

Figure 11b. Logic Tree Structure for Subtrees Addressing Uncertainty in Volcanic Hazard from Specific Sources

The end branches of these logic trees define a discrete joint distribution for the parameters, Θ, required to perform the calculation. Thus, Equation (2) becomes:

$$\nu^I(t|\theta_S) = \sum_i \sum_j \lambda(x_i, y_j, t|\theta_S) \cdot P^I(|x_i, y_j, \theta_S)\Delta x \Delta y \qquad \text{(Eq. 3)}$$

where θ_S is the parameter set associated with an individual end branch of one expert's logic tree. The probability that $\nu^I(t|\theta_S)$ is the correct frequency of intersection, given the expert's characterization of the uncertainty in the process, is given by the probability that the parameter set Θ takes on the specific values defined by θ_S, $P(\Theta = \theta_S)$. This discrete probability is obtained by multiplying all of the conditional probabilities at each node along the path through the logic tree that leads to θ_S. The mean or expected frequency of intersection is given by:

$$\mathrm{E}\left[\nu^I(t)\right] = \sum_s \nu^I(t|\theta_S) \cdot P(\Theta = \theta_S) \qquad \text{(Eq. 4)}$$

and the percentiles of the distribution for $\nu^I(t)$ are obtained by ordering the values of $\nu^I(t|\theta_S)$ and then summing the probabilities $P(\Theta = \theta_S)$ until the desired percentiles are reached.

6.5.1.2 Conditional Distribution for Length and Azimuth of an Intersecting Dike

The above formulation for the PVHA hazard computation gives the overall frequency of intersection, $\nu^I(t)$. However, to compute the consequences of an intersection, one needs to know the distribution for length and orientation of the intersecting dikes. This distribution is developed by breaking down (disaggregating) the total frequency, $\nu^I(t|\theta_S)$, into frequencies for specific values of intersecting dike length, L^I_m, and dike azimuth, ϕ_n. The process involves computing the spatial disaggregation of the frequency of intersection into the contributions from each location (x_i,y_j) in the spatial grid around the potential repository, $\nu^I_{x_i,y_j}(t|\theta_S)$ (see Figure 10). At each point (x_i,y_j), the conditional probability of intersection is the probability that dikes of all lengths and azimuths will intersect the potential repository. The conditional probability of intersection is divided into probabilities for intersection from dikes with specific lengths and azimuths. As a result, the frequency of intersection from volcanic events at point (x_i,y_j) is divided into the frequency of intersection from volcanic events at point (x_i,y_j) that produce specific values of length, L^I_m, and azimuth, ϕ_n, within the potential repository footprint, $\nu^I_{x_i,y_j}(t, L^I_m, \phi_n|\theta_S)$. Summing these frequencies over all locations gives the frequency of intersection with a specific value of length and azimuth from all volcanic events, $\nu^I(t,L^I_m,\phi_n|\theta_S)$. Dividing this frequency by the total frequency of intersection, $\nu^I(t|\theta_S)$, gives the conditional probability that an intersecting dike will produce a specific value of length and azimuth within the potential repository.

The conditional probability of intersection, $P^I(\,|x,y,\theta_S)$, in Equation (3) is computed using the relationship (CRWMS M&O 1996, p. 3-17):

$$P^I(|x_i,y_j,\theta_S) = \int_0^{L_{max}|\theta_S} f(d|\theta_S)\cdot\left[\int_{\phi_1|x,y,d}^{\phi_2|x,y,d} f(\phi|\theta_S)d\phi\right]\mathrm{d}d \qquad \text{(Eq. 5)}$$

where: $f(d|\theta_S)$ is the probability that a dike associated with a volcanic event at (x,y) will extend a distance d toward the potential repository; L_{max} is the maximum length of a dike; $f(\phi|\theta_S)$ is the density function for dike azimuth; and $\phi_1\,|\,x,y,d$ and $\phi_2\,|\,x,y,d$ define the range of azimuths over which a dike extending d from a volcanic event at (x,y) will intersect the footprint of the potential repository. These parameters are illustrated in Figure 12. The integration over dike length in Equation (5) is also computed by summation.

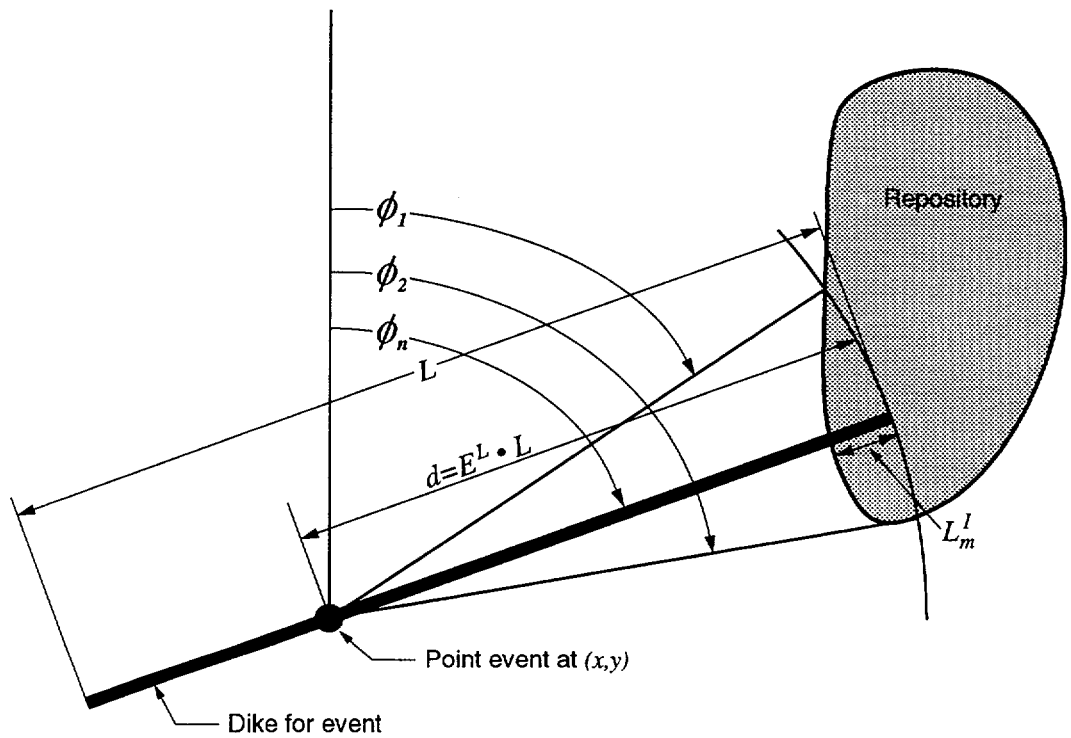

NA - For illustration purposes only

Notes: Parameters are defined in text preceding this figure, except L is the length of the dike, L^I and ϕ are the length and azimuth, respectively for that portion of an intersecting dike within the potential repository footprint, and L^I_m and ϕ_n are specific bins of intersection length and azimuth.

Figure 12. Definition of Parameters Used to Compute the Probability of Intersection of the Potential Repository Footprint by a Volcanic Event

The density function $f(d|\theta_S)$ is computed by convolving the distribution for the total length of the dike, $f(L|\theta_S)$, with a distribution for the normalized location of the dike relative to the volcanic event, $f(E^L|\theta_S)$. Figure 13 illustrates the process using example distributions defined by one of the PVHA expert panel members. Part (a) of Figure 13 shows the probability distribution for the total length of the dike associated with a volcanic event, $f(L|\theta_S)$. Typically these were defined by the PVHA experts to be skewed distributions with long upper tails. Part (b) shows a distribution for the normalized location of the point event [point (x,y)] relative to the total length of the dike, $f(E^L|\theta_S)$. These were defined as symmetric distributions over the range of 0 to 1, typically with higher probability for locations at the midpoint [the dike centered on point (x,y)] than at the ends [the dike extending for its full length in one direction away from point (x,y)]. Part (c) shows the resulting probability and cumulative probability distributions for distance from the potential repository to the end of the dike ($d = E^L \times L$) obtained by convolving the distributions from (a) and (b).

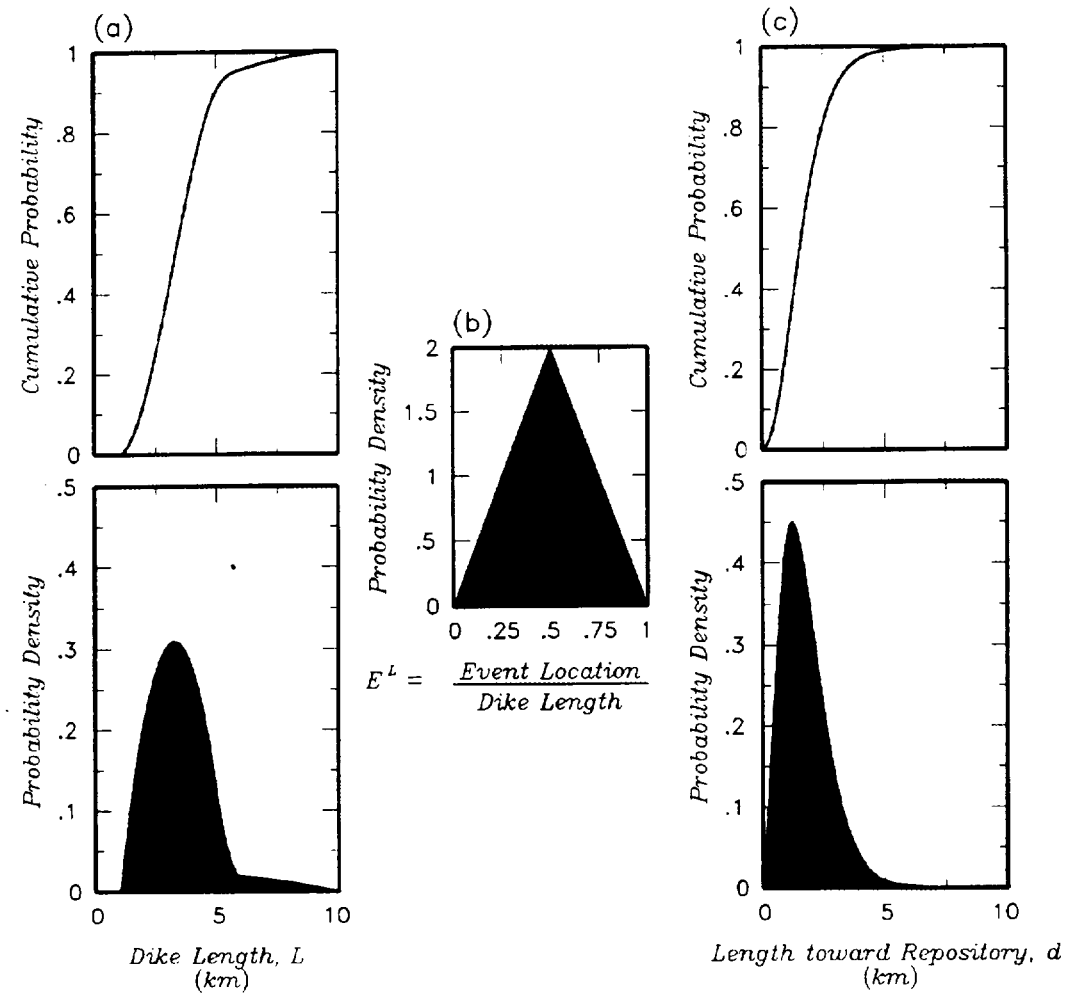

NA - For illustration purposes only

Figure 13. Example Distributions for Dike Length, *L*, (part a); Normalized Location of the Point Volcanic Event Relative to the Total Length of the Dike, E^L, (part b); and the Resulting Distribution for Distance from the Point Volcanic Event to the End of the Dike, *d* (part c)

Using these definitions, the summation form of Equation (5) becomes:

$$P^I(|x_i, y_j, \theta_S) = \sum_{L_p=0}^{L_p=L_{max}|\theta_S} P(L_p|\theta_S) \sum_{E_o^L=0}^{E_o^L=1} P(E_o^L|\theta_S) \sum_{\phi_n=\phi_1|x,y,E_o^L\cdot L_p}^{\phi_n=\phi_2|x,y,E_o^L\cdot L_p} P(\phi_n|\theta_S) \qquad \text{(Eq. 6)}$$

where: $P(L_p|\theta_S)$ is a discrete probability mass function for dike length; $P(E_o^L|\theta_S)$ is a discrete probability mass function for the relative location of the dike on the volcanic event; $P(\phi_n|\theta_S)$ is a discrete probability mass function for dike azimuth; and $\phi_1|x,y,E_o^L \times L_p$ and $\phi_2|x,y,E_o^L \times L_p$ again

define the range of azimuths over which a dike extending $d = E_o^L \times L_p$ from a volcanic event at (x,y) will intersect the potential repository footprint. The three probability mass functions are obtained by discretizing the continuous probability density functions developed for L, E^L, and ϕ by the PVHA experts.

As the summation in Equation (6) is performed, it can be disaggregated into bins defined by azimuth increments, ϕ_n, and intersection length increments, L^I_m, where L^I is the length of penetration of a dike into the potential repository (see Figure 12). As a result, Equation (6) can be rewritten as:

$$P^I(x_i, y_j, \theta_S) = \sum_m \sum_n P^I(L^I_m, \phi_n | x_i, y_j, \theta_S) \qquad \text{(Eq. 7)}$$

The quantity $P^I(L^I_m, \phi_n | x_i, y_j, \theta_S)$ is the probability that a dike associated with a volcanic event at location (x_i, y_j) will intersect the potential repository with length L^I_m and azimuth ϕ_n, and is given by:

$$P^I(L^I_m, \phi_n | x_i, y_j, \theta_S) = \sum_{L_p=0}^{L_p=L_{max}|\theta_S} P(L_p|\theta_S) \sum_{E_o^L=0}^{E_o^L=1} P(E_o^L|\theta_S) \cdot \delta(L^I = L^I_m) \cdot P(\phi_n|\theta_S) \qquad \text{(Eq. 8)}$$

where $\delta(L^I = L^I_m) = 1$ for those combinations of L_p, E_o^L, and ϕ_n that result in $L^I = L^I_m$ for a volcanic event at (x,y), and $\delta(L^I = L^I_m) = 0$ otherwise.

Multiplying Equation (8) by the frequency of volcanic events at (x_i, y_j) and summing over all locations yields the frequency of occurrence for intersections of the potential repository of length L^I_m and azimuth ϕ_n:

$$\nu^I(t, L^I_m, \phi_n | \theta_S) = \sum_i \sum_j \lambda(x_i, y_j, t | \theta_S) \cdot P^I(L^I_m, \phi_n | x_i, y_j, \theta_S) \qquad \text{(Eq. 9)}$$

Because the summation of $\nu^I(t, L^I_m, \phi_n | \theta_S)$ over the $m \times n$ L^I and ϕ intervals equals $\nu^I(t|\theta_S)$ $\left[\nu^I(t|\theta_S) = \sum_m \sum_n \nu^I(t, L^I_m, \phi_n | \theta_S)\right]$, the ratio $\nu^I(t, L^I_m, \phi_n | \theta_S) / \nu^I(t|\theta_S)$ defines the relative frequency of intersection events with length L^I_m and azimuth ϕ_n.

Equation (9) can be recast into the form:

$$\nu^I(t, L^I_m, \phi_n|\theta_S) = \sum_i \sum_j \left[\lambda(x_i, y_j, t|\theta_S) \cdot P^I(|x_i, y_j, \theta_S)\right] \left[\frac{P^I(L^I_m, \phi_n|x_i, y_j, \theta_S)}{P^I(|x_i, y_j, \theta_S)}\right]$$

$$\text{or, if we define : } \nu^I_{x_i, y_j}(t|\theta_S) = \lambda(x_i, y_j, t|\theta_S) \cdot P^I(|x_i, y_j, \theta_S) \qquad \text{(Eq. 10)}$$

$$\nu^I(t, L^I_m, \phi_n|\theta_S) = \sum_i \sum_j \left[\nu^I_{x_i, y_j}(t|\theta_S)\right] \left[\frac{P^I(L^I_m, \phi_n|x_i, y_j, \theta_S)}{P^I(|x_i, y_j, \theta_S)}\right]$$

The first term in brackets defines the contribution to the frequency of intersection from volcanic events occurring at point (x,y), $\nu^I_{x_i, y_j}(t|\theta_S)$. The second term in brackets defines the joint distribution for intersection length and azimuth from volcanic events at point (x,y) conditional on intersection occurring.

The only parameters of θ_S that affect the second term are the specification of the dike length, dike location on the volcanic event, and dike azimuth distributions. The PVHA experts specified these distributions to be independent of the distributions that characterized the spatial density and frequency of volcanic events. Thus Θ can be broken into two independent sets: Θ^D and Θ^E. Parameters Θ^D are those that define the distributions for total length, location relative to the point volcanic event, and azimuth of the dike associated with the volcanic event [the parameters used in the computation of the conditional probability $P^I(|x,y)$]. These are defined by the first two levels of the logic tree shown on Figure 11a. Parameters Θ^E are those that define the distribution for volcanic event frequency, $\lambda(x,y,t)$. These are defined by all of the remaining levels of the logic trees shown on Figures 11a and 11b. Therefore, the expected or mean value of $\nu^I(t, L^I_m, \phi_n|\theta_S)$ [Equation(4)] can be written as:

$$\mathrm{E}\left[\nu^I(t, L^I_m, \phi_n|\Theta)\right] = \sum_{\Theta^D} P(\Theta^D = \theta^D_{S_D}) \left\{ \sum_i \sum_j \left[\frac{P^I(L^I_m, \phi_n|x_i, y_j, \theta^D_{S_D})}{P^I(|x_i, y_j, \theta^D_{S_D})}\right] \times \right.$$

$$\left. \sum_{\Theta^E} P(\Theta^E = \theta^E_{S_E}) \cdot \lambda(x_i, y_j, t|\theta^E_{S_E}) \times P^I(L^I_m, \phi_n|x_i, y_j, \theta^D_{S_D}) \right\}$$

$$\text{or, again using } \nu^I_{x_i, y_j}(t|\theta_S) = \lambda(x_i, y_j, t|\theta_S) \cdot P^I(|x_i, y_j, \theta_S) \qquad \text{(Eq. 11)}$$

$$\mathrm{E}\left[\nu^I(t, L^I_m, \phi_n|\Theta)\right] = \sum_{\Theta^D} P(\Theta^D = \theta^D_{S_D}) \left\{ \sum_i \sum_j \left[\frac{P^I(L^I_m, \phi_n|x_i, y_j, \theta^D_{S_D})}{P^I(|x_i, y_j, \theta^D_{S_D})}\right] \mathrm{E}\left[\nu^I_{x_i, y_j}(t|\theta^D_{S_D})\right] \right\}$$

where $E\left[\nu^{I}_{x_i,y_j}(t|\theta^{D}_{S_D})\right]$ is the expected value of $\nu^{I}_{x_i,y_j}(t)$ conditional on the set of dike parameters $\theta^{D}_{S_D}$. The form of Equation (11) greatly improves the efficiency of the calculation because the terms involving the conditional probability of intersection need to be computed only once for each dike parameter set, $\theta^{D}_{S_D}$, rather than for every combination of the parameters $\theta^{E}_{S_E}$ that define the distribution for volcanic event frequency.

6.5.1.3 Conditional Distribution for the Number of Eruptive Centers

This section develops the mathematical formulation for assessing the conditional distribution for the number of eruptive centers within the footprint of the potential repository. The development is based on the concept that eruptive centers will occur at uncertain locations along the length of the dike associated with a volcanic event. The length of intersection within the potential repository footprint compared to the total length of the dike, the number of eruptive centers per volcanic event, and the spatial distribution of eruptive centers along the length of the dike provide the bases for assessing the likelihood that one or more eruptive centers will occur within the potential repository footprint. The total length of the dike and the length of intersection within the potential repository are computed as part of the formulation presented in Section 6.5.1.2 and are completely defined by the PVHA experts' interpretations. The number of eruptive centers per volcanic event and the spatial distribution of eruptive centers along the length of a dike were not defined as part of the PVHA expert elicitation. However, with the limited set of assumptions (Section 5), these can be derived from the experts' interpretations. There are alternative ways that these assumptions can be applied. In keeping with the concept of uncertainty characterization employed in the PVHA, these alternatives were used to develop alternative assessments of the conditional distribution for the number of eruptive centers within the potential repository footprint. These are then combined using relative weights assigned to each to produce a composite assessment.

The assumptions listed in Section 5.1 and 5.2 provide the basis for using the mapped volcanoes in the YMR to derive assessments of the number of eruptive centers per volcanic event from the PVHA experts' interpretations. Two alternatives are considered. The first uses the number of mapped volcanoes to derive empirical distributions for the number of eruptive centers per volcanic event independent of any assessment of the length of the dike associated with the volcanic event. In this approach, volcanic events can have from 1 to 5 eruptive centers, the range of individual volcanoes associated with a single volcanic event by the PVHA experts. The second alternative uses the number and location of the mapped volcanoes to derive an assessment of the average spacing between eruptive centers. This value, together with the length of the dike associated with a volcanic event determines the number of eruptive centers for a given volcanic event. Attachment III presents the assessments of the distributions for number of eruptive centers per volcanic event and the average spacing between eruptive centers. The use of these results is described in greater detail in Section 6.5.2.2.

The calculation of the likelihood of one or more eruptive centers occurring within the potential repository requires specification of the spatial distribution of eruptive centers along the length of the dike. The minimum information model for the random location of a point on a line is the uniform distribution between the limits of the line length. The assumption listed in Section 5.3

applies the uniform distribution to eruptive center location. Two alternative applications of the uniform distribution were used to capture the range of possible behaviors when multiple eruptive centers occur along the dike for in a single volcanic event.

The first approach specifies the location of each eruptive center independently of the others. Over many volcanic events this approach, on average, will produce eruptive centers spaced out over the length of the volcanic events. However, for an individual event a range of behaviors may occur. Part (a) of Figure 14 shows the results of 20 simulations using this approach, designated the independent, uniformly distributed (*IUD*) approach. Some of the simulations produce relatively uniform spaced eruptive centers and some produce highly clustered eruptive centers.

Dense clustering of multiple eruptive centers can be prevented by imposing a minimum spacing between the eruptive centers. Taking this approach to the limit would result in uniform spacing of eruptive centers along the length of the dike. Part (b) of Figure 14 shows the results of 20 simulations using a model in which the length of the dike is divided into equal length segments, one segment for each eruptive center. Applying the assumption listed in Section 5.3, each eruptive center is randomly located within its segment following a uniform distribution. This approach, designated the uniformly spaced, randomly distributed (*USRD*) approach, produces a broader spread between the eruptive centers in each simulation compared with the *IUD* approach, while still allowing for clustering of two eruptive centers along the length of the dike. Some clustering is expected to occur on occasion, given the close spacing between Little Cones SW and Little Cones NE.

Using these two approaches for the spatial distribution of eruptive centers, the formulation from Section 6.5.1.2 is expanded to define the distribution for the number of eruptive centers that occur within the potential repository. In the previous section the contributions to the frequency of intersection from each location (x,y) in the spatial grid around the potential repository, $\nu^{I}_{x_i,y_j}(t|\theta_S)$,were divided into probabilities for intersection with specific lengths and azimuths, $\nu^{I}_{x_i,y_j}(t, L^{I}_{m}, \phi_n|\theta_S)$.

This calculation involved looping over the possible dike lengths and azimuths. During this calculation, the spatial models described above can be used to compute the number of volcanic events that produce 0, 1, 2, 3, etc., eruptive centers in the potential repository. As a result, $\nu^{I}_{x_i,y_j}(t, L^{I}_{m}, \phi_n|\theta_S)$ is divided into the frequency of intersection from volcanic events at point (x,y) that produce specific numbers of eruptive centers within the potential repository, $\nu^{I}_{x_i,y_j}(t, L^{I}_{m}, \phi_n, r^{EC}|\theta_S)$. Summing these values over all locations (x,y) gives the frequency of intersection with a specific number of eruptive centers in the potential repository, $\nu^{I}(t, L^{I}_{m}, \phi_n, r^{EC}|\theta_S)$. Dividing this frequency by the total frequency of intersection, $\nu^{I}(t|\theta_S)$, gives the conditional probability that an intersecting event will produce a specific number of eruptive centers in the potential repository.

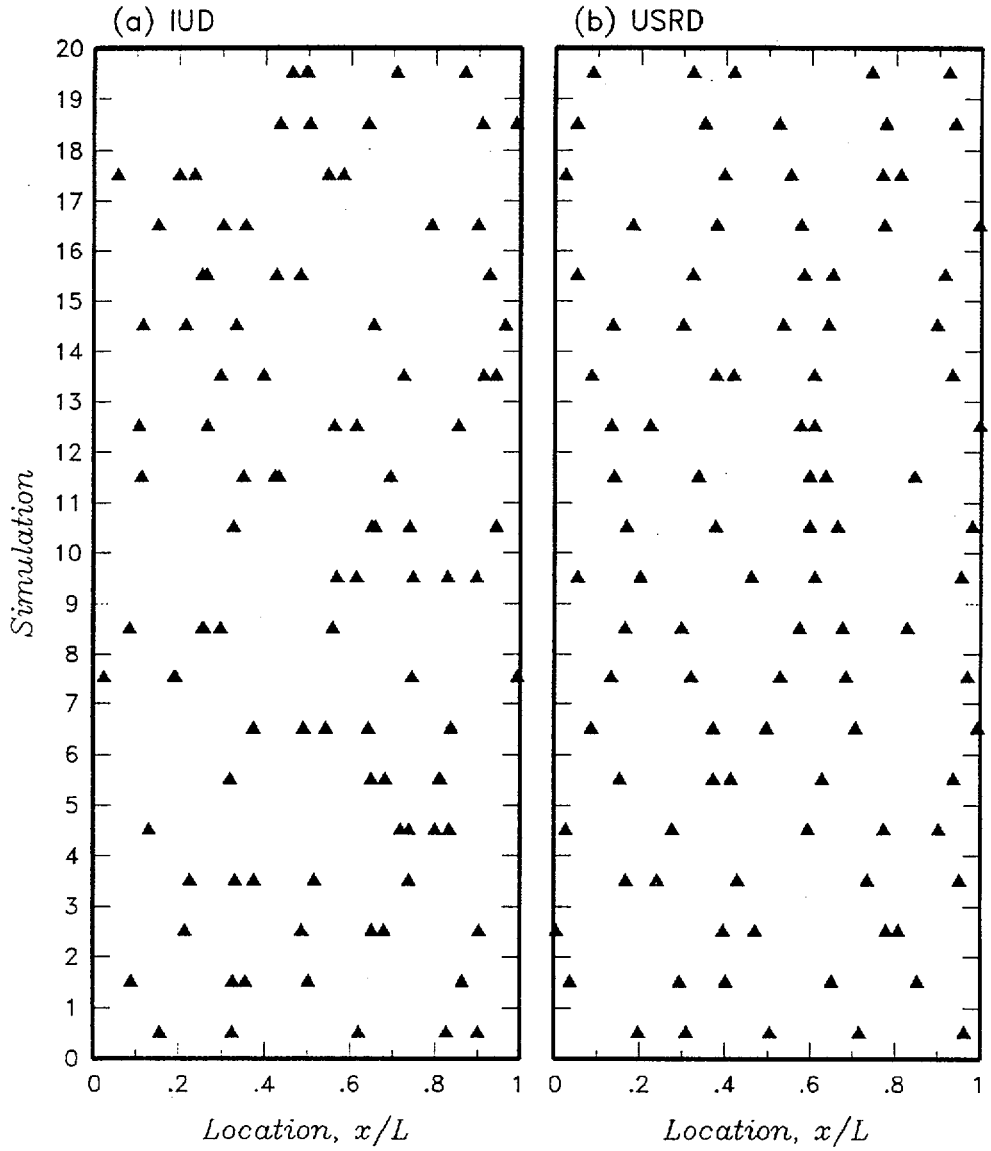

NA - For illustration purposes only

NOTE: The solid triangles show the locations of five eruptive centers for each simulation.

Figure 14. Example Simulations of the Distribution of Eruptive Centers along the Length of a Dike for: (a) the Independent, Uniformly Distributed (*IUD*) Spatial Distribution and (b) the Uniformly Spaced, Randomly Distributed (*USRD*) Spatial Distribution

The disaggregation of $v^{I}_{x_i,y_j}(t, L^{I}_{m}, \phi_n | \theta_S)$ into $v^{I}_{x_i,y_j}(t, L^{I}_{m}, \phi_n, r^{EC} | \theta_S)$ for r^{EC} = 0, 1, 2, ... eruptive centers is accomplished by computing the conditional distribution for r^{EC}, given the total length of the dike, L, the length of intersection within the potential repository footprint, L^{I}, the number of eruptive centers associated with the volcanic event, n^{EC}, and the spatial distribution for the location of eruptive centers. Note that the assumption listed in Section 5.2 results in $n^{EC} \geq 1$.

Independent, Uniformly Distributed (IUD) Spatial Distribution

In this approach, the location of each eruptive center is uniformly distributed along the total length of the dike and the location of each eruptive center is independent of all of the others. Thus, the occurrence of each eruptive center within the footprint of the potential repository is an independent Bernoulli trial with probability of success, p, equal to the length of intersecting dike within the potential repository, L^I, divided by the total length of the dike, L. Under these conditions, the conditional probability distribution for the number of eruptive centers within the potential repository footprint, r^{EC}, given n^{EC} eruptive centers associated with the volcanic event, is given by the binomial distribution:

$$P_{IUD}(r^{EC}|n^{EC}, L, L^I) = \binom{n^{EC}}{r^{EC}}\left(\frac{L^I}{L}\right)^{r^{EC}}\left(1-\frac{L^I}{L}\right)^{n^{EC}-r^{EC}} \qquad \text{(Eq. 12)}$$

where $\binom{n^{EC}}{r^{EC}}$ is the binomial coefficient and the subscript *IUD* refers to independent, uniformly distributed eruptive centers.

Uniformly Spaced, Randomly Distributed (USRD) Spatial Distribution

The alternative approach for the spatial distribution of eruptive centers is that they are spaced more or less equal-distant along the length of the dike. If n^{EC} eruptive centers are generated along the length of the dike, then each eruptive center is located within a segment of length $L^s = L/n^{EC}$. If the location of the eruptive center within each segment is defined by a uniform distribution, the probability that an eruptive center associated with segment q will occur within the potential repository footprint is equal to the length of segment q within the boundary of the potential repository, L^{sI}_q, divided by the total length of the segment, L^s_q. There can be at most two segments of a dike that have partial penetration of the potential repository footprint in one volcanic event (there may be more segments that lie entirely within the potential repository footprint). If only the qth segment penetrates into the potential repository footprint, then the probabilities for zero or one eruptive center within the potential repository are given by:

$$\begin{aligned} P_{USRD}(r^{EC}=0|n^{EC}, L, L^I) &= 1-\frac{L^{sI}_q}{L^s_q} \\ P_{USRD}(r^{EC}=1|n^{EC}, L, L^I) &= \frac{L^{sI}_q}{L^s_q} \end{aligned} \qquad \text{(Eq. 13)}$$

If the qth and $(q+1)^{th}$ segments penetrate into the potential repository footprint, then the probabilities for zero, one, or two eruptive centers within the potential repository are given by:

$$\begin{aligned} P_{USRD}(r^{EC}=0|n^{EC}, L, L^I) &= \left(1-\frac{L^{sI}_q}{L^s_q}\right)\left(1-\frac{L^{sI}_{q+1}}{L^s_{q-1}}\right) \\ P_{USRD}(r^{EC}=1|n^{EC}, L, L^I) &= \left(\frac{L^{sI}_q}{L^s_q}\right)\left(1-\frac{L^{sI}_{q+1}}{L^s_{q+1}}\right)+\left(1-\frac{L^{sI}_q}{L^s_q}\right)\left(\frac{L^{sI}_{q+1}}{L^s_{q+1}}\right) \\ P_{USRD}(r^{EC}=2|n^{EC}, L, L^I) &= \left(\frac{L^{sI}_q}{L^s_q}\right)\left(\frac{L^{sI}_{q+1}}{L^s_{q+1}}\right) \end{aligned} \qquad \text{(Eq. 14)}$$

If one or more segments lie entirely within the potential repository footprint, then the probability of an eruptive center occurring within the potential repository is unity for these segments. In such a case, the value of r^{EC} in Equations (13) and (14) is increased by the number of wholly contained segments. For example, if one segment lies completely within the potential repository and one spans the boundary of the potential repository, then Equation (13) becomes:

$$
\begin{aligned}
P_{USRD}(r^{EC} = 0 | n^{EC}, L, L^{l}) &= 0 \\
P_{USRD}(r^{EC} = 1 | n^{EC}, L, L^{l}) &= 1 - \frac{L_q^{sl}}{L_q^{s}} \\
P_{USRD}(r^{EC} = 2 | n^{EC}, L, L^{l}) &= \frac{L_q^{sl}}{L_q^{s}}
\end{aligned}
\qquad \text{(Eq. 15)}
$$

Figures 15a and 15b compare the probabilities obtained from these two approaches to the spatial distribution of eruptive centers as a function of dike length, L, for L^{l} = 1 kilometer and n^{EC} = 2 (Figure 15a), and for L^{l} = 1 kilometer and n^{EC} = 3 (Fig. 15b). The figures show the computed probabilities for r^{EC} equal to from 0 to n^{EC}, and the probability for at least one eruptive center within the potential repository $P(r^{EC} > 0)$. [Note that $P(r^{EC} > 0)$ is equal to the sum of the probabilities for r^{EC} equal to from 1 to n^{EC}, and is equal to 1 - $P(r^{EC} = 0)$.] For all total lengths, the *USRD* model produces a higher probability for $r^{EC} > 0$, with the difference between the two models diminishing as the dike length increases. Except for short dike lengths, use of the *IUD* spatial distribution produces a higher probability of multiple eruptive centers within the potential repository footprint.

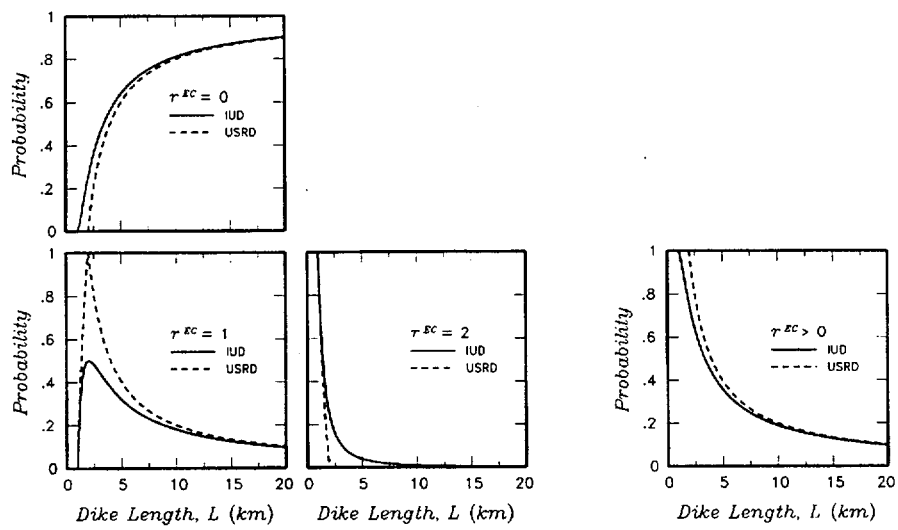

N/A - For illustration purposes only

NOTE: Results are shown for the independent, uniformly distributed (*IUD*) [Equation (12)] and the uniformly spaced, randomly distributed (*USRD*) [Equation (13)] spatial distributions.

Figure 15a. Probability for the Number of Eruptive Centers within the Potential Repository Footprint, r^{EC}, as a Function of Dike Length, L, for the Length of Intersection, L^{l} = 1 Kilometer and the Number of Eruptive Centers Associated with the Volcanic Event, n^{EC}, = 2

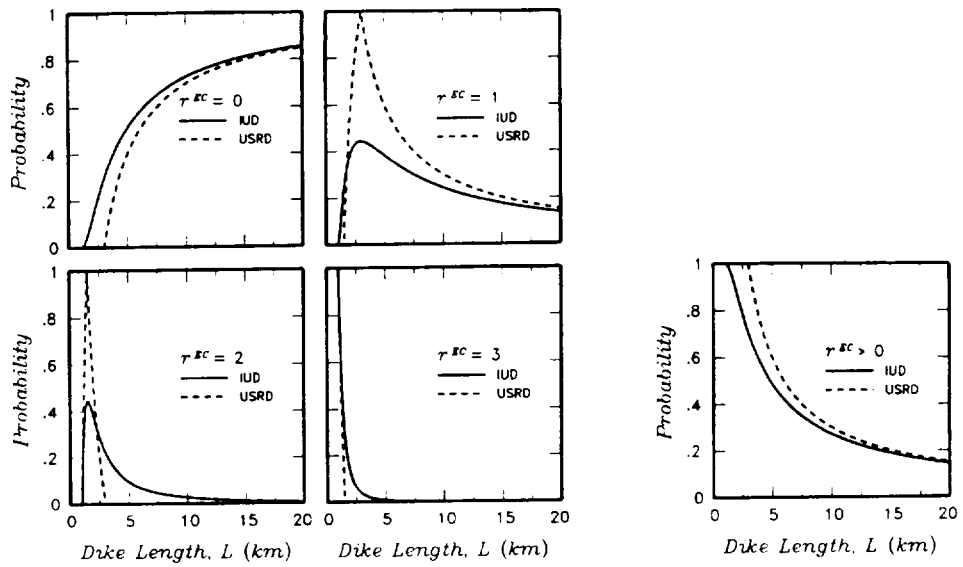

N/A - For illustration purposes only

NOTE: Results are shown for the independent, uniformly distributed (*IUD*) [Equation (12)] and the uniformly spaced, randomly distributed (*USRD*) [Equation (13)] spatial distributions.

Figure 15b. Probability for the Number of Eruptive Centers within the Potential Repository Footprint, r^{EC}, as a Function of Dike Length, *L*, for the Length of Intersection, L^I = 1 Kilometer, and the Number of Eruptive Centers Associated with the Volcanic Event, n^{EC}, = 3

Conditional Distribution

In evaluating the consequences of an intersection of the potential repository footprint by a dike associated with a volcanic event, it is more informative to define $P(r^{EC})$ conditional on the length of intersection, L^I_m. Equation (8) defines the joint probability of intersection length and azimuth for a volcanic event at point (x_i,y_j), $P^I(L^I_m,\phi_n|x_i,y_j,\theta^D_{S_D})$. As indicated in developing Equation (11), the only parameters that affect the calculation of the conditional probability of intersection are $\theta^D_{S_D}$. Thus $P^I(L^I_m,\phi_n|x_i,y_j,\theta_S)$ in Equation (8) can be rewritten as $P^I(L^I_m,\phi_n|x_i,y_j,\theta^D_{S_D})$. In addition, the probability for the number of eruptive centers within the potential repository, Equations (12, 13, and 14) is dependent on the number of eruptive centers per volcanic event, n^{EC}. Attachment III develops distributions for n^{EC}, $P(n^{EC} = \eta|L_p,\theta^D_{S_D})$, which may be conditional on the total length of the dike, L_p. The parameter set $\theta^D_{S_D}$ is expanded to include any alternatives for assessing $P(n^{EC} = \eta)$. Using these definitions, the joint probability of r^{EC} eruptive centers in the potential repository for a volcanic event at (x,y) producing a length of intersection of L^I_m at an azimuth of ϕ_n is given by:

$$P^I(L^I_m,\phi_n,r^{EC}|x_i,y_j,\theta^D_{S_D}) = \sum_{L_p=0}^{L_p=L_{max}|\theta^D_{S_D}} P(L_p|\theta^D_{S_D}) \sum_{E^L_o=0}^{E^L_o=1} P(E^L_o|\theta^D_{S_D})\cdot\delta(L^I=L^I_m)\cdot P(\phi_n|\theta^D_{S_D})\times$$
$$\sum_{\eta=1}^{\eta=n^{EC}_{max}} P(n^{EC}=\eta|L_p,\theta^D_{S_D})P(r^{EC}|L_p,L^I_m,n^{EC}=\eta) \quad \text{(Eq. 16)}$$

with $P(r^{EC}|L_p,L^I_m,n^{EC}=\eta)$ given by either Equation (12) or Equations (13) and (14).

Multiplying Equation (16) by, $\lambda(x_i,y_j,t|\theta^D_{S_D})$ the frequency of volcanic events at (x_i,y_j) and summing over all locations yields the frequency of occurrence for intersections of the potential repository of length L^I_m and azimuth ϕ_n with r^{EC} eruptive centers within the repository:

$$\nu^I(t,L^I_m,\phi_n,r^{EC}|\theta_S) = \sum_i\sum_j \lambda(x_i,y_j,t|\theta^E_{S_E})\cdot P^I(L^I_m,\phi_n,r^{EC}|x_i,y_j,\theta^D_{S_D}) \quad \text{(Eq. 17)}$$

Because the summation of $\nu^I(t,L^I_m,\phi_n,r^{EC}|\theta_S)$ over $r^{EC}=0$ to $r^{EC}=n^{EC}_{max}$ equals $\nu^I(t,L^I_m,\phi_n|\theta_S)$, the ratio $\nu^I(t,L^I_m,\phi_n,r^{EC}|\theta_S)/\nu^I(t,L^I_m,\phi_n|\theta_S)$ defines the relative frequency of intersection events with length L^I_m and azimuth ϕ_n. that produce r^{EC} eruptive centers within the potential repository.
In the same manner that Equation (9) was recast as Equation (10), Equation (17) can be recast into the form:

$$\nu^I(t,L^I_m,\phi_n,r^{EC}|\theta_S) = \sum_i\sum_j \nu^I_{x_i,y_j}(t|\theta^E_{S_E},\theta^D_{S_D})\cdot\left[\frac{P^I(L^I_m,\phi_n,r^{EC}|x_i,y_j,\theta^D_{S_D})}{P^I(|x_i,y_j,\theta^D_{S_D})}\right] \quad \text{(Eq. 18)}$$

where the substitution $\nu^I_{x_i,y_j}(t|\theta^E_{S_E},\theta^D_{S_D}) = \lambda(x_i,y_j,t|\theta^E_{S_E})\cdot P^I(|x_i,y_j,\theta^D_{S_D})$ has been made. Equation (18) may be adapted in a manner similar to Equation (11) to improve the efficiency of the computation of the expected value of $\nu^I(t,L^I_m,\phi_n,r^{EC}|\theta_S)$, producing:

$$\mathrm{E}\left[\nu^I(t,L^I_m,\phi_n,r^{EC}|\Theta)\right] = \sum_{\Theta^D} P(\Theta^D=\theta^D_{S_D})\cdot$$
$$\left\{\sum_i\sum_j\left[\frac{P^I(L^I_m,\phi_n,r^{EC}|x_i,y_j,\theta^D_{S_D})}{P^I(|x_i,y_j,\theta^D_{S_D})}\right]\mathrm{E}\left[\nu^I_{x_i,y_j}(t|\theta^D_{S_D})\right]\right\} \quad \text{(Eq. 19)}$$

6.5.2 Implementation

This section describes the implementation of the formulation presented in Section 6.5.1. Equations (3) and (5) provide the relationships used to compute the frequency of intersection, $\nu^I(t)$. Equations (10), (11), (18), and (19) provide the relationships used to compute the frequency of intersecting volcanic events that produce an intersection length of L^I_m, at an azimuth of ϕ_n, with r^{EC} eruptive centers occurring within the potential repository footprint.

6.5.2.1 Frequency of Intersection of the Potential Repository Footprint by a Dike

The computational scheme used in CRWMS M&O (1996) and repeated in this AMR consists of the steps shown on Figure 1 (repeated for each expert's interpretation).

Step 1: Discrete cumulative distributions for dike length are developed from the experts' assessments using software routines FITCD V1.0 (STN: 10262-1.0-00) or SFCD V1.0 (STN: 10275-1.0-00) [e.g., part (a) of Figure 13]. These are then convolved with the event location of the dike on the volcanic event [e.g. part (b) of Figure 13] to produce distributions for volcanic event length [e.g. part (c) of Figure 13] using software routine DCPELD V1.0 (STN: 10258-1.0-00).

Step 2: The conditional probability of intersection, $P^I(|x_i, y_j, \theta^D_{S_D})$, is computed for each set of parameters $\theta^D_{S_D}$ (defined by an unique event length distribution from step 1 and an unique azimuth distribution) using software routine CPDI V1.0 (STN: 10257-1.0-00).

Step 3: The rate of intersection, $\nu^I(t)$, is computed using software routines specific to the type of source [software routines UZVH V1.0 (STN: 10277-1.0-00) and UZVPVH V1.0 (STN: 10279-1.0-00) for source zones; routines FKVH V1.0 (STN: 10265-1.0-00), FKVPVH V1.0 (STN: 10267-1.0-00), and ZBCKVH V1.0 (STN: 10283-1.0-00) for kernel density sources; and routines PFGVH V1.0 (STN: 10273-1.00-00) and FPFGVH V1.0 (STN: 10269-1.0-00) for 2-D Gaussian field sources]. The characterization of individual volcanic sources is defined by a 12-parameter subset of $\theta^E_{S_E}$. The distribution for these parameters depends upon the alternative source definitions, temporal models, and time periods of interest. To denote this breakdown of $\theta^E_{S_E}$, the parameter set $\theta^E_{S_{ASM}}$ represents the alternative source models (including temporal models) and parameter set $\theta^E_{S_{ISP}}|\theta^E_{S_{ASM}}$ represents the individual source parameters, which are conditional on the chosen source and temporal models $\theta^E_{S_{ASM}}$. The software routines used to compute the hazard from an individual source contain a set of 12 nested DO loops to enumerate all of the alternative versions of $\theta^E_{S_{ISP}}|\theta^E_{S_{ASM}}$ (see Figure 11b). Given a set of parameters, the frequency of volcanic events, $\lambda_\alpha(x_i, y_j, t|\theta^E_{S_{ISP}})$, is computed for a specific source, α, using the formulation appropriate for the source type. This is multiplied by the conditional probability of intersection, $P^I(|x_i, y_j, \theta^D_{S_D})$, from the output of routine CPDI V1.0 and summed over all points within the source to obtain the frequency of intersection from volcanic events associated with source α. The software routines store the mean frequency of intersection and the distribution in the frequency of intersection (computed over the distributions for $\theta^E_{S_{ISP}}|\theta^E_{S_{ASM}}$ in output files for use in the final step of the computations. Separate output files are created for all of the alternative sets of source model parameters, $\theta^E_{S_{ASM}}$, and for the alternative parameters that describe the associated dikes, $\theta^D_{S_D}$.

Step 4: The results from step 3 are combined over the distributions for $\theta^E_{S_{ASM}}$ and $\theta^D_{S_D}$ (see Figures 11a and 11b) to compute the full distribution for frequency of intersection specified by an

individual PVHA expert's interpretations. The results for each expert are then combined to obtain the composite distribution. These calculations are performed using software routine VHTREE V1.0 (STN: 10282-1.0-00). Complete enumeration of all of the alternative parameter sets $\theta^E_{S_{ASM}}$ is again achieved by a series of nested DO loops. The mean value and various percentiles of the distribution for frequency of intersection of the potential repository footprint by a dike were computed from the discrete distribution for $\nu^I(t|\theta^D_{S_D},\theta^E_{S_E})$ as described above in Section 6.5.1.1. These are then combined using equal weights to produce a composite distribution for frequency of intersection.

The calculations performed in the PVHA (CRWMS M&O 1996) used the potential repository footprint shown on Figure 16. The current design (EDA II) calls for a longer and narrower emplacement area. Attachment II presents the coordinates of the drifts in the Primary Block (drifts 1 through 50) and the Primary Block Contingency Area (drifts 51 through 60) and their transformation to UTM kilometers. Figure 16 shows the location of the Primary and Primary Contingency Blocks relative to the 1996 potential repository configuration.

Two footprint polygons of the potential repository were used for the calculations in this AMR. The first polygon envelops the Primary Block (drifts 1 through 50) and the drifts placed 40 meters north of drift 1 and 40 meters south of drift 50. The second polygon envelops the Primary Block (drifts 1 through 50), the Primary Contingency Block (drifts 51 through 60), and the drifts placed 40 meters north of drift 1 and 40 meters south of drift 60. This polygon is referred to as the Primary + Contingency Blocks throughout this AMR. The polygons were constructed to provide a clearance of approximately 10 meters around the drift coordinates (see Figure 16). The polygons encompassing the Primary Block and the Primary + Contingency Blocks were used to calculate the conditional distributions for intersection length, azimuth, and number of eruptive centers using the simulation approach developed in this AMR. These polygons were also used to calculate an updated mean and distribution for the frequency of intersection of the potential repository footprint by a dike using the full enumeration approach employed in PVHA (CRWMS M&O 1996).

6.5.2.2 Distributions for Length, Azimuth, and Number of Eruptive Centers

The computations performed in CRWMS M&O (1996) were made for all possible sets of $\theta^D_{S_D}$ and $\theta^E_{S_E}$ defined by the volcanic hazard characterization of each of the PVHA experts (full enumeration of the logic tree branches (CWRMS M&O 1996, Appendix E)). However, the objective of this analysis is a disaggregation of the intersection frequency, $\nu^I(t|\theta^D_{S_D},\theta^E_{S_E})$, into intersection frequencies with specific values of L^I_m, ϕ_n, and r^{EC}. Repeating the calculation for the spatial disaggregation would require exhaustive computation and storage of the spatial disaggregation of the hazard, $\nu^I_{x_i,y_j}(t|\theta^E_{S_E},\theta^D_{S_D})$, for all possible parameter sets $\theta^E_{S_E}$. Therefore, a simulation approach was used to develop random sample parameter sets $\theta^E_{S_E}$ from the PVHA experts' logic trees to speed up the computation process. As discussed subsequently in the results (Section 6.5.3), the mean and distribution for the frequency of intersection of the potential repository footprint by a dike computed by full enumeration and by simulation for each PVHA expert's interpretation and for the composite result generally agree within a few percent.

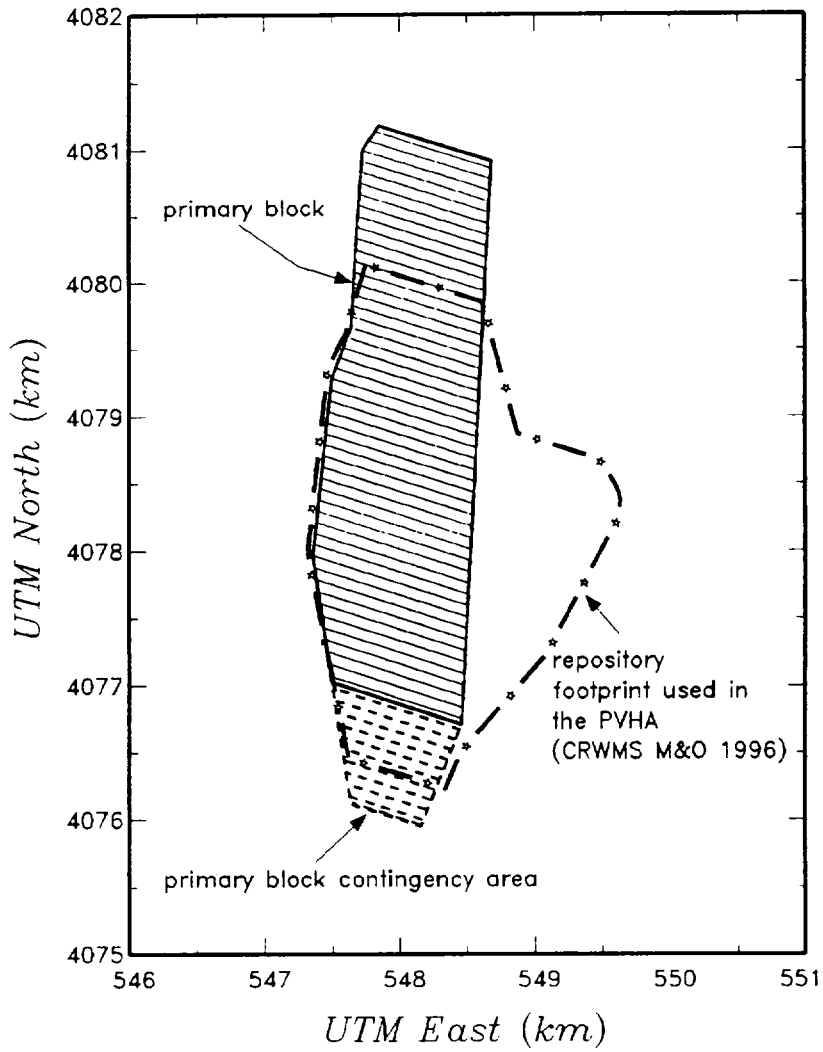

Source: CRWMS M&O 1999f.

NOTE: PVHA reference from CRWMS M&O 1996.

Figure 16. Location of Primary Block and Primary + Contingency Blocks of Current Potential Repository Footprint (EDA II) Compared to Repository Footprint Used in the PVHA

The approach used to obtain the spatial disaggregation of the frequency of intersection consists of the following steps (see Figure 2).

Step 1: The conditional probability of intersection, $P^I(|x_i, y_j, \theta^D_{S_D})$, was taken directly from the computation for the frequency of intersection discussed above. The files containing

$P^I(|x_i, y_j, \theta^D_{S_D})$ for each set of parameters $\theta^D_{S_D}$ were created using routine CPDI V1.0 (STN: 10257-1.0-00) using inputs processed through routines FITCD V1.0 (STN: 10262-1.0-00), SFCD V1.0 (STN: 10275-1.0-00), and DCPELD V1.0 (STN: 10258-1.0-00).

Step 2: The second step in the calculation involved computation of the spatial disaggregation of frequency of intersection hazard for the individual sources specified by the alternative source parameter sets $\theta^E_{S_{ASM}}$ and for the alternative dike parameters $\theta^D_{S_D}$. For the reasons discussed above, simulation is used to select random samples of the parameter subset $\theta^E_{S_{ISP}}|\theta^E_{S_{ASM}}$ used to compute the frequency of intersection for an individual source type. The approach used to generate these parameter subsets is Latin hypercube sampling (McKay et al. 1979, pp. 243-245). The software routines used to compute the frequency of intersection replace the 12 nested DO loops with simulation of 50 parameter sets, $\theta^E_{sim_{ISP}}|\theta^E_{S_{ASM}}$, $sim_{ISP} = 1 \ldots 50$, using Latin hypercube sampling from the 12 independent, discrete parameter distributions that define $\Theta^E_{ISP}|\theta^E_{S_{ASM}}$. Once a parameter subset is defined, the spatial distribution of $\lambda(x,y,t)$ for source α is computed using the same algorithms employed for the PVHA calculation (CRWMS M&O 1996). The disaggregated frequency of intersection, $\nu^I_{\alpha,x_i,y_j}(t|\theta^E_{sim_{ISP}}, \theta^E_{S_{ASM}}, \theta^D_{S_D})$, from each simulation for each source α is output to a file along with the mean frequency of intersection for the source. Each simulated parameter set $\theta^E_{sim_{ISP}}|\theta^E_{S_{ASM}}$ is an equally likely realization of the possible parameter sets from the joint distribution for $\Theta^E_{ISP}|\theta^E_{S_{ASM}}$. Therefore, the mean frequency of intersection for source α, given source model parameter set $\theta^E_{S_{ASM}}$ and dike parameters $\theta^D_{S_D}$, $\mathrm{E}\left[\nu^I_\alpha(t|\theta^E_{S_{ASM}}, \theta^D_{S_D})\right]$, and its spatial disaggregation $\mathrm{E}\left[\nu^I_{\alpha,x_i,y_j}(t|\theta^E_{S_{ASM}}, \theta^D_{S_D})\right]$, may be estimated by the average of the results from the 50 simulations.

$$\mathrm{E}\left[\nu^I_\alpha(t|\theta^E_{S_{ASM}}, \theta^D_{S_D})\right] \sim \frac{1}{50} \sum_{sim_{ISP}=1}^{sim_{ISP}=50} \nu^I_\alpha(t|\theta^E_{sim_{ISP}}, \theta^E_{S_ASM}, \theta^D_{S_D})$$

and (Eq. 20)

$$\mathrm{E}\left[\nu^I_{\alpha,x_i,y_j}(t|\theta^E_{S_{ASM}}, \theta^D_{S_D})\right] \sim \frac{1}{50} \sum_{sim_{ISP}=1}^{sim_{ISP}=50} \nu^I_{\alpha,x_i,y_j}(t|\theta^E_{sim_{ISP}}, \theta^E_{S_ASM}, \theta^D_{S_D})$$

The simulation software routines are designated UZVHLH V1.0 (STN: 10278-1.0-00), UZVPVHLH V1.0 (STN: 10280-1.0-00), FKVHLH V1.0 (STN: 10266-1.0-00), FKVPVHLH V1.0 (STN: 10268-1.0-00), ZBCKVHLH V1.0 (STN: 10284-1.0-00), PFGVHLH V1.0 (STN: 10274-1.0-00), and FPFGVHLH V1.0 (STN: 10270-1.0-00). They use the same input files used to compute the frequency of intersection by full enumeration (Section 6.5.2.1).

Step 3: The third step in the calculation is computation of the distribution for the spatial disaggregation of the hazard for each the PVHA expert's interpretation. The full enumeration of the possible parameter sets $\theta^D_{S_D}$ and $\theta^E_{S_{ASM}}$ is again replaced by simulation of 50 equally likely

parameter sets. The software routine VHTIELHS V1.0 (STN: 10281-1.0-00) is used to perform the following operations for the interpretation developed by each of the PVHA experts.

Step 3a. First, all of the possible sets $\theta^D_{S_D}, \theta^E_{S_{ASM}}$ in the joint distribution for Θ^D and Θ^E_{ASM} are enumerated. The joint probability of each set is computed from the PVHA expert's logic tree.

Step 3b. The mean frequency of intersection for each set of $\theta^D_{S_D}, \theta^E_{S_{ASM}}$ and its spatial disaggregation are estimated from the sum of all the individual source results from Step 2, for those sources present in the parameter set $\theta^E_{S_{ASM}}$,

$$\mathrm{E}\left[\nu^I(t|\theta^E_{S_{ASM}}, \theta^D_{S_D})\right] \sim \sum_{\alpha|\theta^E_{S_{ASM}}} \mathrm{E}\left[\nu^I_\alpha(t|\theta^E_{S_{ASM}}, \theta^D_{S_D})\right]$$

and (Eq. 21)

$$\mathrm{E}\left[\nu^I_{x_i,y_j}(t|\theta^E_{S_{ASM}}, \theta^D_{S_D})\right] \sim \sum_{\alpha|\theta^E_{S_{ASM}}} \mathrm{E}\left[\nu^I_{\alpha,x_i,y_j}(t|\theta^E_{S_{ASM}}, \theta^D_{S_D})\right]$$

Step 3c. The sets of $\theta^D_{S_D}, \theta^E_{S_{ASM}}$ are then ranked in terms of increasing mean frequency of intersection, $\mathrm{E}\left[\nu^I(t|\theta^E_{S_{ASM}}, \theta^D_{S_D})\right]$, defining a distribution for $\mathrm{E}\left[\nu^I(t|\theta^E_{S_{ASM}}, \theta^D_{S_D})\right]$.

Step 3d. Then, 50 parameter sets, $\theta^D_{sim_D}, \theta^E_{sim_{ASM}}$, are selected using Latin hypercube sampling from the distribution for $\mathrm{E}\left[\nu^I(t|\theta^E_{S_{ASM}}, \theta^D_{S_D})\right]$. For each of these, the frequency of intersection and its spatial disaggregation are computed for the 50 simulations of parameters $\theta^E_{sim_{ISP}}\Big|\left(\theta^E_{S_{ASM}} = \theta^E_{sim_{ASM}}\right.$ by:

$$\nu^I(t|\theta^E_{sim_{ISP}}, \theta^E_{sim_{ASM}}, \theta^D_{sim_D}) \sim \sum_{\alpha|\theta^E_{sim_{ASM}}} \nu^I_\alpha(t|\theta^E_{sim_{ISP}}, \theta^E_{sim_{ASM}}, \theta^D_{sim_D})$$

and (Eq. 22)

$$\nu^I_{x_i,y_j}(t|\theta^E_{sim_{ISP}}, \theta^E_{sim_{ASM}}, \theta^D_{sim_D}) \sim \sum_{\alpha|\theta^E_{sim_{ASM}}} \nu^I_{\alpha,x_i,y_j}(t|\theta^E_{sim_{ISP}}, \theta^E_{sim_{ASM}}, \theta^D_{sim_D})$$

In Equation (22), $\nu^I_\alpha(t|\theta^E_{sim_{ISP}}, \theta^E_{sim_{ASM}}, \theta^D_{sim_D})$, and its spatial disaggregation, $\nu^I_{\alpha,x_i,y_j}(t|\theta^E_{sim_{ISP}}, \theta^E_{sim_{ASM}}, \theta^D_{sim_D})$, are the values for source α for the simulated parameter set

$\theta^E_{sim_{ISP}} \middle| \theta^E_{S_{ASM}}, \theta^D_{S_D}$ from (2) with $\theta^E_{S_{ASM}}, \theta^D_{S_D} = \theta^E_{sim_{ASM}}, \theta^D_{sim_D}$, the source model and dike parameter set selected in one simulation. The result is 2,500 equally likely values for frequency of intersection. The resulting values of the spatial disaggregation of the frequency of intersection, $\nu^I_{x_i,y_j}(t \middle| \theta^E_{sim_{ISP}}, \theta^E_{sim_{ASM}}, \theta^D_{sim_D})$, are written to separate files for each of the 2,500 simulated parameter sets.

Step 3e. Finally, the expected value for the spatial disaggregation of the frequency of intersection for each of the possible dike parameter sets is estimated from the average of all of the results from step 3d for which $\theta^D_{sim_D} = \theta^D_{S_D}$.

$$\mathrm{E}\left[\nu^I_{x_i,y_j}(t \middle| \theta^D_{S_D})\right] \sim \frac{\sum_{sim_{ISP,ASP,D}=1}^{sim_{ISP,ASP,D}=2500} \nu^I_{x_i,y_j}(t \middle| \theta^E_{sim_{ISP}}, \theta^E_{sim_{ASM}}, \theta^D_{sim_D}) \cdot \delta(\theta^D_{sim_D} = \theta^D_{S_D})}{\sum_{sim_{ISP,ASP,D}=1}^{sim_{ISP,ASP,D}=2500} \delta(\theta^D_{sim_D} = \theta^D_{S_D})} \qquad \text{(Eq. 23)}$$

where $\delta(\theta^D_{sim_D} = \theta^D_{S_D}) = 1$ for those simulations where $\theta^D_{sim_D} = \theta^D_{S_D}$, and zero otherwise. [Note that $\frac{1}{2{,}500} \sum_{sim_{ISP,ASP,D}=1}^{sim_{ISP,ASP,D}=2500} \delta(\theta^D_{sim_D} = \theta^D_{S_D}) \sim P(\Theta^D = \theta^D_{S_D})$.]

Figure 17, part (b) shows a map of $\mathrm{E}\left[\nu^I_{x_i,y_j}(t \middle| \theta^D_{S_D})\right]$ averaged across all 10 experts. This figure indicates the locations of volcanic events that contribute to the frequency of intersection. Also shown on Figure 17 (part a) is a map of the expected frequency of volcanic events, $\mathrm{E}\left[\lambda(x_i, y_j, t \middle| \theta^D_{S_D})\right]$, averaged across all experts. This map was obtained by repeating the calculation for part (a) with the conditional probability of intersection, $P^I(\phi \middle| x_i, y_j, \theta^D_{S_D})$, set to 1 at every point (x,y).

Step 4: The composite distribution for the frequency of intersection of the potential repository footprint by a dike is now represented by the 2,500×10 simulation results for the 10 PVHA experts. Each expert's distribution was assigned equal weight in the PVHA aggregation process. Thus, the composite 25,000 simulations of $\nu^I(t)$ are all equally likely. The 25,000 simulations of $\nu^I(t)$ are ranked and the simulations that produce various percentile of the distribution for $\nu^I(t)$ are identified (e. g., the 95th percentile is the simulation with rank 0.95×25,000 = 23,750). Simulation results that are close to each percentile (within a rank of ±250) that are for different experts are also identified to capture the range of expert interpretations. These simulations are identified using software routine CFRAC V1.0 (STN: 10254-1.0-00).

Step 5: Steps 1 through 4 provide the values of $\nu^I_{x_i,y_j}(t \middle| \theta^E_{sim_{ISP}}, \theta^E_{sim_{ASM}}, \theta^D_{sim_D})$ and $\mathrm{E}\left[\nu^I_{x_i,y_j}(t \middle| \theta^D_{S_D})\right]$ needed for Equations (10), (11), (18), and (19). What remains is the calculation of

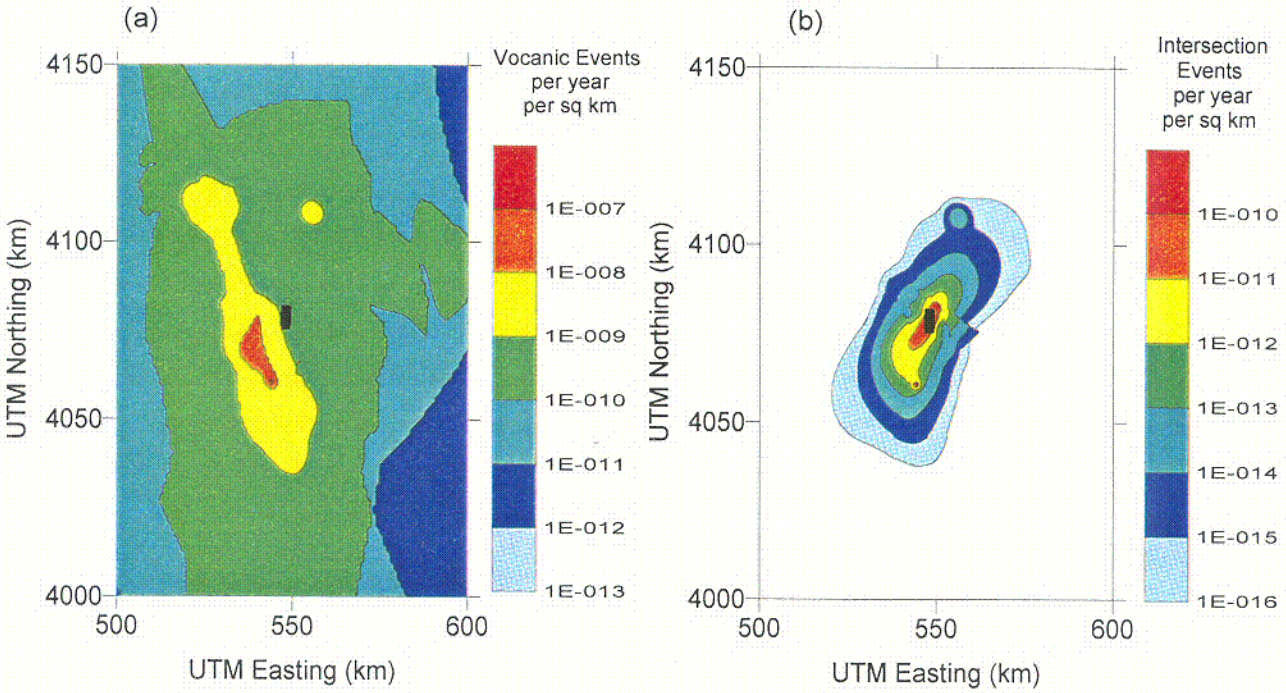

Output data. DTN: LA0005FP831811.001

NOTE: The maps represent the mean results averaged over 10 experts and over each expert's logic tree (CRWMS M&O 1996, Appendix E). Black area in center of maps is the potential repository footprint.

Figure 17. Spatial Distribution of Volcanic Hazard Defined by the PVHA Expert Panel: (a) Map of Expected Volcanic Event Frequency and (b) Map of Spatial Disaggregation of Expected Intersection Frequency

$P^I(L_m^I, \phi_n | x_i, y_j, \theta_{S_D}^D)$ and $P^I(L_m^I, \phi_n, r^{EC} | x_i, y_j, \theta_{S_D}^D)$, the discretization of the conditional probability of intersection into increments of intersection length, intersection azimuth, and number of eruptive centers within the potential repository footprint for each volcanic event location (x,y). Software routine DILECDLH V1.0 (STN: 10259-1.0-00) is used to discretize the conditional probability of intersection, $P^I(\phi | x_i, y_j, \theta_{S_D}^D)$, into the designated bins for length and azimuth within the potential repository. The inputs to program DILECDLH are: (1) the spatial disaggregation of the frequency of intersection (either the mean result conditional on $\theta_{S_D}^D$ for one expert from Step 3 or for one of the hazard simulations representative of the 95th percentile of the composite distribution from Step 4); (2) the dike length and volcanic event location distributions for the corresponding parameter set $\theta_{S_D}^D$; (3) a joint distribution for dike length and the number of eruptive centers on a dike, $P(n^{EC} = \eta | L_p, \theta_{S_D}^D)$ [computed using software routines FITIDSR V1.0 (STN: 10264-1.0-00), SFIDSR V1.0 (STN: 10276-1.0-00), and DLECD V1.0 (STN: 10260-1.0-00)]; and (4) the spatial distribution of eruptive centers along the dike. With the exception of the assessments for the number and spatial distribution of eruptive centers, all of the probability distributions required to perform this calculation are defined in CRWMS M&O (1996).

C-1

Two alternative approaches are developed for the spatial distribution of eruptive centers in Section 6.5.1.3. In the first approach (designated *IUD*) the location of each eruptive center is specified by an independent, uniform distribution over the total length of the dike, L_p. In the second approach (designated *USRD*) the eruptive centers are spaced out over the full length of the dike with the location each of the n^{EC} eruptive centers uniformly distributed in a segment of length L_p/n^{EC}. Calculations of $P^I(L_m^I, \phi_n, r^{EC} | x_i, y_j, \theta_{S_D}^D)$ are performed for both approaches. Distributions for the number of eruptive centers on a dike, $P(n^{EC} = \eta | L_p, \theta_{S_D}^D)$, are developed below.

Each of the PVHA experts made assessments for number of volcanic events represented by the observed eruptive centers. For example, the observed five volcanoes in Crater Flat may have been caused by 1 to 5 volcanic events, with each expert providing a probability distribution for the number of volcanic events. These assessments can be used to produce a distribution for the number of eruptive centers per volcanic event. For example, if Crater Flat contains five individual volcanic events, then the data indicate one eruptive center per volcanic event. If on the other hand, the five volcanoes (and their associated eruptive centers) were created by one volcanic event, then the data indicates five eruptive centers per volcanic event. Using each expert's assessments of volcanic event counts and the number of separate eruptive centers that have occurred in the Quaternary, distributions for the number of separate eruptive centers per volcanic event were developed. These are presented in Attachment III and are shown on Figure 18.

The distributions for $P(n^{EC} = \eta | L_p, \theta_{S_D}^D)$ derived in Attachment III are marginal in the sense that they are defined independent of assessments of dike length and are averaged over an expert's interpretations, Θ^E. (The experts' assessed distributions for dike length are also marginal distributions.) However, the calculations need to use the conditional distribution of number of eruptive centers given dike length. The limiting conditions that define the relationship between two variable parameters are complete independence and complete dependence. These two limiting conditions are used to define the influence of dike length on $P(n^{EC} = \eta | L_p, \theta_{S_D}^D)$. Complete independence implies that the conditional distribution for number of eruptive centers is equal to the marginal distribution, and $P(n^{EC} = \eta | L_p, \theta_{S_D}^D) = P(n^{EC} = \eta | \Theta^E)$ is used in Equation (16). The resulting discretizations of the frequency of intersection are designated: $\nu_{IUD-UC}^I(t, L_m^I, \phi_n, r^{EC} | \theta_S)$ for independent, uniformly distributed spatial locations with the number of eruptive centers uncorrelated with dike length; and $\nu_{USRD-UC}^I(t, L_m^I, \phi_n, r^{EC} | \theta_S)$ for uniformly spaced, randomly distributed spatial locations with the number of eruptive centers uncorrelated with dike length.

Complete dependence implies that the number of eruptive centers varies directly with dike length (it is considered unrealistic to have a negative correlation). The correlation between dike length and number of eruptive centers per event was set to the maximum value by making the marginal distributions for dike length and number of eruptive centers per volcanic event rank correlated.

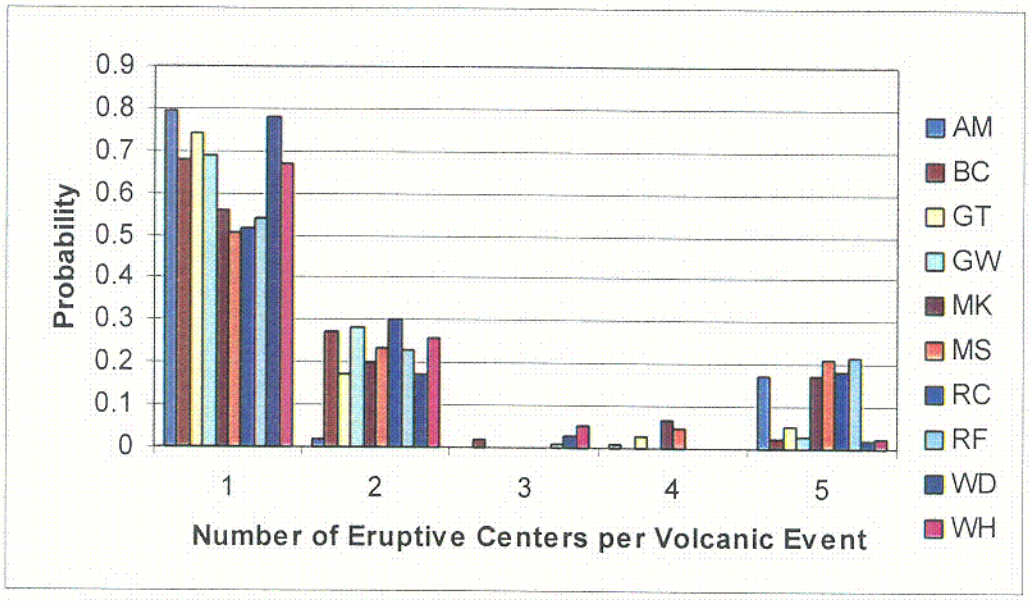

Output data. DTN: LA0005FP831811.001

NOTE: The two-letter code refers to the initials of the 10 PVHA experts in Table 5.

Figure 18. Distributions for Number of Eruptive Centers per Volcanic Event, n^{EC}, Derived from the PVHA Experts' Interpretations (from Attachment III, Figure III-1).

This is achieved by specifying a one-to-one correspondence of the marginal CDF's for the two parameters. The resulting discretizations of the frequency of intersect are designated: $\nu^{I}_{IUD-C}(t, L^{I}_{m}, \phi_n, r^{EC}|\theta_S)$ for independent, uniformly distributed spatial locations and the number of eruptive centers correlated with dike length; and $\nu^{I}_{USRD-C}(t, L^{I}_{m}, \phi_n, r^{EC}|\theta_S)$ for uniformly spaced, randomly distributed spatial locations and the number of eruptive centers correlated with dike length. These two approaches span the range of correlation considered reasonable (zero to maximum).

The longest proposed single-event dike represented by the Quaternary volcanoes in the YMR is the 11.2-kilometer spacing between Little Cones SW and Makani Cone in Crater Flat. However, many of the PVHA experts specified distributions for dike length with upper tails that greatly exceed this length. Thus, the distributions presented in Attachment III may not be representative of conditions for very long dikes. To address this issue, an alternative approach for defining the number of eruptive centers was included in which the number of eruptive centers is defined as an average density per kilometer of dike length, or equivalently, by the average spacing between eruptive centers. For a given dike length, the number of eruptive centers is found by dividing the dike length by the average spacing (rounding to the nearest integer). Consistent with the number of eruptive centers being defined by an average spacing between eruptive centers, the *USRD* spatial distribution is used. The resulting spatial distribution approach is designated *USRD-FD* for uniformly spaced, randomly distributed with fixed density.

The same process used to derive the distribution for number of eruptive centers per volcanic event from the PVHA experts' assessments was be used to evaluate the average spacing between eruptive centers. For example, if the five volcanoes in Crater Flat are considered to constitute a

single volcanic event, then the 11.2-km distance between Little Cones SE and Makani Cone in Crater Flat divided by 4 (the number of intervals between eruptive centers) gives an average spacing of 2.8 kilometers. The other Quaternary volcano cluster with multiple cones is Hidden Cone and Little Black Peak near Sleeping Butte, 2.5 km apart. If these are considered to be the result of a single volcanic event, the average spacing between eruptive centers for this event is 2.5 kilometers. If these are the only two volcanic events with multiple eruptive centers, then one obtains an average spacing for all volcanic events of 2.6 kilometers. An alternative assessment might be that Crater Flat contains two volcanic events. One volcanic event may consist of Makani and Black Cones. These two cones are located 5.4 kilometers apart. The other volcanic event would then consist of Red Cone and the two Little Cones. The distance between Red Cone and Little Cone SW is 3.2 km, resulting in an average spacing for this volcanic event of 1.6 kilometers. The average eruptive center spacing for the three volcanic events would then be 3.1 kilometers. Using each expert's assessments of volcanic event counts and the number of separate eruptive centers that have occurred in the Quaternary, the average spacing of eruptive centers was computed. These are presented in Attachment III and are summarized in Table 7.

Table 7. Average Eruptive Center Spacing
(from Attachment III, Table III-12)

PVHA Expert	Average Spacing between Eruptive Centers (km)
Alex McBirney (AM)	2.7
Bruce Crowe (BC)	1.9
George Thompson (GT)	1.5
George Walker (GW)	1.4
Mel Kuntz (MK)	2.4
Michael Sheridan (MS)	2.5
Richard Carlson (RC)	2.4
Richard Fisher (RF)	2.5
Wendell Duffield (WD)	1.4
William Hackett (WH)	2.0

Output data. DTN: LA0005FP831811.001

The values listed in Table 7 are used as an alternative approach to obtaining n^{EC}. For each simulation of a dike length, L_p, the value of n^{EC} is set to L_p divided by the average spacing from Table 7, with the quotient rounded to the nearest integer.

Figure 19 compares the probability of the occurrence of $r^{EC} = 0$, 1, 2, and $r^{EC} > 0$ [$P(r^{EC} > 0)$ is equal to 1- $P(r^{EC} = 0)$ and is the sum of $P(r^{EC} = 1)$, $P(r^{EC} = 2)$,...] eruptive centers computed using the *USRD-FD* spatial distribution and an average eruptive center spacing of 2.5 kilometers with the probabilities shown on Figure 15a for the *IUD* and *URSD* spatial distribution approaches. For short dike lengths, the *USRD-FD* approach results in a lower probability for one or more centers within the potential repository than the other two approaches. However, as the

dike length increases, the *USRD-FD* approach reaches a nearly constant probability of 0.4 for r^{EC} = 1 [0.4 = (L^l = 1)/2.5 kilometer average spacing of eruptive centers]. The oscillations in the probability about 0.4 are a result of incremental changes in n^{EC} by integer values as the length of the dike increases. The *USRD-FD* approach produces a density of eruptive centers per volcanic event for all dike lengths that is similar to that observed for the Quaternary volcanoes in the YMR. The resulting discretization of the frequency of intersection is designated $v^l_{USRD-FD}(t, L^l_m, \phi_n, r^{EC}|\theta_S)$ for uniformly spaced, randomly distributed spatial locations, with the number of eruptive centers determined by an average spacing between eruptive centers along a dike.

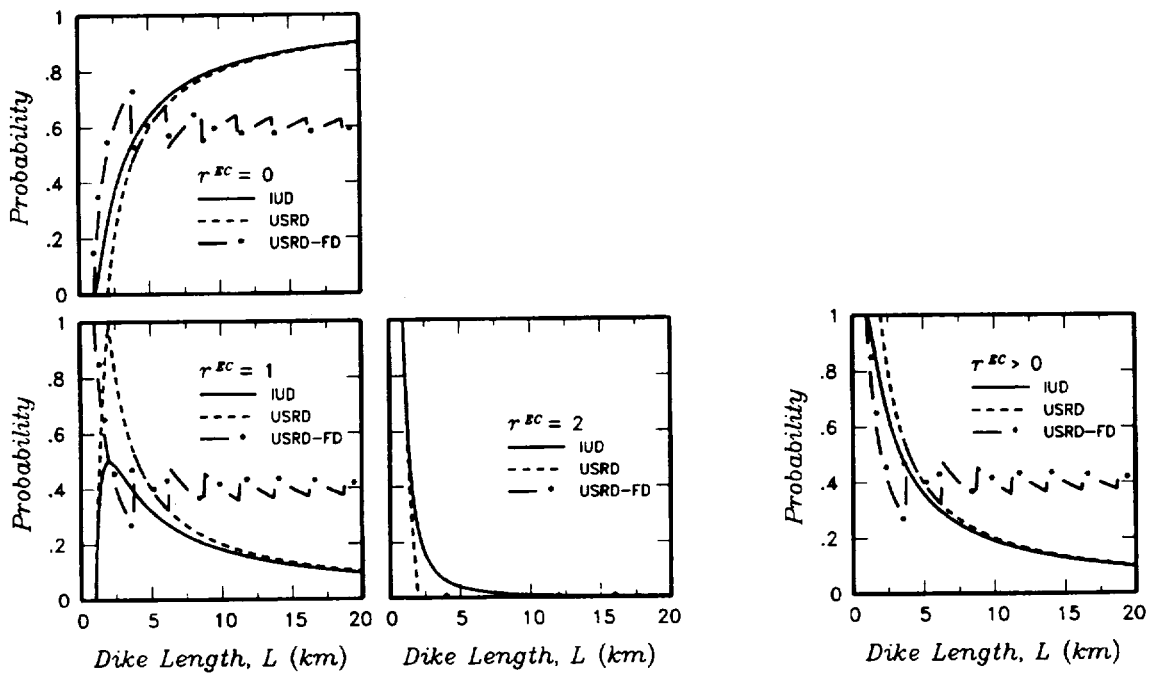

N/A - For illustration purposes only

Figure 19. Probability for the Number of Eruptive Centers within the Potential Repository Footprint, r^{EC}, Computed Using the *USRD-FD* Spatial Distribution of Eruptive Centers and for the Length of Intersection, L^l = 1 kilometer, and an Average Spacing of 2.5 kilometers between Eruptive Centers Compared to the Results for the *IUD* and *USRD* Models Shown on Figure 15a

The computation procedure used in software routine DILECDLH V1.0 is as follows:

Step 5a. An input file is created that contains the probability distributions for the length of the dike, L, and number of eruptive centers per volcanic event, n^{EC}. The probability distribution for L is discretized into the probability mass for L_p in 0.05 kilometer increments using module FITIDSR V1.0 (STN: 10264-1.0-00) or SFIDSR V1.0 (STN: 10276-1.0-00). The marginal distribution for n^{EC} is listed at the top of the file and the rank correlated value for n^{EC} is listed for each value of L by determining the value in the marginal distribution for n^{EC} that has the same cumulative probability as L_p in the marginal distribution for L.

Step 5b. For each of the dike parameter sets, $\theta^D_{S_D}$, the spatial disaggregation of the hazard computed in Steps 3 and 4 is then input into the program. At each location (x,y) that contributes to the frequency of intersection $\{ v^I_{x_i,y_j}(t|\theta^E_{sim_{ISP}}, \theta^E_{sim_{ASM}}, \theta^D_{sim_D})$ or $\mathrm{E}\left[v^I_{x_i,y_j}(t|\theta^D_{S_D}) > 0\right\}$ the direction toward the potential repository is sampled over 5° increments in azimuth, with the probability distribution for $P^I(\phi_n|\theta^D_{S_D})$ obtained by computing the probability mass in the interval ϕ_n-2.5° ≤ ϕ ≤ ϕ_n-2.5°. At each azimuth, ϕ_n, 100 simulations of L_{sim} and E^L_{sim} are created by Latin hypercube sampling from the distributions defined for each. For those combinations of L_p and E^L_o at azimuth ϕ_n that result in intersections with the potential repository footprint, L^I is computed. The probability $P^I(L^I_m, \phi_n|x_i, y_j, \theta^D_{S_D})$ defined in Equation (8) is now approximated by the expression:

$$P^I(L^I_m, \phi_n|x_i, y_j, \theta_S) \sim \tfrac{1}{100}\,\delta(L^I = L^I_m)\cdot P(\phi_n|\theta_S) \qquad \text{(Eq. 24)}$$

and the probability $P^I(r^{EC}, L^I_m, \phi_n|x_i, y_j, \theta^D_{S_D})$ in Equation (16) is approximated by

$$P^I(r^{EC}, L^I_m, \phi_n|x_i, y_j, \theta^D_{S_D}) \sim \tfrac{1}{100}\sum_{sim=1}^{sim=100}\delta(L^I = L^I_m)\cdot P(\phi_n|\theta^D_{S_D})\times \sum_{\eta=1}^{\eta=n^{EC}_{max}} P(n^{EC} = \eta|L_{sim}, \theta^D_{S_D})P(r^{EC}|L_{sim}, L^I_m, n^{EC} = \eta) \qquad \text{(Eq. 25)}$$

where $\delta(L^I = L^I_m)$ = 1 for those simulation values of L_{sim} and E^L_{sim} at azimuth ϕ_n that result in L^I=L^I_m for a volcanic event at (x,y), and $\delta(L^I = L^I_m)$ = 0 otherwise. An increment of 0.05 kilometer is chosen for the intersection length bin size. This length bin size, together with the azimuth bin size of 5° are sufficient to clearly define the variability in the length and azimuth of intersecting dikes. (Note that the computation of the frequency of intersection is independent of these bin sizes.) Equation (25) is used five times for the five alternative approaches for $P(n^{EC} = \eta|L_{sim}, \theta^D_{S_D})$ and $P(r^{EC}|L_{sim}, L^I_m, n^{EC} = \eta)$ described above.

Step 5c. The results of step 5b are then used in Equations (11) and (19) to estimate the expected frequencies of intersection $\mathrm{E}\left[v^I(t, L^I_m, \phi_n|\Theta)\right]$ and $\mathrm{E}\left[v^I(t, L^I_m, \phi_n, r^{EC}|\Theta)\right]$, respectively for each of the PVHA expert's interpretations. The definition for $P(\Theta^D = \theta^D_{S_D})$ used in Equation (23) is used in this calculation. The results for each expert are then averaged to obtain an estimate of the composite expected frequencies over all experts using the expressions:

$$\mathrm{E}\left[\nu^{I}(t,L^{I}_{m},\phi_{n})\right]\sim\tfrac{1}{10}\sum_{\text{expert 1}}^{\text{expert 10}}\mathrm{E}\left[\nu^{I}(t,L^{I}_{m},\phi_{n}|\Theta)\right]$$

and (Eq. 26)

$$\mathrm{E}\left[\nu^{I}(t,L^{I}_{m},\phi_{n},r^{EC})\right]\sim\tfrac{1}{10}\sum_{\text{expert 1}}^{\text{expert 10}}\mathrm{E}\left[\nu^{I}(t,L^{I}_{m},\phi_{n},r^{EC}|\Theta)\right]$$

This calculation is performed using software routine COMBSM V1.0 (STN: 10256-1.0-00). The resulting partial frequencies of intersection are then normalized to produce conditional distributions. At each value of L^{I}_{m} and ϕ_n, the computed vales of $\mathrm{E}\left[\nu^{I}(t,L^{I}_{m},\phi_{n},r^{EC})\right]$ are divided by $\mathrm{E}\left[\nu^{I}(t,L^{I}_{m},\phi_{n})\right]$ to produce a distribution for r^{EC} conditional on L^{I}_{m} and ϕ_n. The values of $\mathrm{E}\left[\nu^{I}(t,L^{I}_{m},\phi_{n})\right]$ are, in turn, divided by $\mathrm{E}\left[\nu^{I}(t)\right]$ to produce a joint distribution for L^{I}_{m} and ϕ_n conditional on the mean frequency of intersection. Because Latin hypercube sampling was used instead of full enumeration in (2), at a few of the points (x,y) that contribute to the frequency of intersection computed in Step (3) the 100 simulated values of L_{sim} and E^{L}_{sim} do not produce any intersections. These occur at locations where only the longest possible dikes combined with values of E^{L} very near 1.0 result in intersections of the potential repository footprint. As a result, the sum of $\mathrm{E}\left[\nu^{I}(t,L^{I}_{m},\phi_{n}|\Theta)\right]$ over L^{I}_{m} and ϕ_n for each expert typically equaled about 97% to 99% of $\mathrm{E}\left[\nu^{I}(t|\Theta)\right]$. Because the purpose of Step 5 is to obtain a conditional distribution, the computed values of $\mathrm{E}\left[\nu^{I}(t,L^{I}_{m},\phi_{n}|\Theta)\right]$ for each expert were normalized in software routine COMBSM V1.0 to sum to the value of $\mathrm{E}\left[\nu^{I}(t|\Theta)\right]$ computed in Step (3). [Note that the true value of $\mathrm{E}\left[\nu^{I}(t|\Theta)\right]$ was computed by full enumeration of the individual expert interpretations.]

Step 5d. Step 4 identified those simulation results that represented the 5th and 95th percentiles of the composite distribution for frequency of intersection. For these parameter sets, designated $\theta^{0.05}$ and $\theta^{0.95}$, the results of step 5b are used in Equations (10) and (18) to compute the values of $\nu^{I}(t,L^{I}_{m},\phi_{n}|\theta^{0.05})$ and $\nu^{I}(t,L^{I}_{m},\phi_{n},r^{EC}|\theta^{0.05})$, respectively, for the 5th percentile hazard and $\nu^{I}(t,L^{I}_{m},\phi_{n}|\theta^{0.95})$ and $\nu^{I}(t,L^{I}_{m},\phi_{n},r^{EC}|\theta^{0.95})$, respectively, for the 95th percentile hazard. The results of the individual simulations are averaged using software routine COMBSF V1.0 (STN: 10255-1.0-00) to produce the final values of $\nu^{I}(t,L^{I}_{m},\phi_{n}|\theta^{0.05})$, $\nu^{I}(t,L^{I}_{m},\phi_{n},r^{EC}|\theta^{0.05})$, $\nu^{I}(t,L^{I}_{m},\phi_{n}|\theta^{0.95})$ and $\nu^{I}(t,L^{I}_{m},\phi_{n},r^{EC}|\theta^{0.95})$. Routine COMBSF V1.0 performed this calculation, including the normalization so that the sum of $\nu^{I}(t,L^{I}_{m},\phi_{n}|\theta^{0.xx})$ over L^{I}_{m} and ϕ_n equals $\nu^{I}(t|\theta^{0.xx})$ obtained in Step 4. The resulting disaggregated frequencies of intersection are then normalized to produce conditional distributions. At each value of L^{I}_{m} and ϕ_n, the computed values of $\nu^{I}(t,L^{I}_{m},\phi_{n},r^{EC}|\theta^{0.05})$ are divided by $\nu^{I}(t,L^{I}_{m},\phi_{n}|\theta^{0.05})$ and the values of $\nu^{I}(t,L^{I}_{m},\phi_{n},r^{EC}|\theta^{0.95})$ are divided by $\nu^{I}(t,L^{I}_{m},\phi_{n}|\theta^{0.95})$ to produce a distribution for r^{EC} conditional on L^{I}_{m} and ϕ_n. The values of $\nu^{I}(t,L^{I}_{m},\phi_{n}|\theta^{0.05})$ are, in turn, divided by $\nu^{I}(t|\theta^{0.05})$ and the values $\nu^{I}(t,L^{I}_{m},\phi_{n}|\theta^{0.95})$ are

divided by $\nu^I(t|\theta^{0.95})$ to produce joint distributions for L^I_m and ϕ_n conditional on the 5th and 95th percentile values for the frequency of intersection.

In summary, the mathematical formulation for computing the conditional distribution for the length and azimuth of intersecting dikes within the potential repository footprint is developed directly from the PVHA formulation presented in CRWMS M&O (1996, Section 3 and Appendix E) without invoking any additional assumptions. The formulation for computing the conditional distribution for the number of eruptive centers occurring within the potential repository footprint requires additional assumptions in order to assess the number of eruptive centers per volcanic event and the spatial distribution of eruptive centers along the length of the dike. Five alternative approaches are developed to implement these assumptions to span the range of available approaches. Calculations are performed for all five approaches to indicate the sensitivity of the results. As a final step, relative weights are assigned to the five approaches in order that a composite result can be obtained. The five approaches are summarized below:

1. The Independent, Uniformly Distributed, Uncorrelated (*IUD-UC*) approach. The distribution for the number of eruptive centers per volcanic event is derived from the PVHA experts' interpretations. These distributions are uncorrelated with the distributions for dike length. The location for each eruptive center is defined by a uniform distribution over the total length of the dike, and if multiple eruptive centers occur in a volcanic event, the distributions for their locations are independent.

2. The Independent, Uniformly Distributed, Correlated (*IUD-C*) approach. The distribution for the number of eruptive centers per volcanic event is derived from the PVHA experts' interpretations. These distributions are completely correlated with the distributions for dike length. The location for each eruptive center is defined by a uniform distribution over the total length of the dike, and if multiple eruptive centers occur in a volcanic event, the distributions for their locations are independent.

3. The Uniformly Spaced, Randomly Distributed, Uncorrelated (*USRD-UC*) approach. The distribution for the number of eruptive centers per volcanic event is derived from the PVHA experts' interpretations. These distributions are uncorrelated with the distributions for dike length. The total length of the dike is divided into equal segments for each eruptive center. Within each segment, the location of the eruptive center is defined by a uniform distribution over the length of the segment.

4. The Uniformly Spaced, Randomly Distributed, Correlated (*USRD-C*) approach. The distribution for the number of eruptive centers per volcanic event is derived from the PVHA experts' interpretations. These distributions are completely correlated with the distributions for dike length. The total length of the dike is divided into equal segments for each eruptive center. Within each segment, the location of the eruptive center is defined by a uniform distribution over the length of the segment.

5. The Uniformly-Spaced, Randomly Distributed, Fixed Density (*USRD-FD*) approach. The number of eruptive centers per volcanic event is determined by dividing the total length of the dike by an average distance between eruptive centers derived from the PVHA experts'

interpretations. The total length of the dike is divided into equal segments for each eruptive center. Within each segment, the location of the eruptive center is defined by a uniform distribution over the length of the segment.

Application of the results of this AMR in assessing the impact of disruptive events will require a rule for combining the results for these five approaches. In the overall framework of the PVHA, this is accomplished by assigning weights to each model. These weights are derived by separately examining the three issues addressed by the alternative approaches.

The first issue is the overall approach for evaluating the number of eruptive centers per volcanic event. The two approaches are to define a distribution for the total number based on the observed Quaternary data or to define the average spacing using the Quaternary data and compute the number for each dike length. These two approaches are considered to be equally credible. They both rely to an equal degree on the observed data and the PVHA experts' interpretations of these data to define the characteristics of volcanic events in the YMR. Thus, the two approaches are given equal weight.

The second issue is the appropriate spatial distribution for eruptive centers along the length of the dike. Two alternative approaches are used, one in which the location of each eruptive center is independent of the others (*IUD*) and one in which the eruptive centers are spaced out along the dike (*USRD*). The simulations shown on Figure 14 indicate that the *IUD* spatial model often produces tight clustering of multiple eruptive centers. This is somewhat at odds with the limited observations for eruptive centers in the vicinity of Yucca Mountain. Therefore, the *URSD* model is strongly preferred over the *IUD* model by a ratio of 3:1, yielding weights of 0.75 for the *USRD* models and 0.25 for the *IUD* models. Note that this assessment applies to the cases where the number of eruptive centers is derived from the distributions shown on Figure 18. When the number of eruptive centers is derived from an average spacing, it is assumed that only the *USRD* model applies.

The third issue addresses the correlation between the distributions for number of eruptive centers per volcanic event shown on Figure 18 and the distributions for the length of the dike associated with a volcanic event developed by the PVHA experts. Two alternatives were used: the two distributions are uncorrelated and the two distributions are fully correlated. It is likely that there is some degree of correlation because longer dikes would provide more opportunity for the formation of vents and presumably result from volcanic events with larger volumes. Thus, the fully correlated model is slightly favored (0.6) to the uncorrelated model (0.4). Again, this assessment applies only to the cases where the number of eruptive centers is derived from the distributions shown in Figure 18.

Combining these three sets of weights yields the following relative weighting of the five approaches for computing the conditional distribution for number of eruptive centers within the potential repository footprint:

- The weight for the *IUD-UC* approach is equal to 0.5 for the approach for number of centers times 0.25 for the spatial approach times 0.4 for uncorrelated number of eruptive centers and dike length distributions, yielding a weight of 0.05.

- The weight for the *IUD-C* approach is equal to 0.5 for the approach for number of centers times 0.25 for the spatial approach times 0.6 for correlated number of eruptive centers and dike length distributions, yielding a weight of 0.075.

- The weight for the *USRD-UC* approach is equal to 0.5 for the approach for number of centers times 0.75 for the spatial approach times 0.4 for uncorrelated number of eruptive centers and dike length distributions, yielding a weight of 0.15.

- The weight for the *USRD-C* approach is equal to 0.5 for the approach for number of centers times 0.75 for the spatial approach times 0.6 for uncorrelated number of eruptive centers and dike length distributions, yielding a weight of 0.225.

- The weight for the *USRD-FD* approach is 0.5 for the approach, with only the *USRD* spatial approach applying and the correlation issue not pertinent, yielding a weight of 0.5.

These weights are used to combine the results of consequence evaluations for the five alternative approaches of number of eruptive centers in downstream analyses.

6.5.3 Results

6.5.3.1 Frequency of Intersection of the Potential Repository Footprint by a Dike

Tables 8 and 9 list the mean annual frequency of intersection of the potential repository footprint and percentiles of the distribution for the frequency of intersection computed by full enumeration and by Latin simulation for the Primary Block and the Primary + Contingency Blocks potential repository configurations, respectively. The results are listed for each expert, indicated by the expert's initials from Table 5, and for the composite distribution over all 10 experts. The results computed by full enumeration of the experts' logic trees are indicated by the suffix –FEn in the column headings (e.g., AM-FEn) and the results computed by simulation are indicated by the suffix –Sim in the column headings (e.g., AM-Sim). The percent difference in the frequency of intersection is also listed in the table. The differences between the frequencies of intersection computed by full enumeration and by simulation are small, indicating that simulation with Latin hypercube sampling reliably represents the full distribution for frequency of intersection.

Table 8. Frequency of Intersection for Primary Block (drifts 1-50)

	AM[1]-FEn[2]	AM-Sim[2]	% difference[3]	BC-Fen	BC-Sim	% difference	GT-FEn	GT-Sim	% difference
Mean	4.79E-09	4.82E-09	0.6	1.05E-08	1.05E-08	-0.3	3.25E-08	3.21E-08	-1.3
0.05	1.18E-09	1.18E-09	0.5	9.55E-10	8.75E-10	-8.4	1.05E-08	9.97E-09	-4.8
0.1	1.45E-09	1.63E-09	12.9	1.55E-09	1.44E-09	-6.8	1.29E-08	1.28E-08	-0.9
0.15	1.66E-09	1.71E-09	2.9	1.95E-09	1.83E-09	-6.2	1.51E-08	1.47E-08	-2.8
0.2	1.82E-09	1.89E-09	3.8	2.29E-09	2.15E-09	-6.0	1.74E-08	1.65E-08	-5.4
0.3	2.09E-09	2.14E-09	2.5	3.09E-09	3.06E-09	-1.0	1.95E-08	1.94E-08	-0.5
0.4	2.34E-09	2.37E-09	1.2	4.37E-09	4.28E-09	-1.9	2.24E-08	2.27E-08	1.6
0.5	2.75E-09	2.67E-09	-3.2	6.46E-09	6.66E-09	3.1	2.69E-08	2.76E-08	2.6
0.6	3.31E-09	3.20E-09	-3.3	1.02E-08	1.06E-08	3.6	3.24E-08	3.33E-08	2.9
0.7	4.17E-09	4.11E-09	-1.4	1.38E-08	1.38E-08	0.3	3.80E-08	3.75E-08	-1.4
0.8	6.17E-09	5.73E-09	-7.0	1.82E-08	1.85E-08	1.4	4.47E-08	4.29E-08	-3.9
0.85	7.41E-09	7.75E-09	4.5	2.04E-08	2.05E-08	0.3	5.37E-08	4.93E-08	-8.3
0.9	1.12E-08	1.02E-08	-8.9	2.34E-08	2.35E-08	0.4	5.75E-08	5.63E-08	-2.1
0.95	1.70E-08	1.75E-08	2.8	3.16E-08	3.07E-08	-2.8	6.76E-08	6.50E-08	-3.9
	GW-FEn	**GW-Sim**	**% difference**	**MK-Fen**	**MK-Sim**	**% difference**	**MS-FEn**	**MS-Sim**	**% difference**
Mean	5.76E-09	5.94E-09	3.0	9.81E-09	9.60E-09	-2.2	1.68E-08	1.61E-08	-4.2
0.05	1.07E-09	9.85E-10	-8.2	3.63E-10	3.65E-10	0.5	2.88E-09	2.96E-09	2.7
0.1	1.48E-09	1.53E-09	3.3	7.41E-10	8.46E-10	14.1	4.17E-09	3.88E-09	-6.9
0.15	1.86E-09	1.78E-09	-4.6	1.48E-09	1.60E-09	8.0	5.25E-09	4.78E-09	-8.9
0.2	2.19E-09	2.03E-09	-7.3	2.09E-09	2.17E-09	3.7	6.31E-09	5.50E-09	-12.9
0.3	2.82E-09	2.65E-09	-6.0	3.39E-09	3.22E-09	-4.9	8.71E-09	7.53E-09	-13.6
0.4	3.47E-09	3.38E-09	-2.5	4.90E-09	4.55E-09	-7.1	1.10E-08	9.72E-09	-11.3
0.5	4.27E-09	4.20E-09	-1.5	6.46E-09	6.22E-09	-3.7	1.38E-08	1.27E-08	-7.8
0.6	5.37E-09	5.09E-09	-5.1	8.51E-09	8.42E-09	-1.1	1.70E-08	1.63E-08	-4.3
0.7	6.76E-09	6.84E-09	1.1	1.15E-08	1.13E-08	-2.0	2.04E-08	2.04E-08	-0.1
0.8	8.71E-09	8.94E-09	2.6	1.48E-08	1.50E-08	1.4	2.46E-08	2.44E-08	-0.5
0.85	1.00E-08	9.92E-09	-0.8	1.74E-08	1.77E-08	1.6	2.75E-08	2.76E-08	0.2
0.9	1.18E-08	1.20E-08	2.2	2.19E-08	2.16E-08	-1.5	3.16E-08	3.14E-08	-0.7
0.95	1.48E-08	1.35E-08	-8.5	2.88E-08	2.84E-08	-1.6	3.98E-08	3.87E-08	-2.7
	RC-FEn	**RC-Sim**	**% difference**	**RF-Fen**	**RF-Sim**	**% difference**	**WD-FEn**	**WD-Sim**	**% difference**
Mean	1.33E-08	1.28E-08	-3.7	1.73E-08	1.71E-08	-1.2	1.50E-09	1.74E-09	16.2
0.05	1.12E-09	1.18E-09	4.7	3.55E-09	3.66E-09	3.3	1.20E-10	1.20E-10	0.0
0.1	1.74E-09	1.74E-09	0.1	5.13E-09	4.86E-09	-5.3	1.86E-10	1.84E-10	-1.2
0.15	2.29E-09	2.26E-09	-1.4	6.31E-09	5.94E-09	-5.9	2.29E-10	2.30E-10	0.4
0.2	3.02E-09	2.88E-09	-4.6	7.41E-09	7.03E-09	-5.2	3.09E-10	3.21E-10	3.8
0.3	4.27E-09	4.12E-09	-3.4	9.55E-09	9.41E-09	-1.4	4.90E-10	4.84E-10	-1.2
0.4	6.31E-09	6.97E-09	10.5	1.20E-08	1.20E-08	0.2	9.12E-10	6.79E-10	-25.6
0.5	8.13E-09	8.28E-09	1.9	1.45E-08	1.47E-08	2.0	1.12E-09	1.13E-09	0.9
0.6	1.05E-08	1.06E-08	1.5	1.74E-08	1.69E-08	-2.6	1.12E-09	1.13E-09	1.1
0.7	1.51E-08	1.53E-08	1.0	2.04E-08	2.02E-08	-1.1	1.38E-09	1.40E-09	1.4
0.8	1.91E-08	1.90E-08	-0.1	2.46E-08	2.46E-08	0.0	2.40E-09	2.10E-09	-12.5
0.85	2.57E-08	2.51E-08	-2.4	2.82E-08	2.78E-08	-1.5	2.69E-09	2.68E-09	-0.4
0.9	3.02E-08	2.98E-08	-1.2	3.24E-08	3.28E-08	1.4	3.47E-09	3.50E-09	1.0
0.95	4.37E-08	3.55E-08	-18.7	4.07E-08	3.94E-08	-3.3	4.17E-09	4.90E-09	17.6

	WH-FEn	WH-Sim	% difference	Composite Fen	Composite sim	% difference
Mean	2.97E-08	2.97E-08	0.1	1.42E-08	1.40E-08	-1.2
0.05	5.62E-09	5.70E-09	1.3	6.61E-10	6.16E-10	-6.8
0.1	7.08E-09	6.95E-09	-1.8	1.20E-09	1.18E-09	-1.5
0.15	8.51E-09	8.45E-09	-0.7	1.78E-09	1.81E-09	1.5
0.2	1.00E-08	9.94E-09	-0.6	2.29E-09	2.21E-09	-3.4
0.3	1.41E-08	1.43E-08	1.1	3.55E-09	3.47E-09	-2.1
0.4	1.95E-08	1.94E-08	-0.5	5.62E-09	5.46E-09	-2.8
0.5	2.46E-08	2.48E-08	1.0	8.32E-09	8.32E-09	0.0
0.6	3.02E-08	3.00E-08	-0.6	1.20E-08	1.19E-08	-1.3
0.7	3.63E-08	3.60E-08	-0.8	1.70E-08	1.69E-08	-0.2
0.8	4.57E-08	4.54E-08	-0.8	2.29E-08	2.30E-08	0.5
0.85	5.13E-08	5.16E-08	0.6	2.75E-08	2.77E-08	0.5
0.9	5.89E-08	5.94E-08	0.9	3.47E-08	3.42E-08	-1.3
0.95	7.41E-08	7.57E-08	2.1	4.68E-08	4.51E-08	-3.5

Output data. DTN: LA0005FP831811.001

NOTES: [1] AM - Alex McBirney, BC – Bruce Crowe, GT – George Thompson, GW – George Walker, MK – Mel Kuntz, MS – Michael Sheridan, RC – Richard Carlson, RF – Richard Fisher, WD – Wendell Duffield, WH – William Hackett

[2] FEn – results from full enumeration, Sim – results from simulations with Latin hypercube sampling.

[3] The percent difference is computed as (Sim – FEn)/FEn. It represents the percent difference between the frequency of intersection computed by full enumeration and by simulation.

Table 9. Frequency of Intersection for Primary+Contingency Blocks (drifts 1-60)

	AM[1]-FEn[2]	AM-Sim[2]	% difference[3]	BC-Fen	BC-Sim	% difference	GT-FEn	GT-Sim	% difference
Mean	5.29E-09	5.34E-09	0.8	1.13E-08	1.13E-08	-0.2	3.49E-08	3.45E-08	-1.3
0.05	1.26E-09	1.26E-09	0.4	1.07E-09	1.00E-09	-6.4	1.12E-08	1.07E-08	-4.5
0.1	1.59E-09	1.74E-09	9.7	1.70E-09	1.60E-09	-5.5	1.38E-08	1.37E-08	-0.6
0.15	1.78E-09	1.86E-09	4.8	2.14E-09	2.02E-09	-5.5	1.62E-08	1.59E-08	-2.1
0.2	1.95E-09	1.99E-09	1.8	2.51E-09	2.37E-09	-5.8	1.86E-08	1.78E-08	-4.6
0.3	2.24E-09	2.32E-09	3.7	3.39E-09	3.38E-09	-0.3	2.14E-08	2.09E-08	-2.5
0.4	2.57E-09	2.56E-09	-0.6	4.68E-09	4.66E-09	-0.3	2.40E-08	2.46E-08	2.4
0.5	2.95E-09	2.86E-09	-3.2	7.08E-09	7.38E-09	4.3	2.95E-08	2.99E-08	1.2
0.6	3.55E-09	3.49E-09	-1.7	1.12E-08	1.14E-08	1.2	3.47E-08	3.58E-08	3.2
0.7	4.47E-09	4.55E-09	1.9	1.48E-08	1.49E-08	0.8	4.17E-08	4.03E-08	-3.4
0.8	6.76E-09	6.32E-09	-6.5	2.00E-08	1.99E-08	-0.1	4.79E-08	4.62E-08	-3.5
0.85	8.32E-09	8.74E-09	5.0	2.19E-08	2.19E-08	0.0	5.75E-08	5.31E-08	-7.8
0.9	1.29E-08	1.14E-08	-11.8	2.57E-08	2.54E-08	-1.1	6.17E-08	6.05E-08	-1.9
0.95	1.86E-08	1.99E-08	6.9	3.47E-08	3.32E-08	-4.2	7.24E-08	6.98E-08	-3.6
	GW-FEn	**GW-Sim**	**% difference**	**MK-Fen**	**MK-Sim**	**% difference**	**MS-FEn**	**MS-Sim**	**% difference**
Mean	6.67E-09	6.87E-09	3.0	1.08E-08	1.06E-08	-2.0	1.86E-08	1.82E-08	-2.0
0.05	1.26E-09	1.16E-09	-7.5	4.07E-10	4.62E-10	13.3	3.31E-09	3.43E-09	3.7
0.1	1.74E-09	1.74E-09	0.2	8.51E-10	9.60E-10	12.7	4.79E-09	4.41E-09	-8.0
0.15	2.19E-09	2.03E-09	-7.1	1.70E-09	1.86E-09	9.3	6.03E-09	5.49E-09	-8.9
0.2	2.51E-09	2.31E-09	-7.9	2.34E-09	2.43E-09	3.5	7.24E-09	6.43E-09	-11.2
0.3	3.24E-09	3.10E-09	-4.1	3.80E-09	3.73E-09	-1.9	9.77E-09	8.62E-09	-11.8
0.4	4.07E-09	3.88E-09	-4.7	5.37E-09	5.20E-09	-3.2	1.26E-08	1.14E-08	-9.5
0.5	5.01E-09	4.83E-09	-3.6	7.24E-09	7.01E-09	-3.3	1.55E-08	1.46E-08	-5.5
0.6	6.17E-09	5.94E-09	-3.7	9.33E-09	9.40E-09	0.7	1.86E-08	1.80E-08	-3.6
0.7	7.76E-09	7.86E-09	1.2	1.26E-08	1.23E-08	-2.5	2.24E-08	2.24E-08	0.1
0.8	1.02E-08	1.03E-08	0.3	1.62E-08	1.66E-08	2.1	2.75E-08	2.74E-08	-0.4
0.85	1.15E-08	1.14E-08	-0.4	1.91E-08	1.95E-08	2.3	3.02E-08	3.15E-08	4.1
0.9	1.35E-08	1.37E-08	1.2	2.40E-08	2.33E-08	-2.8	3.55E-08	3.59E-08	1.3
0.95	1.70E-08	1.57E-08	-7.5	3.16E-08	3.12E-08	-1.3	4.37E-08	4.40E-08	0.7
	RC-FEn	**RC-Sim**	**% difference**	**RF-Fen**	**RF-Sim**	**% difference**	**WD-FEn**	**WD-Sim**	**% difference**
Mean	1.46E-08	1.42E-08	-2.9	1.93E-08	1.91E-08	-1.0	1.64E-09	1.90E-09	15.6
0.05	1.26E-09	1.37E-09	8.4	3.98E-09	4.01E-09	0.7	1.48E-10	1.46E-10	-1.0
0.1	1.95E-09	1.92E-09	-1.4	5.75E-09	5.44E-09	-5.4	2.24E-10	2.24E-10	0.0
0.15	2.63E-09	2.54E-09	-3.3	7.08E-09	6.71E-09	-5.3	2.82E-10	2.80E-10	-0.6
0.2	3.39E-09	3.16E-09	-6.9	8.32E-09	7.97E-09	-4.2	3.47E-10	3.59E-10	3.6
0.3	4.79E-09	4.46E-09	-6.9	1.07E-08	1.06E-08	-0.9	5.89E-10	5.89E-10	0.0
0.4	7.08E-09	7.52E-09	6.2	1.32E-08	1.34E-08	1.8	1.00E-09	7.57E-10	-24.3
0.5	8.91E-09	9.43E-09	5.8	1.62E-08	1.65E-08	1.5	1.26E-09	1.26E-09	0.2
0.6	1.15E-08	1.15E-08	0.2	1.91E-08	1.88E-08	-1.1	1.26E-09	1.26E-09	0.3
0.7	1.66E-08	1.68E-08	1.4	2.29E-08	2.26E-08	-1.6	1.51E-09	1.52E-09	0.1
0.8	2.09E-08	2.17E-08	4.1	2.75E-08	2.69E-08	-2.3	2.63E-09	2.31E-09	-12.1
0.85	2.82E-08	2.78E-08	-1.3	3.09E-08	3.11E-08	0.5	3.02E-09	2.99E-09	-1.1
0.9	3.31E-08	3.28E-08	-1.0	3.63E-08	3.71E-08	2.2	3.72E-09	3.75E-09	1.0
0.95	4.79E-08	3.89E-08	-18.8	4.57E-08	4.39E-08	-4.0	4.47E-09	5.25E-09	17.6

	WH-FEn	WH-Sim	% difference	Composite Fen	Composite Sim	% difference
Mean	3.19E-08	3.23E-08	1.4	1.55E-08	1.54E-08	-0.5
0.05	6.03E-09	6.06E-09	0.6	7.59E-10	6.86E-10	-9.5
0.1	7.76E-09	7.77E-09	0.1	1.35E-09	1.33E-09	-1.8
0.15	9.33E-09	9.23E-09	-1.1	1.95E-09	1.98E-09	1.4
0.2	1.10E-08	1.09E-08	-1.0	2.57E-09	2.45E-09	-4.7
0.3	1.55E-08	1.53E-08	-1.2	3.89E-09	3.86E-09	-0.8
0.4	2.09E-08	2.05E-08	-1.9	6.31E-09	6.12E-09	-3.1
0.5	2.63E-08	2.63E-08	0.0	9.33E-09	9.30E-09	-0.4
0.6	3.24E-08	3.18E-08	-1.7	1.32E-08	1.32E-08	0.1
0.7	3.89E-08	3.88E-08	-0.4	1.86E-08	1.87E-08	0.2
0.8	4.90E-08	4.91E-08	0.2	2.51E-08	2.54E-08	0.9
0.85	5.50E-08	5.50E-08	0.1	3.02E-08	3.02E-08	0.1
0.9	6.31E-08	6.33E-08	0.3	3.80E-08	3.77E-08	-0.9
0.95	7.94E-08	8.24E-08	3.7	5.01E-08	4.91E-08	-2.1

Output data. DTN: LA0005FP831811.001

NOTES: [1] AM - Alex McBirney, BC – Bruce Crowe, GT – George Thompson, GW – George Walker, MK – Mel Kuntz, MS – Michael Sheridan, RC – Richard Carlson, RF – Richard Fisher, WD – Wendell Duffield, WH – William Hackett
[2] FEn – results from full enumeration, Sim – results from simulations with Latin hypercube sampling. sampling.
[3] The percent difference is computed as (Sim – FEn)/FEn. It represents the percent difference between the frequency of intersection computed by full enumeration and by simulation.

The computed distributions for the annual frequency of intersection of the potential repository footprint by a dike are shown on Figures 20 and 21 for the Primary Block and Primary + Contingency Blocks potential repository footprints, respectively. Part (a) of Figures 20 and 21 show the computed distributions for the frequency of intersection aggregated over all of the 10 PVHA experts' interpretations together with the median and mean values obtained for each expert's interpretation. Part (b) of Figures 20 and 21 compare the 5th to 95th percentile range for frequency of intersection obtained for each expert's interpretation with that for the aggregate distributions.

The computed mean annual frequencies of intersection of the potential repository footprint by a dike are 1.4×10^{-8} for the Primary Block case and 1.6×10^{-8} for the Primary + Contingency Blocks case as compared to 1.5×10^{-8} obtained in the PVHA (CRWMS M&O 1996). The computed 5th percentiles of the uncertainty distribution for frequency of intersection are 6.6×10^{-10} for the Primary Block case and 7.6×10^{-10} for the Primary + Contingency Blocks case as compared to 5.4×10^{-10} obtained in the PVHA (CRWMS M&O 1996). The computed 95th percentiles of the uncertainty distribution for frequency of intersection are 4.7×10^{-8} for the Primary Block case and 5.0×10^{-8} for the Primary + Contingency Blocks case as compared to 4.9×10^{-8} obtained in the PVHA (CRWMS M&O 1996).

The composite uncertainty distributions for frequency of intersection are located in the output files PVHA-PB.DST and PVHA-PCB.DST for transmittal to users of the results of this AMR.

Each file consists of a title record, a record giving the number of points in the composite distribution, and *n* records containing the *n* discrete values of frequency of intersection, the associated probability mass, and the cumulative probability (CDF).

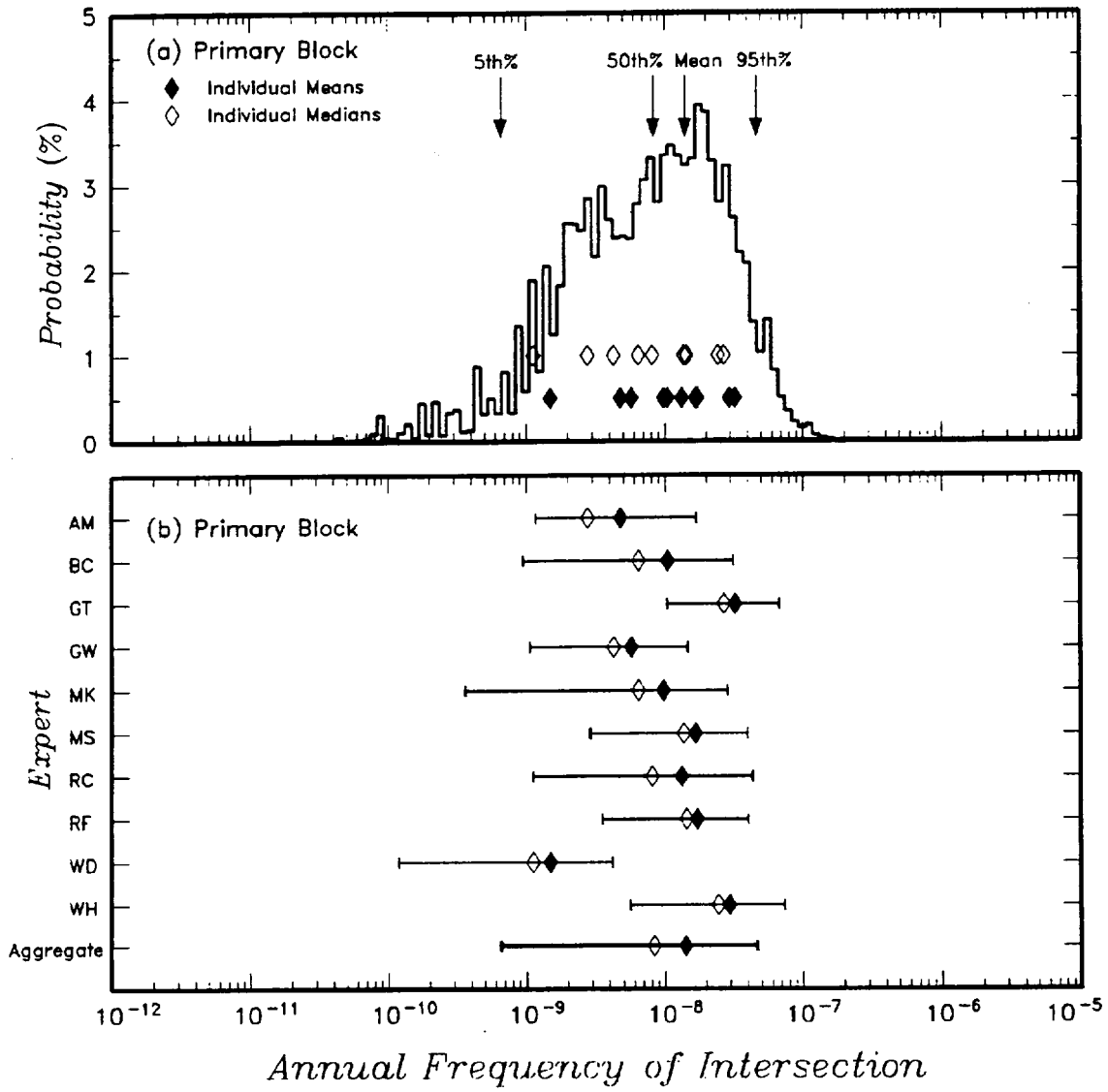

Output data. DTN: LA0005FP831811.001

Figure 20. Annual Frequency of Intersecting the Potential Repository Footprint for the Primary Block Case

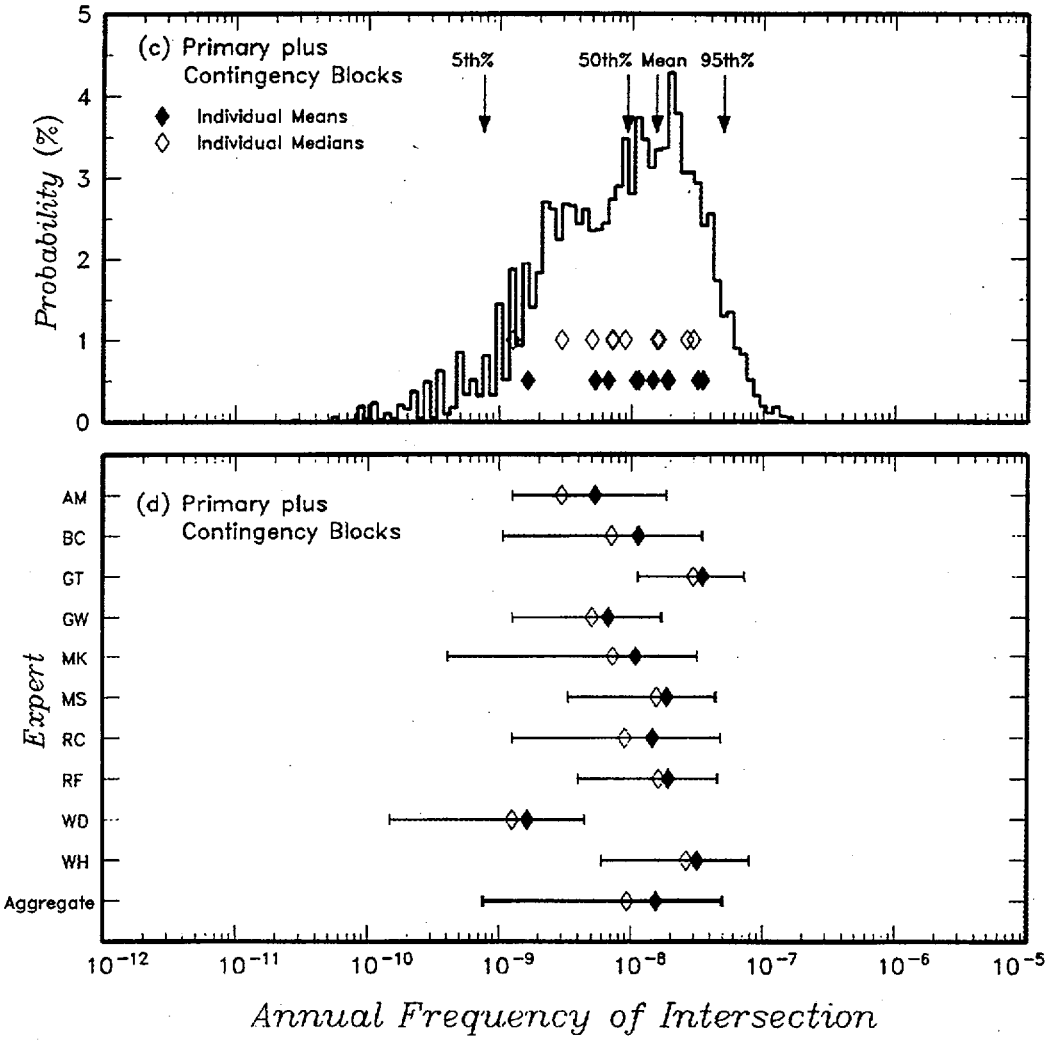

Output data. DTN: LA0005FP831811.001

NOTES: (a) Aggregate distribution and median and means for individual PVHA expert interpretations for the Primary + Contingency Blocks case. (b) Range for 5th to 95th percentiles for results from individual PVHA expert interpretations compared to range for aggregate distribution for the Primary + Contingency Blocks case. Two-letter code indicates initials of experts from Table 5.

Figure 21. Annual Frequency of Intersecting the Potential Repository Footprint for the Primary + Contingency Blocks Case

6.5.3.2 Conditional Distributions for Intersection Length, Azimuth, and Number of Eruptive Centers within the Potential Repository Footprint

The Latin hypercube sampling process described above was used to compute conditional joint distributions for length and azimuth of dike intersection and distributions for the number of eruptive centers within the potential repository footprint conditional on the length and azimuth of the intersecting dike within the repository. The computed values for frequency of intersection obtained from the simulation process are compared to the results obtained from full enumeration in Tables 9 and 10. The simulation results are indicated by the suffix –Sim in the column headings (e.g., AM-Sim). The simulation results are generally within a few percent of the full enumeration results, indicating that the simulation process accurately reproduces the full hazard distribution. The conditional joint distributions are listed in six output files (DTN: LA0005FP831811.001) for transmittal to users of the results of this AMR: CCSM-PB.OUT providing the mean hazard results for the Primary Block case, CCSM-PCB.OUT providing the mean hazard results for the Primary + Contingency Blocks case, CC05-PB.OUT providing the 5th-percentile hazard results for the Primary Block case, CC05-PCB.OUT providing the 5th-percentile hazard results for the Primary + Contingency Blocks case, CC95-PB.OUT providing the 95th-percentile hazard results for the Primary Block case, and CC95-PCB.OUT providing the 95th-percentile hazard results for the Primary + Contingency Blocks case. Each file consists of a title record, a record giving the number of points in the conditional joint distribution for dike intersection length and azimuth, and n records containing the n pairs of intersection length and azimuth (L^I_m and ϕ_n) and the conditional joint probability of an intersection having that length and azimuth within the potential repository. Also listed for each L^I_m and ϕ_n pair are the five conditional distributions for the number of eruptive centers within the potential repository given the pair L^I_m and ϕ_n. These are given in the order: *IUD-UC*, *USRD-UC*, *IUD-C*, *USRD-C*, and *USRD-FD* and give probabilities for r^{EC} = 0, 1, 2, 3, 4, and 5.

Figures 22, 23, and 24 show the conditional marginal distributions for intersection length, intersection azimuth, and number of eruptive centers, respectively, computed from the conditional joint distributions. These results are also summarized in Tables 10, 11, and 12. The marginal distributions are computed from the joint distributions using software routine MARGIN V1.0 (STN: 10271-1.0-00) (Figure 2) are placed in output files for transmittal to users of the results of this AMR. The output files of marginal conditional distributions for the Primary Block case are: 05PB-DIL.CDF, MPB-DIL.CDF, and 95PB-DIL.CDF for dike intersection length conditional on the 5th-percentile, mean, and 95th-percentile frequency of intersection; and 05PB-PEC.PMF, MPB-PEC.PMF, and 95PB-PEC.PMF for number of eruptive centers conditional on the 5th-percentile, mean, and 95th-percentile frequency of intersection. The output files of marginal conditional distributions for the Primary + Contingency Blocks case are: 05PCB-DIL.CDF, MPCB-DIL.CDF, and 95PCB-DIL.CDF for dike intersection length conditional on the 5th-percentile, mean, and 95th-percentile frequency of intersection; and 05PCB-PEC.PMF, MPCB-PEC.PMF, and 95PCB-PEC.PMF for number of eruptive centers conditional on the 5th-percentile, mean, and 95th-percentile frequency of intersection.

The marginal conditional distributions at the mean hazard and at the 5th and 95th percentile hazards are very similar. The marginal conditional distribution for the number of eruptive centers shows some sensitivity to the approach for the number and spatial distribution of eruptive

centers along the length of the dike. The *IUD-UC* approach produces the lowest probability of one or more eruptive centers within the potential repository, approximately one chance in three, and the *USRD-FD* approach produces the highest probability, approximately one chance in two.

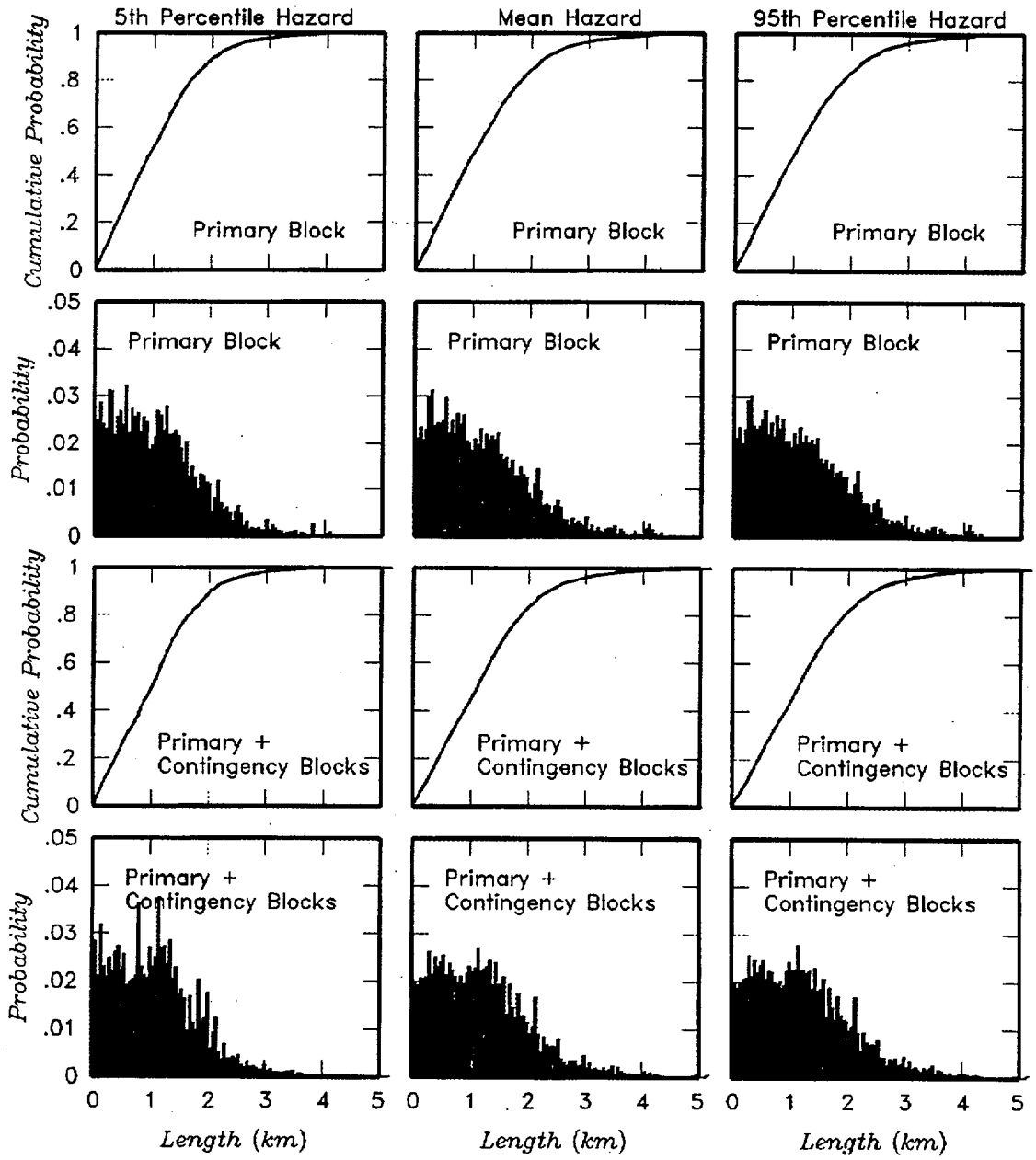

Output data. DTN: LA0005FP831811.001

NOTE: These distributions are conditional on the occurrence on an intersection.

Figure 22. Marginal Conditional Distributions for Dike Intersection Length, L', for Mean and 95th Percentile Frequency of Intersection and for the Primary Block and Primary + Contingency Block Cases

Table 10. Marginal Conditional Distributions for Dike Intersection Length, Conditional on the Occurrence of an Intersection

Dike Intersection Length (km)	Primary Block			Primary + Contingency Blocks		
	5th percentile hazard	Mean Hazard	95th percentile hazard	5th percentile hazard	Mean Hazard	95th percentile hazard
0.0-0.25	0.1570	0.1403	0.1388	0.1486	0.1213	0.1196
>0.25-0.50	0.1292	0.1284	0.1266	0.1226	0.1199	0.1169
>0.50-0.75	0.1337	0.1249	0.1216	0.1060	0.1139	0.1097
>0.75-1.00	0.1106	0.1092	0.1096	0.1281	0.1050	0.1058
>1.00-1.25	0.1246	0.1047	0.1081	0.1398	0.1164	0.1181
>1.25-1.50	0.1066	0.1033	0.0992	0.1123	0.1100	0.1044
>1.50-1.75	0.0753	0.0769	0.0749	0.0721	0.0875	0.0857
>1.75-2.00	0.0577	0.0620	0.0621	0.0709	0.0669	0.0662
>2.00-2.25	0.0373	0.0497	0.0512	0.0361	0.0507	0.0528
>2.25-2.50	0.0256	0.0323	0.0346	0.0225	0.0344	0.0380
>2.50-2.75	0.0132	0.0196	0.0207	0.0142	0.0209	0.0232
>2.75-3.00	0.0093	0.0152	0.0170	0.0091	0.0162	0.0179
>3.00-3.25	0.0073	0.0084	0.0096	0.0055	0.0101	0.0120
>3.25-3.50	0.0041	0.0086	0.0093	0.0049	0.0087	0.0100
>3.50-3.75	0.0023	0.0047	0.0054	0.0025	0.0053	0.0057
>3.75-4.00	0.0036	0.0037	0.0034	0.0016	0.0030	0.0038
>4.00-4.25	0.0022	0.0070	0.0067	0.0013	0.0039	0.0036
>4.25-4.50	0.0003	0.0013	0.0011	0.0007	0.0017	0.0019
>4.50-4.75	0.0000	0.0000	0.0000	0.0005	0.0011	0.0013
>4.75-5.00	0.0000	0.0000	0.0000	0.0006	0.0025	0.0027
>5.00-5.25	0.0000	0.0000	0.0000	0.0001	0.0007	0.0008

Output data. DTN: LA0005FP831811.001

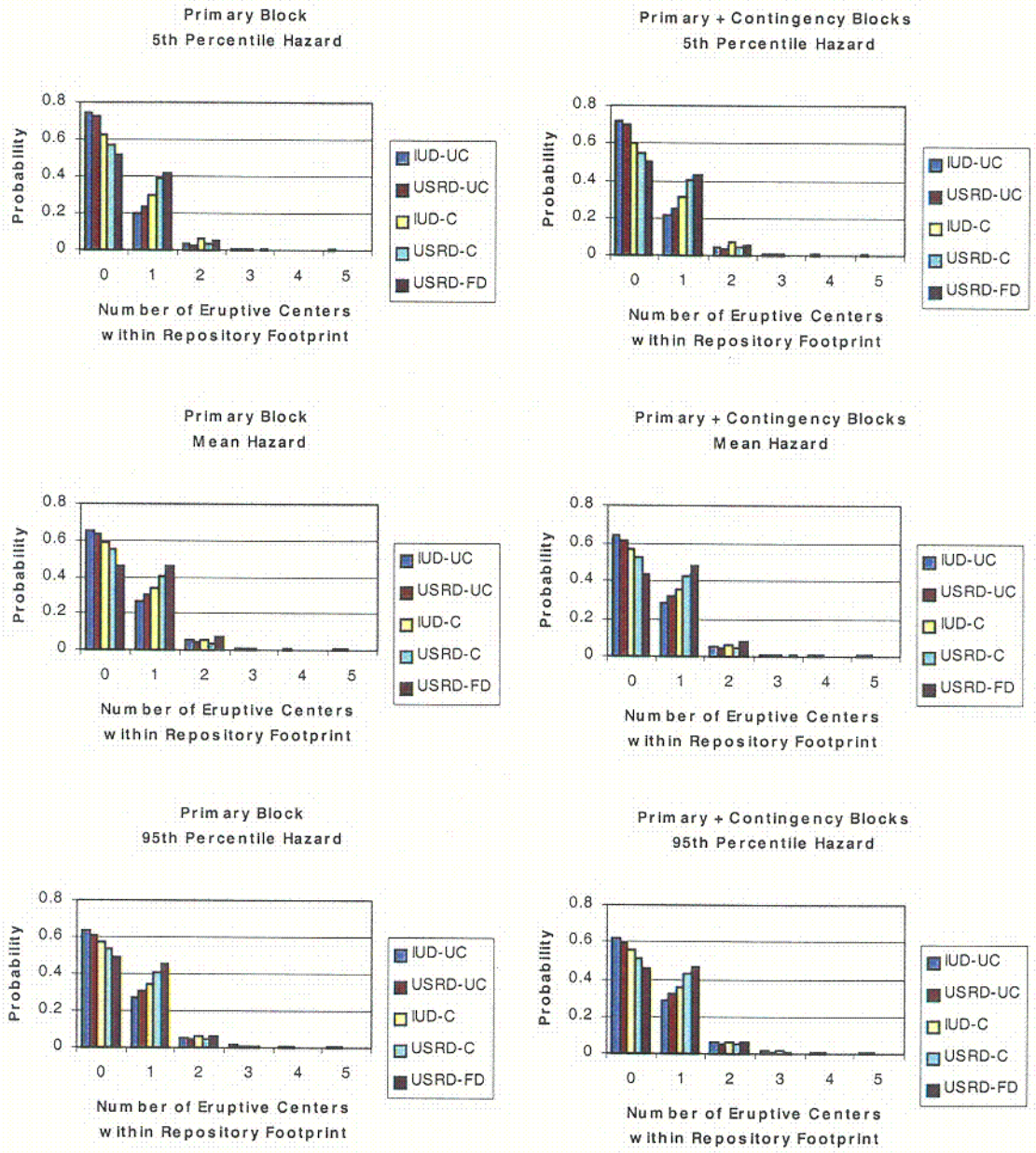

Output data. DTN: LA0005FP831811.001

NOTES: *IUD* – independent, uniformly distributed; *USRD* – uniformly spaced, randomly distributed; *UC* – uncorrelated length and number of eruptive centers per volcanic event distributions; *C* – correlated length and number of eruptive centers per volcanic event distributions; *FD* – fixed density for number of eruptive centers per volcanic event.

Figure 24. Marginal Conditional Distributions for the Number of Eruptive Centers within the Potential Repository Footprint, r^{EC}, for 5th Percentile, Mean, and 95th Percentile Frequency of Intersection and for the Primary Block and Primary + Contingency Block Cases

C-3

Table 11. Marginal Conditional Distribution for Intersecting Dike Azimuth, Conditional on the Occurrence of an Intersection

Intersecting Dike Azimuth (°)	Primary Block			Primary + Contingency Blocks		
	5th percentile hazard	Mean hazard	95th percentile hazard	5th percentile hazard	Mean hazard	95th percentile hazard
>0-10	0.0427	0.0705	0.0747	0.0407	0.0637	0.0729
>10-20	0.1176	0.1465	0.1579	0.0938	0.1442	0.1539
>20-30	0.2217	0.2832	0.2733	0.2106	0.2842	0.2689
>30-40	0.2170	0.2478	0.2239	0.2278	0.2527	0.2260
>40-50	0.1551	0.1191	0.1017	0.1648	0.1222	0.1049
>50-60	0.0897	0.0491	0.0426	0.0930	0.0506	0.0440
>60-70	0.0468	0.0162	0.0197	0.0466	0.0167	0.0203
>70-80	0.0215	0.0050	0.0098	0.0230	0.0054	0.0103
>80-90	0.0087	0.0020	0.0053	0.0114	0.0022	0.0058
>90-100	0.0034	0.0009	0.0029	0.0037	0.0010	0.0031
>100-110	0.0009	0.0004	0.0015	0.0010	0.0005	0.0016
>110-120	0.0006	0.0003	0.0008	0.0005	0.0004	0.0008
>120-130	0.0020	0.0010	0.0013	0.0018	0.0011	0.0015
>130-140	0.0069	0.0032	0.0045	0.0068	0.0036	0.0049
>140-150	0.0165	0.0087	0.0133	0.0172	0.0091	0.0140
>150-160	0.0230	0.0157	0.0258	0.0267	0.0158	0.0267
>160-170	0.0181	0.0189	0.0278	0.0222	0.0173	0.0277
>170-180	0.0076	0.0115	0.0132	0.0083	0.0095	0.0127

Output data. DTN: LA0005FP831811.001

Table III-12. Summary of Average Spacing Between Eruptive Center Calculation Results

PVHA Expert	Average Spacing between Eruptive Centers (km)
Alex McBirney (AM)	2.7
Bruce Crowe (BC)	1.9
George Thompson (GT)	1.5
George Walker (GW)	1.4
Mel Kuntz (MK)	2.4
Michael Sheridan (MS)	2.5
Richard Carlson (RC)	2.4
Richard Fisher (RF)	2.5
Wendell Duffield (WD)	1.4
William Hackett (WH)	2.0

Output data. DTN: LA0005FP831811.001.

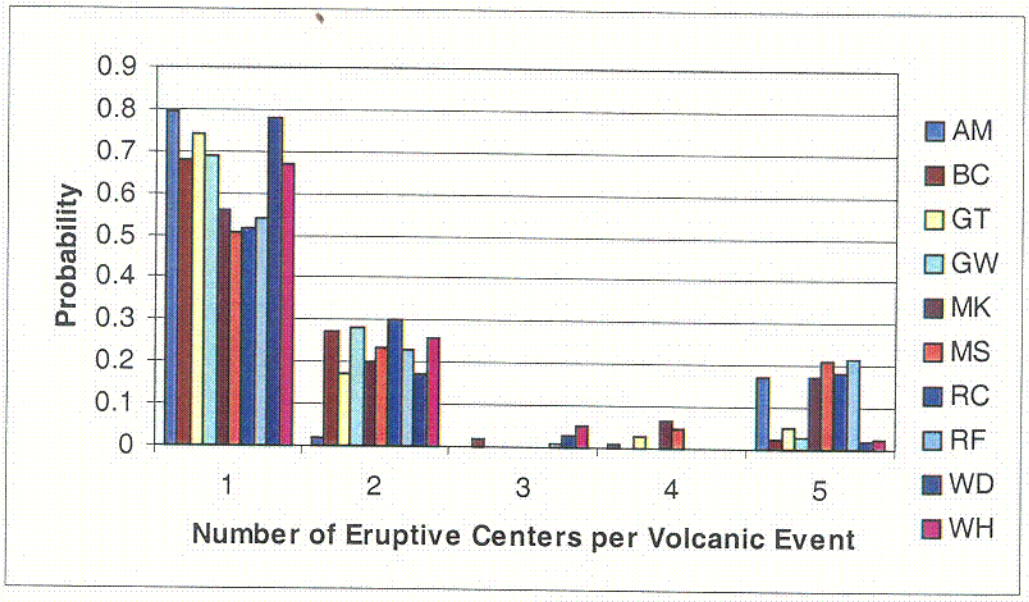

Output data. DTN: LA0005FP831811.001.

NOTE: The two-letter code indicates the PVHA expert's initials from Table III-12.

Figure III-1. Distributions for Number of Eruptive Centers per Volcanic Event, n^{EC}, Derived from the PVHA Experts' Interpretations

C-4

Table 12. Marginal Conditional Distribution for Number of Eruptive Centers within the Potential Repository, Conditional on the Occurrence of an Intersection

Number of Eruptive Centers with Potential Repository r^{EC}	Formulation for Eruptive Centers				
	Independent, Uniformly Distributed, Uncorrelated, *IUD-UC* (weight 0.05)	**Uniformly Spaced, Randomly Distributed, Uncorrelated, *USRD-UC* (weight 0.15)**	**Independent, Uniformly Distributed, Correlated, *IUD-C* (weight 0.075))**	**Uniformly Spaced, Randomly Distributed, Correlated, *USRD-C* (weight 0.225)**	**Uniformly Spaced, Randomly Distributed, Fixed Density, *USRD-FD* (weight 0.5)**
Primary Block 5th Percentile Hazard					
0	0.744	0.725	0.627	0.575	0.519
1	0.203	0.234	0.297	0.387	0.419
2	0.037	0.029	0.063	0.035	0.058
3	0.008	0.006	0.011	0.003	0.005
4	0.004	0.003	0.002	0.0002	0.00006
5	0.005	0.004	0.0003	0	0
Primary Block Mean Hazard					
0	0.653	0.632	0.589	0.550	0.460
1	0.271	0.304	0.340	0.406	0.462
2	0.052	0.044	0.058	0.040	0.074
3	0.012	0.010	0.010	0.004	0.004
4	0.006	0.004	0.002	0.0003	0.00008
5	0.007	0.005	0.0003	0.00001	0
Primary Block 95th Percentile Hazard					
0	0.636	0.612	0.576	0.534	0.487
1	0.277	0.314	0.344	0.414	0.451
2	0.056	0.050	0.063	0.047	0.060
3	0.014	0.013	0.013	0.005	0.003
4	0.008	0.006	0.003	0.0006	0.00001
5	0.008	0.006	0.0005	0.00001	0
Primary + Contingency Blocks 5th Percentile Hazard					
0	0.723	0.702	0.602	0.547	0.506
1	0.215	0.248	0.313	0.407	0.435
2	0.042	0.034	0.069	0.041	0.056
3	0.009	0.008	0.013	0.004	0.002
4	0.005	0.004	0.003	0.0006	0.0001
5	0.006	0.004	0.0005	0.00004	0
Primary + Contingency Blocks Mean Hazard					
0	0.637	0.614	0.569	0.527	0.435
1	0.282	0.318	0.354	0.425	0.480
2	0.055	0.047	0.063	0.043	0.079
3	0.012	0.011	0.011	0.004	0.005
4	0.006	0.005	0.003	0.0005	0.0002
5	0.007	0.005	0.0004	0.00003	0
Primary + Contingency Blocks 95th Percentile Hazard					
0	0.622	0.597	0.557	0.513	0.461
1	0.288	0.325	0.357	0.429	0.469
2	0.059	0.052	0.067	0.050	0.067
3	0.015	0.013	0.014	0.006	0.003
4	0.008	0.006	0.004	0.0009	0.00004
5	0.008	0.006	0.0007	0.00007	0

Output data. DTN: LA0005FP831811.001

INTENTIONALLY LEFT BLANK

7. CONCLUSIONS

The result of the PVHA (CRWMS M&O 1996) has been recalculated using PVHA outputs to account for the current footprint of the potential repository and extended to include the probability of an eruption within the potential repository footprint, conditional on a dike intersection (Table 13). A conceptual framework for the probability calculations, based on PVHA outputs and subsequent studies, accounts for deep (mantle) and shallow (structural control) processes that influence volcanic event distribution in the YMR. The framework presented here emphasizes the close correlation between the distribution of volcanic events and areas of crustal extension and faulting in the YMR, and within this context, the appropriateness of volcanic source zone boundaries defined in the PVHA. It also emphasizes the appropriate selection of parameter distributions that affect probability models and provides support for comparison of alternative conceptual frameworks and parameter selection, within the framework of the volcanic history of the YMR. Alternative models presented by the NRC (Reamer 1999) that result in higher eruption probabilities (10^{-7} versus $\sim 8\times10^{-9}$ per year) than those presented here are found to employ input parameters that either represent extreme values (e.g., event length) or assume a specific geologic control (i.e., crustal density) on spatial distribution while not considering more defensible and observable controls (i.e., crustal extension and structure). Spatial density models weighted by crustal density result in higher event frequencies at the potential repository site, while the same models weighted by an alternative geologic control such as cumulative crustal extension across the Crater Flat structural domain would likely lead to decreased event frequencies at the site. The NRC states that the highest value (10^{-7} per year) in their range of calculated probability values (10^{-8}–10^{-7} per year) cannot be considered more or less likely than any other value they have calculated using alternative probability models (Reamer 1999, p. 61). The analysis in this AMR suggests that the choice of input parameters used by the NRC compared to those used in the PVHA logically places the highest NRC probability value at the extreme upper tail of a probability distribution.

The annual frequency of intersection of the potential repository footprint by a dike associated with a volcanic event, and the annual frequency of a volcanic event producing one or more eruptive centers within the potential repository has been recalculated, based on the current potential repository footprint (Table 13). The latter frequency is obtained by multiplying the frequency of intersection from Figure 15 by the conditional probability of the occurrence of at least one eruptive center (1 minus the conditional probability of 0 centers) from Table 12. The values listed in Table 13 are the weighted combination of the five models for eruptive centers listed in Table 12.

Conditional distributions for the length and azimuth of the intersecting dike and the number of eruptive centers occurring within the potential repository footprint are developed for the six values of frequency of intersection in Table 13. These distributions are very similar for all six conditions. The five alternative models for specifying the number and spatial distribution for eruptive centers associated with a volcanic event have relatively small effects on the conditional distribution for the number of eruptive centers occurring within the potential repository footprint.

The inputs to this AMR are the results of an expert elicitation conducted in a manner consistent with the guidance in the Branch Technical Position on Expert Elicitation (Kotra et al. 1996). The

PVHA experts explicitly quantified the uncertainties in their interpretations and they are represented in the outputs of this AMR in the form of probability distributions. The assumptions used to extend the PVHA interpretations to calculate conditional distributions for the number of eruptive conduits within the potential repository are conservative and need not be verified. Thus, it is concluded that the results of this AMR form an appropriate basis for the evaluation of the consequences of volcanic hazards in the YMR.

The inputs to this AMR from the PVHA are qualified. The footprint of the potential repository is not yet qualified because the EDA II drift coordinates are not yet qualified. However, minor changes in location by a tens of meters will not have a significant impact on the results of this AMR. The software used to perform the calculations in this AMR has been qualified following procedure AP-SI.1Q, Revision 2, ICN 4.

7.1 OUTPUTS OF THIS AMR

The outputs of this AMR are described in Section 6.5.3. They consist of the following.

1. Probability distributions for annual frequency of intersection of the potential repository footprint by a dike for the Primary Block and Primary + Contingency Blocks potential repository configurations of EDA II in output files PVHA-PB.DST and PVHA-PCB.DST (DTN: LA0005FP831811.001) and summary frequencies of disruptive volcanic events (Table 13, DTN: LA0004FP831811.004)

2. Conditional joint probability distributions for length and azimuth of an intersecting dike, and number of eruptive centers within the potential repository footprint for the Primary Block and Primary + Contingency Blocks potential repository configurations of EDA II, output files CCSM-PB.OUT, CCSM-PCB.OUT, CC05-PB.OUT, CC05-PCB.OUT, CC95-PB.OUT, and CC95-PCB.OUT (DTN: LA0005FP831811.001). In addition, conditional marginal distributions for length of intersecting dike and number of eruptive centers within the potential repository footprint for the Primary Block and Primary + Contingency Blocks potential repository configurations of EDA II, output files 05PB-DIL.CDF, MPB-DIL.CDF, 95PB-DIL.CDF, 05PB-PEC.PMF, MPB-PEC.PMF, 95PB-PEC.PMF, 05PCB-DIL.CDF, MPCB-DIL.CDF, 95PCB-DIL.CDF, 05PCB-PEC.PMF, MPCB-PEC.PMF, and 95PCB-PEC.PMF (DTN: LA0005FP831811.001).

These outputs will be used as input to the "Number of Waste Packages Hit" calculation (CRWMS M&O 2000c) and the *Igneous Consequence Modeling* AMR (CRWMS M&O 2000a).

The results presented in this document, computed using the qualified software, differ slightly from the preliminary results in DTN: LA004FP831811.001. The typical difference is only a few percent. For example, the preliminary mean frequency of intersection for the Primary + Contingency Blocks case was 1.50×10^{-8} per year and the final mean frequency of intersection is 1.55×10^{-8} per year. The final conditional distributions for the length and azimuth of intersecting dikes and the number of eruptive centers within the potential repository footprint also differ by a few percent from the preliminary results. The largest differences are at the lower tails of the distributions for annual frequency of intersection. The 5th percentile of the distributions

increased by about 30 percent, with the difference decreasing to below 10 percent by the 25th percentile of the distributions for frequency of intersection. Given that the preliminary and final results are small in comparison to the range of the distribution for frequency of intersection, and that the differences are smallest in the upper portion of the distribution which will dominate the results of analyses that use the outputs of this AMR, the preliminary and final results can be considered equivalent.

Table 13. Summary Frequencies of Disruptive Volcanic Events

Potential Repository Footprint (EDA II)	Hazard Level	Annual Frequency of Intersection of Potential Repository by a Dike	Weighted Conditional Probability of No Eruptive Centers	Annual Frequency of Occurrence of One or More Eruptive Centers within Potential Repository
Primary Block	5th percentile	6.6×10^{-10}	0.58	2.8×10^{-10}
	Mean	**1.4×10^{-8}**	0.53	**6.7×10^{-9}**
	95th percentile	4.7×10^{-8}	0.53	2.2×10^{-8}
Primary + Contingency Blocks	5th percentile	7.6×10^{-10}	0.56	3.3×10^{-10}
	Mean	**1.6×10^{-8}**	0.50	**7.7×10^{-9}**
	95th percentile	5.0×10^{-8}	0.51	2.5×10^{-8}

Output data. DTN: LA0004FP831811.004

This document may be affected by technical product input information that requires confirmation. Any changes to the document that may occur as a result of completing the confirmation activities will be reflected in subsequent revisions. The status of the input information quality may be confirmed by review of the Document Input Reference System database.

INTENTIONALLY LEFT BLANK

8. INPUTS AND REFERENCES

8.1 DOCUMENTS CITED

Brocher, T.M.; Hunter, W.C.; and Langenheim, V.E. 1998. "Implications of Seismic Reflection and Potential Field Geophysical Data on the Structural Framework of the Yucca Mountain-Crater Flat Region, Nevada." *Geological Society of America Bulletin, 110* (8), 947-971. Boulder, Colorado: Geological Society of America. TIC: 238643.

Brocoum, S.J. 1997. "Evaluation of Data Provided at U.S. Department of Energy (DOE) and U.S. Nuclear Regulatory Commission (NRC) Igneous Activity Technical Exchange, February 25-26, 1997." Letter from S.J. Brocoum (DOE/OCRWM) to J.T. Greeves (NRC), June 4, 1997, with enclosure. ACC: MOL.19970722.0276; MOL.19970722.0277.

Byers, F.M., Jr. and Barnes, H. 1967. *Geologic Map of the Paiute Ridge Quadrangle, Nye and Lincoln Counties, Nevada.* Map GQ-577. Washington, D.C.: U.S. Geological Survey. ACC: HQS.19880517.1104.

Connor, C.B. and Hill, B.E. 1995. "Three Nonhomogeneous Poisson Models for the Probability of Basaltic Volcanism: Application to the Yucca Mountain Region, Nevada." *Journal of Geophysical Research, 100* (B6), 10,107–10,125. Washington, D.C.: American Geophysical Union. TIC: 237682.

Connor, C.B.; Stamatakos, J.; Ferrill, D.; Hill, B.E.; Magsino, S.B.L.; La Femina, P.; and Martin, R.H. 1997. "Integrating Structural Models into Probabilistic Volcanic Hazard Analyses: An Example from Yucca Mountain, NV." *Abstracts with Programs – Geological Society of America, 28*, (7), A-192. Boulder, Colorado: Geological Society of America. TIC: 247409.

Connor, C.B.; Stamatakos, J.A.; Ferrill, D.A.; and Hill, B.E. 1998. "Technical Comments: Detecting Strain in the Yucca Mountain Area, Nevada." *Science, 282*, (5391), 1007b. Washington, D.C.: American Association for the Advancement of Science. TIC: 243445.

Crowe, B.; Perry, F.; Geissman, J.; McFadden, L.; Wells, S.; Murrell, M.; Poths, J.; Valentine, G.A.; Bowker, L.; and Finnegan, K. 1995. *Status of Volcanism Studies for the Yucca Mountain Site Characterization Project.* LA-12908-MS. Los Alamos, New Mexico: Los Alamos National Laboratory. ACC: HQO.19951115.0017.

Crowe, B.M. and Perry, F.V. 1990. "Volcanic Probability Calculations for the Yucca Mountain Site: Estimation of Volcanic Rates." *Proceedings of the Topical Meeting on Nuclear Waste Isolation in the Unsaturated Zone, FOCUS '89, September 17-21, 1989, Las Vegas, Nevada.* 326–334. La Grange Park, Illinois: American Nuclear Society. TIC: 212738.

Crowe, B.M.; Johnson, M.E.; and Beckman, R.J. 1982. "Calculation of the Probability of Volcanic Disruption of a High-Level Radioactive Waste Repository Within Southern Nevada, USA." *Radioactive Waste Management and the Nuclear Fuel Cycle, 3* (2), 167-190. New York, New York: Harwood Academic Publishers. TIC: 222179.

Crowe, B.M.; Perry, F.V.; Valentine, G.A.; Wallmann, P.C.; and Kossik, R. 1993. "Simulation Modeling of the Probablity of Magmatic Disruption of the Potential Yucca Mountain Site." *Proceedings of the Topical Meeting on Site Characterization and Model Validation, Focus '93, September 26-29,1993*. 182-191. La Grange Park, Illinois: American Nuclear Society. TIC: 225003.

CRWMS M&O (Civilian Radioactive Waste Management System Management and Operating Contractor). 1996. *Probabilistic Volcanic Hazard Analysis for Yucca Mountain, Nevada*. BA0000000-01717-2200-00082, Rev 0. Las Vegas, Nevada: CRWMS M&O. ACC: MOL.19971201.0221.

CRWMS M&O 1998a. "Disruptive Events." Chapter 10 of *Total System Performance Assessment–Viability Assessment (TSPA-VA) Analyses Technical Basis Document*. B00000000-01717-4301-00010, REV 00. Las Vegas, Nevada: CRWMS M&O. ACC: MOL.19980724.0399.

CRWMS M&O 1998b. "Geochemistry." Book 3 - Section 6 of *Yucca Mountain Site Description*. B00000000-01717-5700-00019, REV 00. Las Vegas, Nevada: CRWMS M&O. ACC: MOL.19980729.0052.

CRWMS M&O 1998c. *Synthesis of Volcanism Studies for the Yucca Mountain Site Characterization Project*. Deliverable 3781MR1. Las Vegas, Nevada: CRWMS M&O. ACC: MOL.19990511.0400.

CRWMS M&O 1999a. *Characterize Igneous Framework for Yucca Mountain, NV*. Development Plan. TDP-CRW-GS-000002 REV 00. Las Vegas, Nevada: CRWMS M&O. ACC: MOL.19990811.0288.

CRWMS M&O 1999b. *Analysis to Characterize the Igneous Framework for Yucca Mountain, Nevada*. Activity Evaluation, July 26, 1999. Las Vegas, Nevada: CRWMS M&O. ACC: MOL.19990917.0048.

CRWMS M&O 1999c. *Analysis to Characterize the Eruptive Processes at Yucca Mountain, Nevada*. Activity Evaluation, July 26, 1999. Las Vegas, Nevada: CRWMS M&O. ACC: MOL.19990917.0049.

CRWMS M&O 1999d. *Analysis to Characterize the Framework for Seismicity and Structural Deformation at Yucca Mountain, NV*. Activity Evaluation, July 26, 1999. Las Vegas, Nevada: CRWMS M&O. ACC: MOL.19990917.0050.

CRWMS M&O 1999e. *License Application Design Selection Report*. B00000000-01717-4600-00123 REV 01 ICN 01. Las Vegas, Nevada: CRWMS M&O. ACC: MOL.19990908.0319.

CRWMS M&O 1999f. *Layout of Repository Drifts for Site-Recommendation Design, Including Information on Those Which are Anticipated to Contain Emplaced Waste*. Input Transmittal

NEP-EBS-99332.T. Las Vegas, Nevada: CRWMS M&O. ACC: MOL.20000131.0184; MOL.19990901.0312; MOL.19990901.0311.

CRWMS M&O 2000a. *Igneous Consequence Modeling for TSPA-SR*. ANL-WIS-MD-000017 REV 00. Las Vegas, Nevada: CRWMS M&O. ACC: MOL.20000501.0225.

CRWMS M&O 2000b. *Characterize Eruptive Processes at Yucca Mountain, Nevada*. ANL-MGR-GS-000002 REV 00. Las Vegas, Nevada: CRWMS M&O. ACC: MOL.20000517.0259.

CRWMS M&O 2000c. *Number of Waste Packages Hit by Igneous Intrusion*. CAL-WIS-PA-000001. Las Vegas, Nevada: CRWMS M&O. ACC: MOL.20000602.0054.

Day, W.C.; Dickerson, R.P.; Potter, C.J.; Sweetkind, D.S.; San Juan, C.A.; Drake II, R.M.; and Fridrich, C.J. 1998. *Bedrock Geologic Map of the Yucca Mountain Area, Nye County, Nevada*. Geologic Investigations Series I-2627. Denver, Colorado: U.S. Geological Survey. ACC: MOL.19981014.0301.

Delaney, P.T. and Gartner, A.E. 1997. "Physical Processes of Shallow Mafic Dike Emplacement Near the San Rafael Swell, Utah." *Geological Society of America Bulletin, 109* (9), 1177–1192. Boulder, Colorado: Geological Soceity of America. TIC: 247421.

DOE (U.S. Department of Energy) 1998. *Total System Performance Assessment*. Volume 3 of *Viability Assessment of a Repository at Yucca Mountain*. DOE/RW-0508. Washington, D.C.: U.S. Department of Energy, Office of Civilian Radioactive Waste Management. ACC: MOL.19981007.0030.

DOE 2000. *Quality Assurance Requirements and Description*. DOE/RW-0333P, Rev. 10. Washington, D.C.: U.S. Department of Energy, Office of Civilian Radioactive Waste Management. ACC: MOL.20000427.0422.

Dyer, J.R. 1999. "Revised Interim Guidance Pending Issuance of New U.S. Nuclear Regulatory Commission (NRC) Regulations (Revision 01, July 22, 1999), for Yucca Mountain, Nevada." Letter from J.R. Dyer (DOE/YMSCO) to D.R. Wilkins (CRWMS M&O), September 3, 1999, OL&RC:SB-1714, with enclosure, "Interim Guidance Pending Issuance of New NRC Regulations for Yucca Mountain (Revision 01)." ACC: MOL.19990910.0079.

Earthfield Technology. 1995. *Summary Report: Magnetic and Gravity Study of the Yucca Mountain Area, Nevada*. Houston, Texas: Earthfield Technology. ACC: MOL.20000228.0374.

Farmer, G.L.; Perry, F.V.; Semken, S.; Crowe, B.; Curtis, D.; and Depaulo, D.J. 1989. "Isotopic Evidence on the Structure and Origin of Subcontinental Lithospheric Mantle in Southern Nevada." *Journal of Geophysical Research, 94*, (B6), 7885-7898. Washington, D.C.: American Geophysical Union. TIC: 201800.

Feighner, M.A. and Majer, E.L. 1996. *Results of the Analysis of the Timber Mt., Lathrop Wells, and Yucca Mt. Aeromagnetic Data*. Milestone SPT23KM4. Berkeley, California: Lawrence Berkeley National Laboratory. ACC: MOL.19971204.0767.

Ferrill, D.A.; Stamatakos, J.A.; Jones, S.M.; Rahe, B.; McKague, H.L.; Martin, R.H.; and Morris, A.P. 1996. "Quaternary Slip History of the Bare Mountain Fault (Nevada) from the Morphology and Distribution of Alluvial Fan Deposits." *Geology, 24*, (6), 559-562. Boulder, Colorado: Geological Society of America. TIC: 234557.

Fridrich, C. J. 1999. "Tectonic Evolution of the Crater Flat Basin, Yucca Mountain Region, Nevada." *Cenozoic Basins of the Death Valley Region: Boulder, Colorado*. Wright, L.A. and Troxel, B.W., eds. Special Paper 333, 169-195. Boulder, Colorado: Geological Society of America. TIC: 245355.

Fridrich, C.J.; Whitney, J.W.; Hudson, M.R.; and Crowe, B.M. 1999. "Space-Time Patterns of Late Cenozoic Extension, Vertical Axis Rotations, and Volcanism in the Crater Flat Basin, Southwest Nevada." *Cenozoic Basins of the Death Valley Region*. Wright, L.A., and Troxel, B.W., eds. Special Paper 333. pp. 197-212. Boulder, Colorado: Geological Society of America. TIC: 245358.

Heizler, M.T.; Perry, F.V.; Crowe, B.M.; Peters, L.; and Appelt, R. 1999. "The Age of Lathrop Wells Volcanic Center: An $^{40}Ar/^{39}Ar$ Dating Investigation." *Journal of Geophysical Research, 104* (B1), 767-804. Washington, D.C.: American Geophysical Union. TIC: 243399.

Ho, C.-H. and Smith, E.I. 1998. "A Spatial-Temporal/3-D Model for Volcanic Hazard Assessment: Application to the Yucca Mountain Region, Nevada." *Mathematical Geology, 30* (5), 497–510. New York, New York: Plenum Publishing Corporation. TIC: 245110.

Hudson, M.R.; Minor, S.A.; and Fridrich, C.J. 1996. "The Distribution, Timing, and Character of Steep-Axis Rotations in a Broad Zone of Dextral Shear in Southwestern Nevada." *Abstracts with Programs, 28*, (7), A-451. Boulder, Colorado: Geological Society of America. TIC: 234723.

Kotra, J.P.; Lee, M.P.; Eisenberg, N.A.; and De Wispelare, A.R. 1996. *Branch Technical Position on the Use of Expert Elicitation in the High-Level Radioactive Waste Program*. NUREG-1563. Washington, D.C.: U.S. Nuclear Regulatory Commission. TIC: 226832.

Langenheim, V.E.; Kirchoff-Stein, K.S., and Oliver, H.W. 1993. "Geophysical Investigations of Buried Volcanic Centers Near Yucca Mountain, Southwest Nevada." *High-Level Radioactive Waste Management, Proceedings of the Fourth Annual International Conference, Las Vegas, Nevada, April 26-30, 1993*. 2, 1840-1846. La Grange Park, Illinois: American Nuclear Society. TIC: 208542.

Magsino, S.L.; Connor, C.B.; Hill, B.E.; Stamatakos, J.A.; La Femina, P.C.; Sims, D.A.; and Maratin, R.H. 1998. *CNWRA Ground Magnetic Surveys in the Yucca Mountain Region, Nevada*

(1996-1997). CNWRA 98-001. San Antonio, Texas: Center for Nuclear Waste Regulatory Analyses. TIC: 247807.

McKay, M.D.; Beckman, R.J.; and Conover, W.J. 1979. "A Comparison of Three Methods for Selecting Values of Input Variables in the Analysis of Output from a Computer Code." *Technometrics, 21*, (2), 239-245. Alexandria, Virginia: American Statistical Association. TIC: 221741.

Ratcliff, C.D.; Geissman, J.W.; Perry, F.V.; Crowe, B.M.; and Zeitler, P.K. 1994. "Paleomagnetic Record of a Geomagnetic Field Reversal from Late Miocene Mafic Intrusions, Southern Nevada." *Science, 266*, 412-416. Washington, D.C.: American Association for the Advancement of Science. TIC: 234818.

Reamer, C.W. 1999. "Issue Resolution Status Report (Key Technical Issue: Igneous Activity. Revision 2.)" Letter from C.W. Reamer (NRC) to Dr. S. Brocoum (DOE), July 16, 1999 with enclosure. ACC: MOL.19990810.0639.

Rosenbaum, J.G.; Hudson, M.R.; and Scott, R.B. 1991. "Paleomagnetic Constraints on the Geometry and Timing of Deformation at Yucca Mountain, Nevada." *Journal of Geophysical Research, 96*, (B2), 1963-1979. Washington, D.C.: American Geophysical Union. TIC: 225126.

Savage, J.C.; Svarc, J.L.; and Prescott, W.H. 1999. "Strain Accumulation at Yucca Mountain, Nevada, 1983-1998." *Journal of Geophysical Research, 104* (B8), 17627-17631. Washington, D.C.: American Geophysical Union. TIC: 245645.

Sawyer, D.A.; Fleck, R.J.; Lanphere, M.A.; Warren, R.G.; Broxton, D.E.; and Hudson, M.R. 1994. "Episodic Caldera Volcanism in the Miocene Southwestern Nevada Volcanic Field: Revised Stratigraphic Framework, $^{40}Ar/^{39}Ar$ Geochronology, and Implications for Magmatism and Extension." *Geological Society of America Bulletin, 106*, (10), 1304-1318. Boulder, Colorado: Geological Society of America. TIC: 222523.

Smith, E.I.; Feuerbach, D.L.; Nauman, T.R.; and Faulds, J.E. 1990. "The Area of Most Recent Volcanism Near Yucca Mountain, Nevada: Implications for Volcanic Risk Assessment." *High-Level Radioactive Waste Management, Proceedings of the International Topical Meeting, Las Vegas, Nevada, April 8-12, 1990.* 1, 81-90. La Grange Park, Illinois: American Nuclear Society. TIC: 202058.

Stamatakos, J.A.; Connor, C.B.; and Martin, R.H. 1997. "Quaternary Basin Evolution and Basaltic Volcanism of Crater Flat, Nevada, from Detailed Ground Magnetic Surveys of the Little Cones." *Journal of Geology, 105*, 319-330. Chicago, Illinois: University of Chicago. TIC: 245108.

Wemheuer, R.F. 1999. "First Issue of FY00 NEPO QAP-2-0 Activity Evaluations." Interoffice correspondence from R.F. Wemheuer (CRWMS M&O) to R.A. Morgan, October 1, 1999. LV.NEPO.RTPS.TAG.10/99-155, with enclosures. ACC: MOL.19991028.0162.

Wernicke, B.; Davis, J.L.; Bennett, R.A.; Elosegui, P.; Abolins, M.J.; Brady, R.J.; House, M.A.; Niemi, N.A.; and Snow, J.K. 1998. "Anomalous Strain Accumulation in the Yucca Mountain Area, Nevada." *Science, 279*, 2096-2100. New York, New York: American Association for the Advancement of Science. TIC: 235956.

Wilkins, D.R. and Heath, C.A. 1999. "Direction to Transition to Enhanced Design Alternative II." Letter from Dr. D.R. Wilkins (CRWMS M&O) and Dr. C.A. Heath (CRWMS M&O) to Distribution, June 15, 1999, LV.NS.JLY.06/99-026, with enclosures, "Strategy for Baselining EDA II Requirements: and "Guidelines for Implementation of EDA II." ACC: MOL.19990622.0126; MOL.19990622.0127; MOL.19990622.0128.

Yogodzinski, G.M. and Smith, E.I. 1995. "Isotopic Domains and the Area of Interest for Volcanic Hazard Assessment in the Yucca Mountain Area." *Transactions of the American Geophysical Union, 76* (46), F669. Washington, D.C.: American Geophysical Union. TIC: 237939.

8.2 CODES, STANDARDS, REGULATIONS, AND PROCEDURES

AP-3.10Q, Rev. 2, ICN 2. *Analysis and Models*. Washington, D.C.: U.S. Department of Energy, Office of Civilian Radioactive Waste Management. ACC: MOL.20000619.0576.

AP-3.15Q, Rev. 1, ICN 1. *Managing Technical Product Inputs*. Washington, D.C.: U.S. Department of Energy, Office of Civilian Radioactive Waste Management. ACC: MOL.20000218.0069.

AP-SI.1Q, Rev 2, ICN 4. Office of Civilian Radioactive Waste Management (OCRWM) Procedure: *Software Management*. Washington, D.C.: OCRWM. ACC: MOL.20000223.0508.

AP-SV.1Q, Rev. 0, ICN 1. *Control of Electronic Management of Data*. Washington, D.C.: U.S. Department of Energy, Office of Civilian Radioactive Waste Management. ACC: MOL.20000512.0068.

LANL-YMP-QP-S5.01, Rev 0. 2000. *Electronic Data Management*. Los Alamos, New Mexico: Los Alamos National Laboratory. ACC: MOL.20000621.0094.

QAP-2-0, Rev. 5. *Conduct of Activities*. Las Vegas, Nevada: CRWMS M&O. ACC: MOL.19980826.0209.

8.3 SOFTWARE

Dynamic Graphics. 1997. *Software Code: EarthVision V4.0*. V4.0. Silicon Graphics Indigo R4000. 30035-1 V4.0; 30035-2 V4.0.

Los Alamos National Laboratory. 2000. *Software Routine*: *CFRAC.FOR V1.0*. V1.0. 10254-1.0-00.

Los Alamos National Laboratory. 2000. *Software Routine*: *COMBDELD.FOR V1.0*. V1.0. 10288-1.0-00.

Los Alamos National Laboratory. 2000. *Software Routine*: *COMBSF.FOR V1.0*. V1.0. 10255-1.0-00.

Los Alamos National Laboratory. 2000. *Software Routine: COMBSM.FOR V1.0*. V1.0. 10256-1.0-00.

Los Alamos National Laboratory. 2000. *Software Routine*: *CPDI.FOR V1.0*. V1.0. 10257-1.0-00.

Los Alamos National Laboratory. 2000. *Software Routine*: *DCPELD.FOR V1.0*. V1.0. 10258-1.0-00.

Los Alamos National Laboratory. 2000. *Software Routine*: *DILECDLH.FOR V1.0*. V1.0. 10259-1.0-00.

Los Alamos National Laboratory. 2000. *Software Routine*: *DLECD.FOR V1.0*. V1.0. 10260-1.0-00.

Los Alamos National Laboratory. 2000. *Software Routine*: *FIT2CNTR.FOR V1.0*. V1.0. 10261-1.0-00.

Los Alamos National Laboratory. 2000. *Software Routine*: *FITCD.FOR V1.0*. V1.0. 10262-1.0-00.

Los Alamos National Laboratory. 2000. *Software Routine*: *FITFIELD.FOR V1.0*. V1.0. 10263-1.0-00.

Los Alamos National Laboratory. 2000. *Software Routine*: *FITIDSR.FOR V1.0*. V1.0. 10264-1.0-00.

Los Alamos National Laboratory. 2000. *Software Routine*: *FKVH.FOR V1.0*. V1.0. 10265-1.0-00.

Los Alamos National Laboratory. 2000. *Software Routine*: *FKVHLH.FOR V1.0*. V1.0. 10266-1.0-00.

Los Alamos National Laboratory. 2000. *Software Routine*: *FKVPVH.FOR V1.0*. V1.0. 10267-1.0-00.

Los Alamos National Laboratory. 2000. *Software Routine*: *FKVPVHLH.FOR V1.0*. V1.0. 10268-1.0-00.

Los Alamos National Laboratory. 2000. *Software Routine*: *FPFGVH.FOR V1.0*. V1.0. 10269-1.0-00.

Los Alamos National Laboratory. 2000. *Software Routine*: *FPFGVHLH.FOR V1.0*. V1.0. 10270-1.0-00.

Los Alamos National Laboratory. 2000. *Software Routine*: *MARGIN.FOR V1.0*. V1.0. 10271-1.0-00.

Los Alamos National Laboratory. 2000. *Software Routine*: *NECPDS.FOR V1.0*. V1.0. 10272-1.0-00.

Los Alamos National Laboratory. 2000. *Software Routine*: *PFGVH.FOR V1.0*. V1.0. 10273-1.0-00.

Los Alamos National Laboratory. 2000. *Software Routine*: *PFGVHLH.FOR V1.0*. V1.0. 10274-1.0-00.

Los Alamos National Laboratory. 2000. *Software Routine*: *SFCD.FOR V1.0*. V1.0. 10275-1.0-00.

Los Alamos National Laboratory. 2000. *Software Routine*: *SFIDSR.FOR V1.0*. V1.0. 10276-1.0-00.

Los Alamos National Laboratory. 2000. *Software Routine*: *UZVH.FOR V1.0*. V1.0. 10277-1.0-00.

Los Alamos National Laboratory. 2000. *Software Routine*: *UZVHLH.FOR V1.0*. V1.0. 10278-1.0-00.

Los Alamos National Laboratory. 2000. *Software Routine*: *UZVPVH.FOR V1.0*. V1.0. 10279-1.0-00.

Los Alamos National Laboratory. 2000. *Software Routine*: *UZVPVHLH.FOR V1.0*. V1.0. 10280-1.0-00.

Los Alamos National Laboratory. 2000. *Software Routine*: *VHTIELHS.FOR V1.0*. V1.0. 10281-1.0-00.

Los Alamos National Laboratory. 2000. *Software Routine*: *VHTREE.FOR V1.0*. V1.0. 10282-1.0-00.

Los Alamos National Laboratory. 2000. *Software Routine*: *ZBCKVH.FOR V1.0*. V1.0. 10283-1.0-00.

Los Alamos National Laboratory. 2000. *Software Routine*: *ZBCKVHLH.FOR V1.0*. V1.0. 10284-1.0-00.

8.4 SOURCE DATA, LISTED BY DATA TRACKING NUMBER

LA0004FP831811.002. Volume of Volcanic Centers in the Yucca Mountain Region. Submittal date: 04/14/2000. (Data are used for reference only).

LAFP831811AQ97.001. Chemical and Geochronology Data for the Revision and Final Publication of the Volcanism Synthesis Report. Submittal date: 08/29/1997. (Data are used for reference only).

MO0002PVHA0082.000. Probabilistic Volcanic Hazard Analysis for Yucca Mountain, Nevada. Submittal date: 02/17/2000.

MO0003YMP98126.001. Quaternary and Pliocene Basalt. Submittal date: 03/02/2000. (Data are used for reference only).

8.5 OUTPUT DATA, LISTED BY DATA TRACKING NUMBER

LA0004FP831811.004. Summary Frequencies of Disruptive Volcanic Events. Submittal date: 04/17/2000.

LA0005FP831811.001. Compilation and Summaries of Data Supporting Computation of Volcanic Event Intersection Frequencies. Submittal date: 06/15/2000.

ATTACHMENT I: AMR FEEDS TO TSPA IGNEOUS ACTIVITY

Activities external to the Disruptive Events PMR are shown in dashed boxes

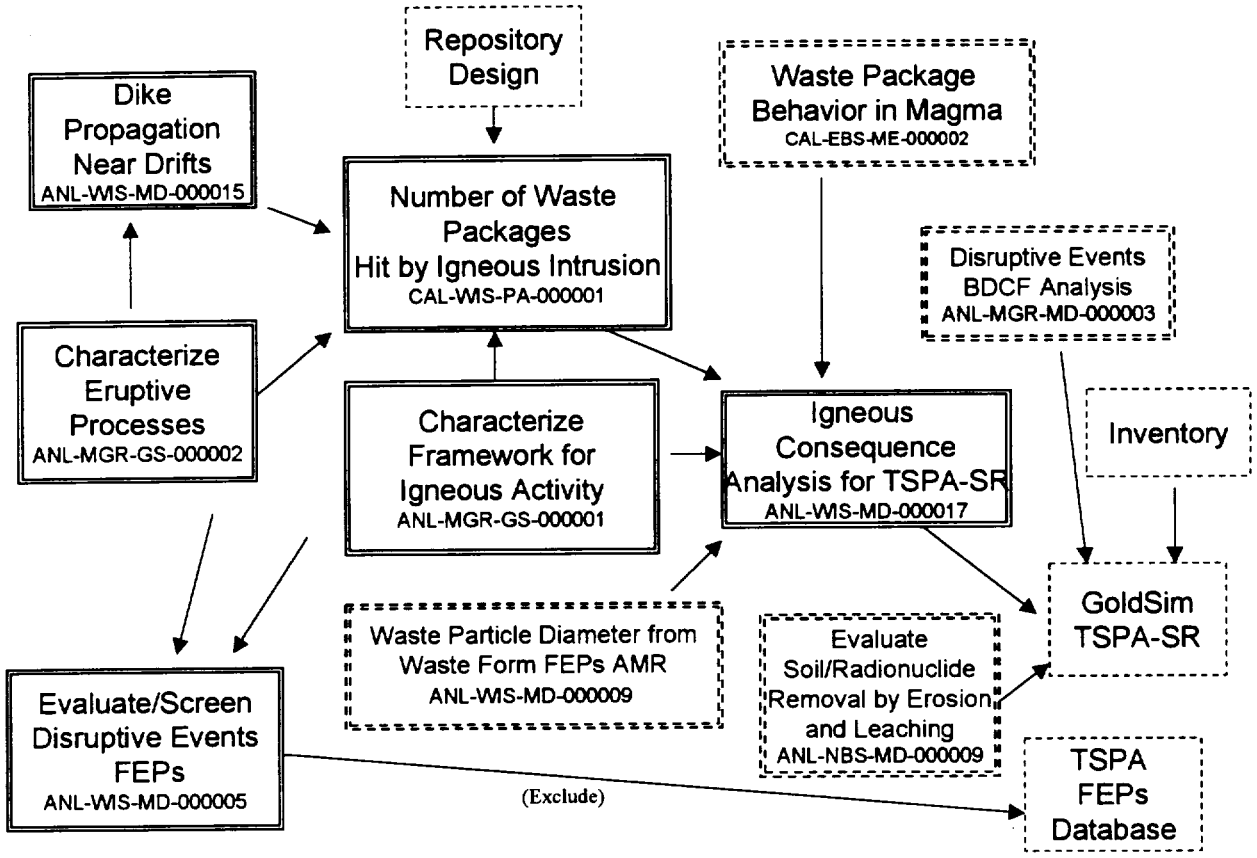

ATTACHMENT II: DEVELOPMENT OF FOOTPRINT POLYGONS FOR POTENTIAL REPOSITORY

The coordinates of the drifts that make up the Primary Block and the Primary Block Contingency Area of EDA-II were obtained from CRWMS M&O (1999f). These coordinates, listed in Table II-1, are given in terms of the Nevada State Plane Coordinate System, Central Zone. The coordinate system used in the PVHA hazard assessment is UTM. The Nevada State Plane coordinates were transformed to UTM as follows.

Columns one and two of Table II-2 list coordinates at the north and south ends of the Primary and Secondary blocks and the Primary and Secondary Block Contingency areas in Nevada Coordinates taken from CRWMS M&O (1999f). These 16 sets of coordinates were transformed to UTM meters (Columns 3 and 4 of Table II-2) by Robert Clayton at the M&O project office in Las Vegas, Nevada, using EARTHVISION V4.0 (STN: 30035-1 V4.0). The difference in the East and North coordinates between UTM and Nevada State Plane was calculated for each point (Columns 5 and 6 of Table II-2). Listed at the bottom of columns five and 6 of Table II-2 are the average value of the differences and the standard error in the differences between UTM meters and Nevada State Plane meters. The standard errors are much smaller than the bin size of 50 meters used in the calculation of the conditional distributions for intersecting dike length. Thus, it is sufficient to use the addition of a constant to transform the drift coordinates from Nevada State Plane meters to UTM meters within the area defined by the EDA-II footprint. Accordingly, the drift coordinates in Nevada State Plane meters listed in Table II-1 were converted to UTM meters by adding the constant 377311.19 meters to the Nevada State Plane Easting and the constant 3845170.47 meters to the Nevada State Plane Northing. The resulting values were divided by 1,000 to obtain the UTM kilometer coordinates listed in Table II-1.

The calculations performed in this AMR input data from files that contain the vertices of a polygon for the potential repository footprint. Encompassing polygons were constructed for the Primary Block and Primary + Contingency Blocks by locating points approximately 10 meters outside of the region defined by the drift coordinates in Table II-1. The resulting polygon vertices were placed in input files REPOS99.PB and REPOS99.PCB used in the calculations presented in this AMR. These files are listed below and are shown in Figure 16, Section 6.5.

**** File: repos99.pb ****

Polygon to encompass Primary Block potential repository footprint from CRWMS M&O (1999f).

9

548.684	4080.913	Primary only
548.461	4076.713	
547.496	4077.027	
547.358	4077.965	
547.497	4079.282	
547.640	4079.662	
547.727	4080.996	
547.846	4081.178	
548.684	4080.913	

**** File: repos99.pcb ****

Polygon to encompass Primary + Contingency Blocks potential repository footprint from CRWMS M&O (1999f).

11

548.684	4080.913	Primary + contingency .
548.461	4076.713	
548.157	4075.953	
547.637	4076.116	
547.496	4077.027	
547.358	4077.965	
547.497	4079.282	
547.640	4079.662	
547.727	4080.996	
547.846	4081.178	
548.684	4080.913	

Table II-1. Potential Repository Drift Coordinates

Primary Block								
	Nevada State Plane Coordinates from CRWMS M&O (1999f)				Translated to UTM using Average from Table II-2			
	East Side		West Side		East Side		West Side	
Drift	North (m)	East (m)	North (m)	East (m)	East (km)	North (km)	East (km)	North (km)
North end	235732.05	171362.51	235997.80	170544.61	548.674	4080.903	547.856	4081.168
1	235690.53	171359.24	235964.55	170515.90	548.670	4080.861	547.827	4081.135
2	235607.39	171353.01	235898.04	170458.47	548.664	4080.778	547.770	4081.069
3	235523.64	171348.62	235823.52	170425.70	548.660	4080.694	547.737	4080.994
4	235439.90	171344.23	235742.01	170414.44	548.655	4080.610	547.726	4080.912
5	235356.16	171339.84	235658.52	170409.26	548.651	4080.527	547.720	4080.829
6	235272.42	171335.46	235575.03	170404.11	548.647	4080.443	547.715	4080.745
7	235188.67	171331.07	235491.54	170398.95	548.642	4080.359	547.710	4080.662
8	235104.93	171326.68	235408.05	170393.78	548.638	4080.275	547.705	4080.579
9	235021.19	171322.29	235324.56	170388.62	548.633	4080.192	547.700	4080.495
10	234937.45	171317.90	235241.07	170383.45	548.629	4080.108	547.695	4080.412
11	234853.70	171313.51	235157.42	170378.77	548.625	4080.024	547.690	4080.328
12	234769.96	171309.12	235073.66	170374.38	548.620	4079.940	547.686	4080.244
13	234686.22	171304.73	234989.94	170369.99	548.616	4079.857	547.681	4080.160
14	234602.48	171300.35	234906.19	170365.60	548.612	4079.773	547.677	4080.077
15	234518.73	171295.98	234822.45	170361.21	548.607	4079.689	547.672	4079.993
16	234434.99	171291.57	234738.71	170356.83	548.603	4079.605	547.668	4079.909
17	234351.25	171287.18	234654.97	170352.44	548.598	4079.522	547.664	4079.825
18	234267.51	171282.79	234571.22	170348.05	548.594	4079.438	547.659	4079.742
19	234183.76	171278.40	234489.19	170338.41	548.590	4079.354	547.650	4079.660
20	234100.02	171274.01	234412.77	170311.48	548.585	4079.270	547.623	4079.583
21	234016.28	171269.62	234337.46	170281.06	548.581	4079.187	547.592	4079.508
22	233932.54	171265.24	234262.20	170250.64	548.576	4079.103	547.562	4079.433
23	233848.79	171260.85	234186.91	170220.23	548.572	4079.019	547.531	4079.357
24	233765.05	171256.46	234109.63	170195.95	548.568	4078.936	547.507	4079.280
25	233681.31	171252.07	234027.47	170186.69	548.563	4078.852	547.498	4079.198
26	233597.57	171247.68	233945.12	170178.03	548.559	4078.768	547.489	4079.116
27	233513.82	171243.29	233862.76	170169.37	548.554	4078.684	547.481	4079.033
28	233430.08	171238.90	233780.41	170160.72	548.550	4078.601	547.472	4078.951
29	233346.34	171234.51	233698.05	170152.06	548.546	4078.517	547.463	4078.869
30	233262.60	171230.13	233615.69	170143.41	548.541	4078.433	547.455	4078.786
31	233178.85	171225.74	233533.34	170134.75	548.537	4078.349	547.446	4078.704

32	233095.11	171221.35	233450.98	170126.10	548.533	4078.266	547.437	4078.621
33	233011.37	171216.96	233368.63	170117.44	548.528	4078.182	547.429	4078.539
34	232927.63	171212.57	233286.27	170108.78	548.524	4078.098	547.420	4078.457
35	232843.88	171208.18	233203.91	170100.13	548.519	4078.014	547.411	4078.374
36	232760.14	171203.79	233121.66	170091.47	548.515	4077.931	547.403	4078.292
37	232676.40	171199.40	233039.20	170082.82	548.511	4077.847	547.394	4078.210
38	232592.68	171195.02	232956.85	170074.16	548.506	4077.763	547.385	4078.127
39	232508.92	171190.63	232874.49	170065.50	548.502	4077.679	547.377	4078.045
40	232425.17	171186.24	232792.13	170056.85	548.497	4077.596	547.368	4077.963
41	232341.43	171181.85	232706.11	170059.48	548.493	4077.512	547.371	4077.877
42	232257.69	171177.46	232616.32	170073.70	548.489	4077.428	547.385	4077.787
43	232173.95	171173.07	232526.53	170087.93	548.484	4077.344	547.399	4077.697
44	232090.20	171168.68	232436.74	170102.15	548.480	4077.261	547.413	4077.607
45	232006.48	171164.29	232346.95	170116.37	548.475	4077.177	547.428	4077.517
46	231922.72	171159.91	232257.16	170130.59	548.471	4077.093	547.442	4077.428
47	231838.96	171155.52	232167.37	170144.81	548.467	4077.009	547.456	4077.338
48	231755.23	171151.13	232077.58	170159.03	548.462	4076.926	547.470	4077.248
49	231671.49	171146.74	231987.80	170173.25	548.458	4076.842	547.484	4077.158
50	231587.75	171142.35	231898.01	170187.47	548.454	4076.758	547.499	4077.068
South end	231545.88	171140.16	231853.11	170194.58	548.451	4076.716	547.506	4077.024
Primary Contingency Block								
51	231504.01	171137.96	231808.22	170201.70	548.449	4076.674	547.513	4076.979
52	231428.20	171109.14	231718.43	170215.92	548.420	4076.599	547.527	4076.889
53	231353.47	171077.01	231628.64	170230.14	548.388	4076.524	547.541	4076.799
54	231278.74	171044.89	231538.85	170244.36	548.356	4076.449	547.556	4076.709
55	231204.01	171012.77	231449.05	170258.58	548.324	4076.374	547.570	4076.620
56	231129.26	170980.65	231359.27	170272.80	548.292	4076.300	547.584	4076.530
57	231054.55	170948.52	231269.48	170287.02	548.260	4076.225	547.598	4076.440
58	230979.82	170916.40	231179.69	170301.24	548.228	4076.150	547.612	4076.350
59	230905.08	170884.26	231089.90	170315.46	548.195	4076.076	547.627	4076.260
60	230830.35	170852.16	231000.11	170329.69	548.163	4076.001	547.641	4076.171
South end	230792.99	170836.10	230955.22	170336.80	548.147	4075.963	547.648	4076.126

Data source: CRWMS M&O (1999f) (input); DTN: LA0005FP831811.001 (output data).

Table II-2. Coordinate Transformation Data

Nevada State Plane Coordinates		UTM Coordinates from EARTHVISION V4.0		Difference Between UTM and Nevada State Plane Coordinates (UTM-Nevada State Plane)	
East (m)	North (m)	East (m)	North (m)	East (m)	North (m)
171362.51	235732.05	548664.74	4080902.14	377302.23	3845170.09
170544.61	235997.80	547846.15	4081164.96	377301.54	3845167.16
171140.16	231545.88	548457.06	4076716.37	377316.90	3845170.49
170194.58	231853.11	547510.67	4077020.22	377316.09	3845167.11
171137.96	231504.01	548455.01	4076674.51	377317.05	3845170.50
170201.70	231808.22	547517.95	4076975.37	377316.25	3845167.15
170836.10	230792.99	548155.71	4075962.64	377319.61	3845169.65
170336.80	230955.22	547655.99	4076123.08	377319.19	3845167.86
171889.47	235623.62	549191.94	4080795.58	377302.47	3845171.96
171505.58	235741.86	548807.73	4080912.45	377302.15	3845170.59
172116.10	233332.26	549426.49	4078505.66	377310.39	3845173.40
171607.89	233494.23	548917.86	4078665.81	377309.97	3845171.58
172096.67	233292.83	549407.21	4078466.17	377310.54	3845173.34
171604.97	233452.59	548915.09	4078624.17	377310.12	3845171.58
172088.63	232741.85	549401.09	4077915.32	377312.46	3845173.47
171567.12	232911.30	548879.14	4078082.90	377312.02	3845171.60
			Average	**377311.19**	**3845170.47**
			Standard Error	**6.26**	**2.20**

Output data. DTN: LA0005FP831811.001.

ATTACHMENT III: DEVELOPMENT OF DISTRIBUTIONS FOR NUMBER OF ERUPTIVE CENTERS PER VOLCANIC EVENT AND AVERAGE SPACING BETWEEN ERUPTIVE CENTERS

III.1 INTRODUCTION

This attachment presents the derivation of discrete distributions for the number of eruptive centers per volcanic event, n^{EC}, and the average spacing between eruptive centers. These assessments are derived from the PVHA experts' assessments of the number of volcanic events at the three Quaternary volcanic centers in the site region, Lathrop Wells (LW), Sleeping Butte (SB), and Northwest Crater Flat (NWCF). As defined in the PVHA (CRWMS M&O 1996), the number of eruptive centers at each of these sites is: two at Sleeping Butte (Little Black Peak and Hidden Cone); five at Crater Flat (Little Cones southwest, Little Cones northeast, Red Cone, Black Cone, and Makani Cone); and one at Lathrop Wells.

III.2 ILLUSTRATION OF THE PROCESS

The process is illustrated using the assessments of Alex McBirney (AM) [from Table AM-1, p. AM-13 of Appendix E in CRWMS M&O (1996)]. For Lathrop Wells (LW), AM assigned probabilities of 0.3, 0.2, 0.4, and 0.1 to there having been 1, 2, 3, or 4 volcanic events, respectively. If only one event occurred, then the data from LW are one event with one eruptive center per event ($n^{EC} = 1$). If there were two events, then the data are two events with $n^{EC} = 1$. For the three and four volcanic event scenarios the data are three events with $n^{EC} = 1$ and four events with $n^{EC} = 1$, respectively. These assessments are summarized in Table III-1.

For Sleeping Butte (SB), AM assigned probabilities of 0.05, 0.8, and 0.15 to there being 1, 2, or 3 volcanic events, respectively. For the one event scenario, the data are one event with $n^{EC} = 2$ (Hidden Cone and Little Black Peak). For the two-event scenario, the data are two events with $n^{EC} = 1$. For the three-event scenario, the data are three events with $n^{EC} = 1$.

For Northwest Crater Flat (NWCF), AM assigned probabilities of 0.9, 0.05, 0.025, 0.015, and 0.01 to there having been 1, 2, 3, 4, or 5 volcanic events, respectively. For the one event scenario, the data are one event with $n^{EC} = 5$ (Little Cones SW, Little Cones NE, Red Cone, Black Cone, and Makani Cone). For the two-event scenario, AM linked Little Cones (SW and NE), Red Cone, and Black Cone into one event and considered Makani Cone to be the second event. Thus, the data are one event with $n^{EC} = 4$ and one event with $n^{EC} = 1$. For the three-event scenario, AM considered Red Cone and Black Cone to be one event, Little Cones SW and NE to be one event, and Makani Cone to be the third event. Thus, the data are two events with $n^{EC} = 2$ and one event with $n^{EC} = 1$. For the four-event scenario, AM considered Little Cones SW and NE to be one event, and Red Cone, Black Cone, and Makani Cone to each be separate events. Thus, the data are one event with $n^{EC} = 2$ and four events with $n^{EC} = 1$. Finally, for the five-event scenario, the data are five events with $n^{EC} = 1$.

The PVHA experts defined their assessments at each of the volcanic centers to be independent of the assessments at the other centers. As a result, for the assessments from Alex McBirney, there

are 4×3×5 = 60 possible combined scenarios for the number of Quaternary volcanic events. Each of these combined scenarios represents a possible empirical data set for evaluating the distribution for n^{EC}. For example, if LW scenario 1, SB scenario 1, and NWCF scenario 1 are the correct assessments for the number of events, then the combined data set consists of one event with $n^{EC} = 1$, one event with $n^{EC} = 2$, and one event with $n^{EC} = 5$. The resulting empirical distribution defining the relative frequency for various values of n^{EC} is:

$$P(n^{EC} = 1) = 1/3 = 0.333$$
$$P(n^{EC} = 2) = 1/3 = 0.333$$
$$P(n^{EC} = 3) = 0/3 = 0$$
$$P(n^{EC} = 4) = 0/3 = 0$$
$$P(n^{EC} = 5) = 1/3 = 0.333$$

The joint probability that this combined scenario represents the correct data is the product of the three independent probabilities for each scenario and is equal to 0.3×0.05×0.9 = 0.0135. There are 59 other possible combined data sets, each resulting in an empirical distribution for n^{EC}. The weighted average of these is used to represent the expected distribution for n^{EC} based on the assessments of Alex McBirney.

A similar process is followed to compute the average spacing between eruptive centers. Whenever a volcanic event is defined to contain more than one of the eruptive centers, then the assessment provides a data point that can be used to evaluate the average spacing between eruptive centers. In the above combined scenario, there are two volcanic events with multiple eruptive centers. The single event at Sleeping Butte consists of eruptive centers at Little Black Peak and Hidden Cone. These cones are located 2.45 kilometers apart. The single event at Crater Flat consists of five eruptive centers. The distance between Makani Cone and Little Cones SW is 11.19 kilometers. Dividing this by 4, which is the number of intervals between eruptive centers, gives an average spacing of 2.80 kilometers. Thus, the combined scenario provides an average value of 2.6 kilometers based on two data points. The process is repeated for the 59 other scenarios, and the weighted average provides the expected average spacing between eruptive centers. In performing this calculation, those scenarios that result in only volcanic events with no multiple eruptive centers are removed from the weighting process.

III.3 CALCULATION INPUT AND RESULTS

The inputs to the calculation are the distributions for the number of volcanic events represented by the mapped Quaternary volcanoes defined by the PVHA experts and the locations of the volcanoes. Tables III-1 through III-10 summarize the interpretations of the assessments made by the 10 PVHA experts.

Table III-1. Assessments from Alex McBirney's Volcanic Hazard Model

Volcanic Center	Scenario	Number of Events *	Probability	Number of Events with n^{EC} =				
				1	2	3	4	5
Lathrop Wells	1	1 LW	0.3	1				
	2	2 LW, LW	0.2	2				
	3	3 LW, LW, LW	0.4	3				
	4	4 LW, LW, LW, LW	0.1	4				
Sleeping Butte	1	1 LBP+HC	0.05		1			
	2	2 LBP, HC	0.8	2				
	3	3 LBP, HC, ?	0.15	3				
Crater Flat	1	1 MC+BC+RC+ LCne+LCsw	0.9					1
	2	2 MC, BC+RC+ LCne+LCsw	0.05	1			1	
	3	3 MC, BC+RC, LCne+LCsw	0.025	1	2			
	4	4 MC, BC, RC, LCne+LCsw	0.015	3	1			
	5	5 MC, BC, RC, LCne, LCsw	0.01	5				

Data source: CRWMS M&O (1996, Appendix E, Table AM-1, p. AM-13). DTN: MO0002PVHA0082.000.

NOTE: * LW Lathrop Wells, HC Hidden Cone, LBP Little Black Peak, MC Makani Cone, BC Black Cone, RC Red Cone, LCne Little Cones North East, LCsw Little Cones southwest, ? undetected. A + indicates eruptive centers considered to be part of a single volcanic event.

Table III-2. Assessments from Bruce Crowe's Volcanic Hazard Model

Volcanic Center	Scenario	Number of Events *	Probability	Number of Events with n^{EC} =				
				1	2	3	4	5
Lathrop Wells	1	1 LW	0.9	1				
	2	2 LW, LW	0.06	2				
	3	3 LW, LW, LW	0.03	3				
	4	4 LW, LW, LW, LW	0.01	4				
Sleeping Butte	1	1 LBP+HC	0.35		1			
	2	2 LBP, HC	0.45	2				
	3	3 LBP, HC, ?	0.2	3				
Crater Flat	1	1 MC+BC+RC+ LCne+LCsw	0.1					1
	2	2 MC+BC, RC+LCne+LCsw	0.1		1	1		
	3	3 MC, BC+RC, LCne+LCsw	0.45	1	2			
	4	4 MC, BC, RC, LCne+LCsw	0.2	3	1			
	5	5 MC, BC, RC, Lcne, LCsw	0.1	5				
	6	6 MC, BC, RC, Lcne, LCsw, ?	0.025	6				
	7	7 MC, BC, RC, Lcne, LCsw, ?, ?	0.025	7				

Data source: CRWMS M&O (1996, Appendix E, Table BC-3, p. BC-39). DTN: MO0002PVHA0082.000.

NOTE: * LW Lathrop Wells, HC Hidden Cone, LBP Little Black Peak, MC Makani Cone, BC Black Cone, RC Red Cone, LCne Little Cones North East, LCsw Little Cones southwest, ? undetected. A + indicates eruptive centers considered to be part of a single volcanic event.

Table III-3. Assessments from George Thompson's Volcanic Hazard Model

Volcanic Center	Scenario	Number of Events*	Probability	Number of Events with n^{EC} =				
				1	2	3	4	5
Lathrop Wells	1	1 LW	0.75	1				
	2	2 LW, LW	0.09	2				
	3	3 LW, LW, LW	0.08	3				
	4	4 LW, LW, LW, LW	0.08	4				
Sleeping Butte	1	1 LBP+HC	0.35		1			
	2	2 LBP, HC	0.65	2				
Crater Flat	1	1 MC+BC+RC+ LCne+LCsw	0.2					1
	2	2 MC, BC+RC+ LCne+LCsw	0.15	1			1	
	3	3 MC, BC+RC, LCne+LCsw	0.1	1	2			
	4	4 MC, BC, RC, LCne+LCsw	0.5	3	1			
	5	5 MC, BC, RC, Lcne, LCsw	0.05	5				

Data source: CRWMS M&O (1996, Appendix E, Table GT-1, p. GT-11). DTN: MO0002PVHA0082.000.

NOTE: * LW Lathrop Wells, HC Hidden Cone, LBP Little Black Peak, MC Makani Cone, BC Black Cone, RC Red Cone, LCne Little Cones North East, LCsw Little Cones southwest, ? undetected. A + indicates eruptive centers considered to be part of a single volcanic event.

Table III-4. Assessments from George Walker's Volcanic Hazard Model

Volcanic Center	Scenario	Number of Events*	Probability	Number of Events with n^{EC} =				
				1	2	3	4	5
Lathrop Wells	1	1 LW	0.9	1				
	2	2 LW, LW	0.07	2				
	3	3 LW, LW, LW	0.02	3				
	4	4 LW, LW, LW, LW	0.01	4				
Sleeping Butte	1	1 LBP+HC	0.4		1			
	2	2 LBP, HC	0.6	2				
Crater Flat	1	1 MC+BC+RC+ LCne+LCsw	0.1					1
	3	3 MC, BC+RC, LCne+LCsw	0.35	1	2			
	4	4 MC, BC, RC, LCne+LCsw	0.55	3	1			

Data source: CRWMS M&O (1996, Appendix E, Table GW-1, p. GW-11). DTN: MO0002PVHA0082.000.

NOTE: * LW Lathrop Wells, HC Hidden Cone, LBP Little Black Peak, MC Makani Cone, BC Black Cone, RC Red Cone, LCne Little Cones North East, LCsw Little Cones southwest, ? undetected. A + indicates eruptive centers considered to be part of a single volcanic event.

Table III-5. Assessments from Mel Kuntz's Volcanic Hazard Model

Volcanic Center	Scenario	Number of Events *	Probability	Number of Events with n^{EC} =				
				1	2	3	4	5
Lathrop Wells	1	1 LW	0.95	1				
	2	2 LW, LW	0.03	2				
	3	3 LW, LW, LW	0.019	3				
	4	4 LW, LW, LW, LW	0.001	4				
Sleeping Butte	1	1 LBP+HC	0.6		1			
	2	2 LBP, HC	0.3	2				
	3	3 LBP, HC, ?	0.1	3				
Crater Flat	1	1 MC+BC+RC+ LCne+LCsw	0.6					1
	2	2 MC, BC+RC+ LCne+LCsw	0.3	1			1	
	3	3 MC, BC+RC, LCne+LCsw	0.05	1	2			
	4	4 MC, BC, RC, LCne+LCsw	0.05	3	1			

Data source: CRWMS M&O (1996, Appendix E, Table MK-1, p. MK-18). DTN: MO0002PVHA0082.000.

NOTE: * LW Lathrop Wells, HC Hidden Cone, LBP Little Black Peak, MC Makani Cone, BC Black Cone, RC Red Cone, LCne Little Cones North East, LCsw Little Cones southwest, ? undetected. A + indicates eruptive centers considered to be part of a single volcanic event.

Table III-6. Assessments from Michael Sheridan's Volcanic Hazard Model

Volcanic Center	Scenario	Number of Events *	Probability	Number of Events with n^{EC} =				
				1	2	3	4	5
Lathrop Wells	1	1 LW	0.9	1				
	2	2 LW, LW	0.1	2				
Sleeping Butte	1	1 LBP+HC	0.67		1			
	2	2 LBP, HC	0.33	2				
Crater Flat	1	1 MC+BC+RC+ LCne+LCsw	0.7					1
	2	2 MC, BC+RC+ LCne+LCsw	0.2	1			4	
	3	3 MC, BC+RC, LCne+LCsw	0.1	1	2	2		

Data source: CRWMS M&O (1996, Appendix E, Table MS-1, p. MS-16 and from text on pages MS-6 to MS-7).
DTN: MO0002PVHA0082.000.

NOTE: * LW Lathrop Wells, HC Hidden Cone, LBP Little Black Peak, MC Makani Cone, BC Black Cone, RC Red Cone, LCne Little Cones North East, LCsw Little Cones southwest, ? undetected. A + indicates eruptive centers considered to be part of a single volcanic event.

Table III-7. Assessments from Richard Carlson's Volcanic Hazard Model

Volcanic Center	Scenario	Number of Events *	Probability	Number of Events with n^{EC} =				
				1	2	3	4	5
Lathrop Wells	1	1 LW	0.95	1				
	2	2 LW, LW	0.05	2				
Sleeping Butte	1	1 LBP+HC	0.7		1			
	2	2 LBP, HC	0.2	2				
	3	3 LBP, HC, ?	0.1	3				
Crater Flat	1	1 MC+BC+RC+ LCne+LCsw	0.6					1
	3	3 MC, BC+RC, LCne+LCsw	0.3	1	2			
	5	5 MC, BC, RC, Lcne, LCsw	0.01	5				

Data source: CRWMS M&O (1996, Appendix E, Table RC-1, p. RC-16). DTN: MO0002PVHA0082.000.

NOTE: * LW Lathrop Wells, HC Hidden Cone, LBP Little Black Peak, MC Makani Cone, BC Black Cone, RC Red Cone, LCne Little Cones North East, LCsw Little Cones southwest, ? undetected. A + indicates eruptive centers considered to be part of a single volcanic event.

Table III-8. Assessments from Richard Fisher's Volcanic Hazard Model

Volcanic Center	Scenario	Number of Events *	Probability	Number of Events with n^{EC} =				
				1	2	3	4	5
Lathrop Wells	1	1 LW	0.6	1				
	2	2 LW, LW	0.3	2				
	3	3	0.05	3				
	4	4	0.05	4				
Sleeping Butte	1	1 LBP+HC	0.7		1			
	2	2 LBP, HC	0.25	2				
	3	3 LBP, HC, HC	0.05	3				
Crater Flat	1	1 MC+BC+RC+ LCne+LCsw	0.8					1
	2	2 MC+BC, RC+LCne+LCsw	0.05		1	1		
	3	3 MC, BC+RC, LCne+LCsw	0.05	1	2			
	4	4 MC, BC, RC, LCne+LCsw	0.1	3	1			

Data source: CRWMS M&O (1996, Appendix E, Table RF-1, p. RF-12). DTN: MO0002PVHA0082.000.

NOTE: * LW Lathrop Wells, HC Hidden Cone, LBP Little Black Peak, MC Makani Cone, BC Black Cone, RC Red Cone, LCne Little Cones North East, LCsw Little Cones southwest, ? undetected. A + indicates eruptive centers considered to be part of a single volcanic event.

Table III-9. Assessments from Wendell Duffield's Volcanic Hazard Model

Volcanic Center	Scenario	Number of Events*	Probability	Number of Events with n^{EC} =				
				1	2	3	4	5
Lathrop Wells	1	1 LW	0.9	1				
	2	2 LW, LW	0.1	2				
Sleeping Butte	1	1 LBP+HC	0.05		1			
	2	2 LBP, HC	0.95	2				
Crater Flat	1	1 MC+BC+RC+ LCne+LCsw	0.07					1
	2	2 MC+BC+RC, LCne+LCsw	0.14		1	1		
	3	3 MC, BC+RC, LCne+LCsw	0.26	1	2			
	4	4 MC, BC, RC, LCne+LCsw	0.34	3	1			
	5	5 MC, BC, RC, Lcne, LCsw	0.19	5				

Data source: CRWMS M&O (1996, Appendix E, Table WD-1, p. WD-11 and page WD-5). DTN: MO0002PVHA0082.000.

NOTE: * LW Lathrop Wells, HC Hidden Cone, LBP Little Black Peak, MC Makani Cone, BC Black Cone, RC Red Cone, LCne Little Cones North East, LCsw Little Cones southwest, ? undetected. A + indicates eruptive centers considered to be part of a single volcanic event.

Table III-10. Assessments from William Hackett's Volcanic Hazard Model

Volcanic Center	Scenario	Number of Events*	Probability	Number of Events with n^{EC} =				
				1	2	3	4	5
Lathrop Wells	1	1 LW	0.4	1				
	2	2 LW, LW	0.1	2				
	3	3 LW, LW, LW	0.4	3				
	4	4 LW, LW, LW, LW	0.05	4				
	5	5 LW, LW, LW, LW, LW	0.05	5				
Sleeping Butte	1	1 LBP+HC	0.4		1			
	2	2 LBP, HC	0.5	2				
	3	3 LBP, HC, ?	0.1	3				
Crater Flat	1	1 MC+BC+RC+ LCne+LCsw	0.1					1
	2	2 MC+BC+RC, LCne+LCsw	0.3		1	1		
	3	3 MC, BC+RC, LCne+LCsw	0.4	1	2			
	4	4 MC, BC, RC, LCne+LCsw	0.1	3	1			
	5	5 MC, BC, RC, Lcne, LCsw	0.05	5				
	6	6 MC, BC, RC, Lcne, LCsw, ?	0.05	6				

Data source: CRWMS M&O (1996, Appendix E, Table WH-1, p. WH-16). DTN: MO0002PVHA0082.000.

NOTE: * LW Lathrop Wells, HC Hidden Cone, LBP Little Black Peak, MC Makani Cone, BC Black Cone, RC Red Cone, LCne Little Cones North East, LCsw Little Cones southwest, ? undetected. A + indicates eruptive centers considered to be part of a single volcanic event.

The locations of the Quaternary volcanoes are listed in Table III-11. These values were used in the PVHA calculation (CRWMS M&O 1996) and were taken from Connor and Hill (1995).

Table III-11. Volcano Locations

UTM East (km)	UTM North (km)	Volcano
543.780	4060.380	Lathrop Wells
523.230	4112.530	Hidden Cone
522.130	4110.340	Little Black Peak Cone
540.330	4079.130	Makani Cone (North Cone)
538.840	4073.990	Black Cone
537.450	4071.470	Red Cone
535.500	4069.490	Little Cone northwest
535.131	4069.220	Little Cone southeast

DTN: MO0002PVHA0082.000.

The calculation of the distribution for the number of eruptive centers per volcanic event and the average spacing between eruptive centers was performed using the software routine NECPDS V1.0 (STN: 10272-1.0-00). The data in Tables III-1 through III-11 were used to create the following input files. The resulting output files are listed after each input file.

```
**** File: AMNECPDS.IN ****
vxy.dat
amnecpds.out
AM no ec on dikes at LW, SB, NWCF
4 0.3 0.2 0.4 0.1
1 1 1
2 1 1 1 1
3 1 1 1 1 1 1
4 1 1 1 1 1 1 1 1
3 0.05 0.8 0.15
1 2 2 3
2 1 2 1 3
3 1 2 1 3 1 3
5 0.9 0.05 0.025 0.015 0.01
1 5 4 5 6 7 8
2 4 5 6 7 8 1 4
3 2 7 8 2 5 6 1 4
4 2 7 8 1 5 1 6 1 4
5 1 4 1 5 1 6 1 7 1 8
q
```

```
**** File: AMNECPDS.OUT ****
AM no ec on dikes at LW, SB, NWCF
NEC 1 2 3 4 5
0.797067 0.020689 0.000000 0.008057 0.174188
average spacing = 2.69
```

```
**** File: BCNECPDS.IN ****
vxy.dat
bcnecpds.out
```

```
BC no ec on dikes at LW, SB, NWCF
4 0.9 0.06 0.03 0.01
1 1 1
2 1 1 1 1
3 1 1 1 1 1 1
4 1 1 1 1 1 1 1 1
3 0.35 0.45 0.2
1 2 2 3
2 1 2 1 3
3 1 2 1 3 1 3
7 0.1 0.1 0.45 0.2 0.1 0.025 0.025
1 5 4 5 6 7 8
2 3 6 7 8 2 4 5
3 2 7 8 2 5 6 1 4
4 2 7 8 1 4 1 5 1 6
5 1 4 1 5 1 6 1 7 1 8
6 1 4 1 5 1 6 1 7 1 8 1 8
7 1 4 1 5 1 6 1 7 1 8 1 8 1 8
q
```

```
**** File: BCNECPDS.OUT ****
BC no ec on dikes at LW, SB, NWCF
NEC 1 2 3 4 5
0.681609 0.271645 0.020588 0.000000 0.026158
average spacing = 1.87
```

```
**** File: GTNECPDS.IN ****
vxy.dat
GTnecpds.out
GT no ec on dikes at LW, SB, NWCF
4 0.75 0.09 0.08 0.08
1 1 1
2 1 1 1 1
3 1 1 1 1 1 1
4 1 1 1 1 1 1 1 1
2 0.35 0.65
1 2 2 3
2 1 2 1 3
5 0.2 0.15 0.1 0.5 0.05
1 5 4 5 6 7 8
2 4 5 6 7 8 1 4
3 2 7 8 2 5 6 1 4
4 2 7 8 1 5 1 6 1 4
5 1 4 1 5 1 6 1 7 1 8
q
```

```
**** File: GTNECPDS.OUT ****
GT no ec on dikes at LW, SB, NWCF
NEC 1 2 3 4 5
0.744308 0.174364 0.000000 0.030266 0.051062
average spacing = 1.53
```

```
**** File: GWNECPDS.IN ****
vxy.dat
gwnecpds.out
GW no ec on dikes at LW, SB, NWCF
4 0.9 0.07 0.02 0.01
1 1 1
2 1 1 1 1
3 1 1 1 1 1 1
4 1 1 1 1 1 1 1 1
2 0.4 0.6
1 2 2 3
2 1 2 1 3
```

```
3 0.1 0.35 0.55
1 5 4 5 6 7 8
3 2 7 8 2 5 6 1 4
4 2 7 8 1 4 1 5 1 6
q
```

```
**** File: GWNECPDS.OUT ****
GW no ec on dikes at LW, SB, NWCF
NEC 1 2 3 4 5
0.690211 0.282237 0.000000 0.000000 0.027552
average spacing = 1.36
```

```
**** File: MKNECPDS.IN ****
vxy.dat
MKnecpds.out
MK no ec on dikes at LW, SB, NWCF
4 0.95 0.03 0.019 0.001
1 1 1
2 1 1 1 1
3 1 1 1 1 1 1
4 1 1 1 1 1 1 1 1
3 0.6 0.3 0.1
1 2 2 3
2 1 2 1 3
3 1 2 1 3 1 3
4 0.6 0.3 0.05 0.05
1 5 4 5 6 7 8
2 4 5 6 7 8 1 4
3 2 7 8 2 5 6 1 4
4 2 7 8 1 4 1 5 1 6
q
```

```
**** File: MKNECPDS.OUT ****
MK no ec on dikes at LW, SB, NWCF
NEC 1 2 3 4 5
0.559011 0.199381 0.000000 0.067184 0.174424
average spacing = 2.40
```

```
**** File: MSNECPDS.IN ****
vxy.dat
MSnecpds.out
MS no ec on dikes at LW, SB, NWCF
2 0.9 0.1
1 1 1
2 1 1 1 1
2 0.67 0.33
1 2 2 3
2 1 2 1 3
3 0.7 0.2 0.1
1 5 4 5 6 7 8
2 4 5 6 7 8 1 4
3 2 7 8 2 5 6 1 4
q
```

```
**** File: MSNECPDS.OUT ****
MS no ec on dikes at LW, SB, NWCF
NEC 1 2 3 4 5
0.509542 0.235628 0.000000 0.045810 0.209020
average spacing = 2.49
```

```
**** File: RCNECPDS.IN ****
vxy.dat
RCnecpds.out
RC no ec on dikes at LW, SB, NWCF
```

```
2 0.95 0.05
1 1 1
2 1 1 1 1
3 0.7 0.2 0.1
1 2 2 3
2 1 2 1 3
3 1 2 1 3 1 3
3 0.6 0.3 0.1
1 5 4 5 6 7 8
3 2 7 8 2 5 6 1 4
5 1 4 1 5 1 6 1 7 1 8
q
```

```
**** File: RCNECPDS.OUT ****
RC no ec on dikes at LW, SB, NWCF
NEC 1 2 3 4 5
0.518637 0.301513 0.000000 0.000000 0.179850
average spacing = 2.40
```

```
**** File: RFNECPDS.IN ****
vxy.dat
RFnecpds.out
RF no ec on dikes at LW, SB, NWCF
4 0.6 0.3 0.05 0.05
1 1 1
2 1 1 1 1
3 1 1 1 1 1 1
4 1 1 1 1 1 1 1 1
3 0.7 0.25 0.05
1 2 2 3
2 1 2 1 3
3 1 2 1 3 1 3
4 0.8 0.05 0.05 0.1
1 5 4 5 6 7 8
2 3 6 7 8 2 4 5
3 2 7 8 2 5 6 1 4
4 2 7 8 1 4 1 5 1 6
q
```

```
**** File: RFNECPDS.OUT ****
RF no ec on dikes at LW, SB, NWCF
NEC 1 2 3 4 5
0.540624 0.232107 0.010571 0.000000 0.216698
average spacing = 2.51
```

```
**** File: WDNECPDS.IN ****
vxy.dat
WDnecpds.out
WD no ec on dikes at LW, SB, NWCF
2 0.9 0.1
1 1 1
2 1 1 1 1
2 0.05 0.95
1 2 2 3
2 1 2 1 3
5 0.07 0.14 0.26 0.34 0.19
1 5 4 5 6 7 8
2 2 7 8 3 4 5 6
3 2 7 8 2 5 6 1 4
4 2 7 8 1 4 1 5 1 6
5 1 4 1 5 1 6 1 7 1 8
q
```

```
**** File: WDNECPDS.OUT ****
```

```
WD no ec on dikes at LW, SB, NWCF
NEC 1 2 3 4 5
0.782655 0.172043 0.027872 0.000000 0.017430
average spacing = 1.40

**** File: WHNECPDS.IN ****
vxy.dat
WHnecpds.out
WH no ec on dikes at LW, SB, NWCF
5 0.4 0.1 0.4 0.05 0.05
1 1 1
2 1 1 1 1
3 1 1 1 1 1 1
4 1 1 1 1 1 1 1 1
5 1 1 1 1 1 1 1 1 1 1
3 0.4 0.5 0.1
1 2 2 3
2 1 2 1 3
3 1 2 1 3 1 3
6 0.1 0.3 0.4 0.1 0.05 0.05
1 5 4 5 6 7 8
2 3 4 5 6 2 7 8
3 2 5 6 2 7 8 1 4
4 2 7 8 1 4 1 5 1 6
5 1 4 1 5 1 6 1 7 1 8
6 1 4 1 5 1 6 1 7 1 8 1 8
q

**** File: WHNECPDS.OUT ****
WH no ec on dikes at LW, SB, NWCF
NEC 1 2 3 4 5
0.668581 0.256513 0.053095 0.000000 0.021812
average spacing = 1.97
```

The distributions for n^{EC} for each expert are plotted on Figure III-1. The expected value for the average spacing between eruptive centers computed from each PVHA Expert's hazard model is listed in Table III-12.

Table III-12. Summary of Average Spacing Between Eruptive Center Calculation Results

PVHA Expert	Average Spacing between Eruptive Centers (km)
Alex McBirney (AM)	2.7
Bruce Crowe (BC)	1.9
George Thompson (GT)	1.5
George Walker (GW)	1.4
Mel Kuntz (MK)	2.4
Michael Sheridan (MS)	2.5
Richard Carlson (RC)	2.4
Richard Fisher (RF)	2.5
Wendell Duffield (WD)	1.4
William Hackett (WH)	2.0

Output data. DTN: LA0005FP831811.001.

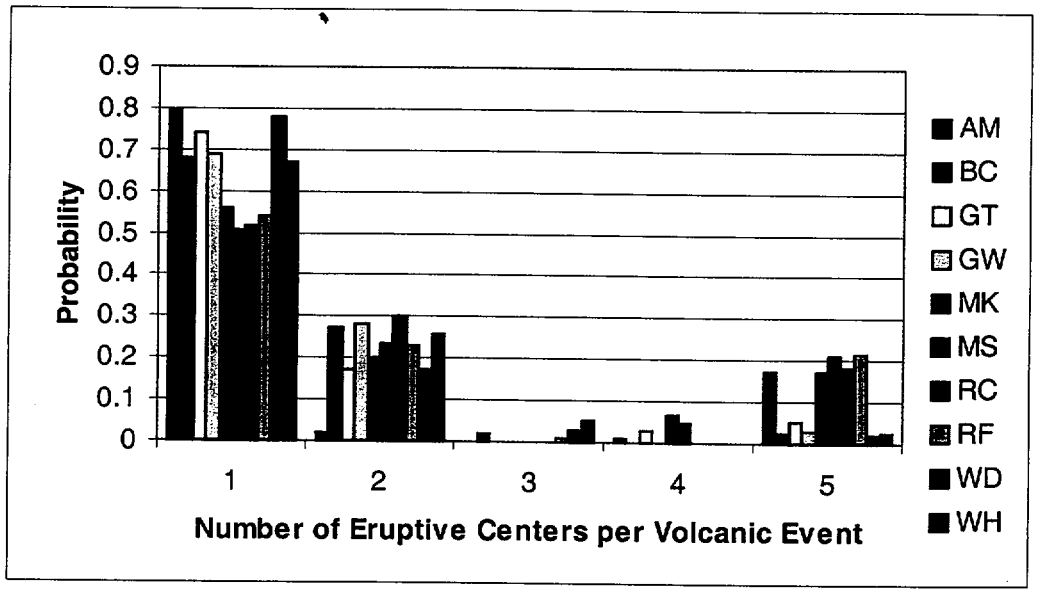

Output data. DTN: LA0005FP831811.001.

NOTE: The two-letter code indicates the PVHA expert's initials from Table III-12.

Figure III-1. Distributions for Number of Eruptive Centers per Volcanic Event, n^{EC}, Derived from the PVHA Experts' Interpretations